US009198733B2

(12) **United States Patent**
Neal, II et al.

(10) **Patent No.:** **US 9,198,733 B2**
(45) **Date of Patent:** **Dec. 1, 2015**

(54) **TREATMENT PLANNING FOR ELECTROPORATION-BASED THERAPIES**

(75) Inventors: **Robert E. Neal, II**, Richmond, VA (US); **Paulo A. Garcia**, Christiansburg, VA (US); **Rafael V. Davalos**, Blacksburg, VA (US); **John H. Rossmeisl**, Blacksburg, VA (US); **John L. Robertson**, Floyd, VA (US)

(73) Assignee: **Virginia Tech Intellectual Properties, Inc.**, Blacksburg, VA (US)

(*) Notice: Subject to any disclaimer, the term of this patent is extended or adjusted under 35 U.S.C. 154(b) by 1006 days.

(21) Appl. No.: **12/906,923**

(22) Filed: **Oct. 18, 2010**

Related U.S. Application Data

(63) Continuation-in-part of application No. 12/432,295, filed on Apr. 29, 2009, and a continuation-in-part of application No. 12/491,151, filed on Jun. 24, 2009, now Pat. No. 8,992,517, and a continuation-in-part of

(Continued)

(51) **Int. Cl.**
A61N 1/32 (2006.01)
A61B 19/00 (2006.01)
(Continued)

(52) **U.S. Cl.**
CPC *A61B 19/50* (2013.01); *C12N 13/00* (2013.01); *A61B 2018/00613* (2013.01); *A61B 2019/504* (2013.01); *A61B 2019/505* (2013.01); *A61N 1/0412* (2013.01); *G06F 19/3437* (2013.01)

(58) **Field of Classification Search**
CPC A61B 2018/00613; A61B 2019/505; A61N 1/3277; G06F 19/3437
USPC 606/34, 41; 435/173.6
See application file for complete search history.

(56) **References Cited**

U.S. PATENT DOCUMENTS

| 1,653,819 | A | 12/1927 | Northcott et al. |
| 4,016,886 | A | 4/1977 | Doss et al. |

(Continued)

FOREIGN PATENT DOCUMENTS

| DE | 863111 | 1/1953 |
| DE | 4000893 | 7/1991 |

(Continued)

OTHER PUBLICATIONS

Co-Pending U.S. Appl. No. 12/432,295, filed Apr. 29, 2009.
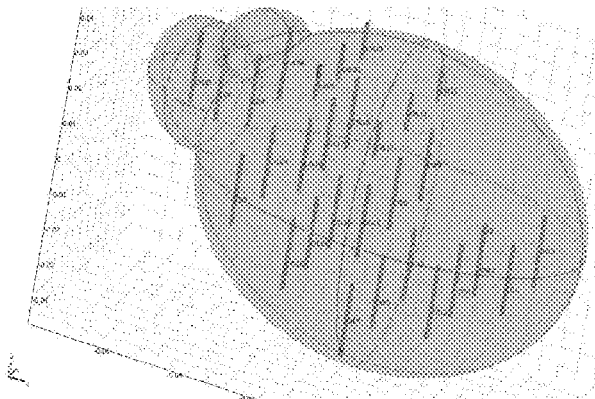
(Continued)

Primary Examiner — Joseph Stoklosa
Assistant Examiner — Jocelyn D Ram
(74) *Attorney, Agent, or Firm* — New River Valley IP Law, PC; Michele L. Mayberry

(57) **ABSTRACT**

The present invention provides systems, methods, and devices for electroporation-based therapies (EBTs). Embodiments provide patient-specific treatment protocols derived by the numerical modeling of 3D reconstructions of target tissue from images taken of the tissue, and optionally accounting for one or more of physical constraints or dynamic tissue properties. The present invention further relates to systems, methods, and devices for delivering bipolar electric pulses for irreversible electroporation exhibiting reduced or no damage to tissue typically associated with an EBT-induced excessive charge delivered to the tissue.

30 Claims, 33 Drawing Sheets

Related U.S. Application Data

application No. 12/609,779, filed on Oct. 30, 2009, now Pat. No. 8,465,484, and a continuation-in-part of application No. 12/757,901, filed on Apr. 9, 2010, now Pat. No. 8,926,606.

(60) Provisional application No. 61/252,445, filed on Oct. 16, 2009, provisional application No. 61/167,997, filed on Apr. 9, 2009, provisional application No. 61/285,618, filed on Dec. 11, 2009, provisional application No. 61/157,670, filed on Mar. 5, 2009, provisional application No. 61/075,216, filed on Jun. 24, 2008, provisional application No. 61/171,564, filed on Apr. 22, 2009, provisional application No. 61/125,840, filed on Apr. 29, 2008.

(51) **Int. Cl.**

C12N 13/00	(2006.01)
A61B 18/00	(2006.01)
A61N 1/04	(2006.01)
G06F 19/00	(2011.01)

(56) **References Cited**

U.S. PATENT DOCUMENTS

4,226,246 A	10/1980	Fragnet
4,262,672 A	4/1981	Kief
4,407,943 A	10/1983	Cole et al.
4,416,276 A	11/1983	Newton et al.
4,810,963 A	3/1989	Blake-Coleman et al.
4,822,470 A	4/1989	Chang
4,907,601 A	3/1990	Frick
4,946,793 A	8/1990	Marshall, III
5,019,034 A	5/1991	Weaver et al.
5,052,391 A	10/1991	Silberstone et al.
5,058,605 A	10/1991	Slovak
5,098,843 A	3/1992	Calvin
5,134,070 A	7/1992	Casnig
5,173,158 A	12/1992	Schmukler
5,192,312 A	3/1993	Orton
5,193,537 A	3/1993	Freeman
5,273,525 A	12/1993	Hofmann
5,283,194 A	2/1994	Schmukler
5,318,563 A	6/1994	Malis et al.
5,328,451 A	7/1994	Davis et al.
5,389,069 A	2/1995	Weaver
5,403,311 A	4/1995	Abele et al.
5,425,752 A	6/1995	Vu Nguyen
5,439,440 A	8/1995	Hofmann
5,458,625 A	10/1995	Kendall
5,533,999 A	7/1996	Hood et al.
5,536,240 A	7/1996	Edwards et al.
5,575,811 A	11/1996	Reid et al.
5,626,146 A	5/1997	Barber et al.
5,634,899 A	6/1997	Shapland et al.
5,674,267 A	10/1997	Mir et al.
5,702,359 A	12/1997	Hofmann et al.
5,718,246 A	2/1998	Vona
5,720,921 A	2/1998	Meserol
5,778,894 A	7/1998	Dorogi et al.
5,782,882 A	7/1998	Lerman et al.
5,800,378 A	9/1998	Edwards et al.
5,810,762 A	9/1998	Hofmann
5,836,905 A	11/1998	Lemelson et al.
5,843,026 A	12/1998	Edwards et al.
5,843,182 A	12/1998	Goldstein
5,873,849 A	2/1999	Bernard
5,919,142 A	7/1999	Boone et al.
5,947,889 A	9/1999	Hehrlein
5,983,131 A	11/1999	Weaver et al.
5,991,697 A	11/1999	Nelson et al.
5,999,847 A	12/1999	Elstrom
6,009,347 A	12/1999	Hofmann
6,010,613 A	1/2000	Walters et al.
6,016,452 A	1/2000	Kasevich
6,029,090 A	2/2000	Herbst
6,041,252 A	3/2000	Walker et al.
6,055,453 A	4/2000	Hofmann et al.
6,068,650 A	5/2000	Hofmann et al.
6,085,115 A	7/2000	Weaver et al.
6,090,106 A	7/2000	Goble et al.
6,102,885 A	8/2000	Bass
6,106,521 A	8/2000	Blewett et al.
6,109,270 A	8/2000	Mah et al.
6,122,599 A	9/2000	Mehta
6,132,419 A	10/2000	Hofmann
6,159,163 A	12/2000	Strauss et al.
6,208,893 B1	3/2001	Hofmann
6,210,402 B1	4/2001	Olsen et al.
6,212,433 B1	4/2001	Behl
6,216,034 B1	4/2001	Hofmann et al.
6,219,577 B1	4/2001	Brown, III et al.
6,241,702 B1	6/2001	Lundquist et al.
6,241,725 B1	6/2001	Cosman
6,261,831 B1	7/2001	Agee
6,278,895 B1	8/2001	Bernard
6,300,108 B1	10/2001	Rubinsky et al.
6,326,177 B1	12/2001	Schoenbach et al.
6,347,247 B1	2/2002	Dev et al.
6,349,233 B1	2/2002	Adams
6,351,674 B2	2/2002	Silverstone
6,387,671 B1	5/2002	Rubinsky et al.
6,403,348 B1	6/2002	Rubinsky et al.
6,470,211 B1	10/2002	Ideker et al.
6,482,619 B1	11/2002	Rubinsky et al.
6,493,592 B1	12/2002	Leonard et al.
6,500,173 B2	12/2002	Underwood et al.
6,526,320 B2	2/2003	Mitchell
6,562,604 B2	5/2003	Rubinsky et al.
6,607,529 B1	8/2003	Jones et al.
6,611,706 B2	8/2003	Avrahami et al.
6,613,211 B1	9/2003	Mccormick et al.
6,627,421 B1	9/2003	Unger et al.
6,653,091 B1	11/2003	Dunn et al.
6,669,691 B1	12/2003	Taimisto
6,678,558 B1	1/2004	Dimmer et al.
6,692,493 B2	2/2004	Mcgovern et al.
6,697,669 B2	2/2004	Dev et al.
6,697,670 B2	2/2004	Chomenky et al.
6,702,808 B1	3/2004	Kreindel
6,795,728 B2	9/2004	Chornenky et al.
6,801,804 B2	10/2004	Miller et al.
6,865,416 B2	3/2005	Dev et al.
6,892,099 B2	5/2005	Jaafar et al.
6,912,417 B1	6/2005	Bernard et al.
6,927,049 B2	8/2005	Rubinsky et al.
6,962,587 B2	11/2005	Johnson et al.
6,972,014 B2	12/2005	Eum et al.
6,994,706 B2	2/2006	Chornenky et al.
7,012,061 B1	3/2006	Reiss et al.
7,053,063 B2	5/2006	Rubinsky et al.
7,054,685 B2	5/2006	Dimmer et al.
7,063,698 B2	6/2006	Whayne et al.
7,113,821 B1	9/2006	Sun et al.
7,130,697 B2	10/2006	Chornenky et al.
7,211,083 B2	5/2007	Chornenky et al.
7,232,437 B2	6/2007	Berman et al.
7,267,676 B2	9/2007	Chornenky et al.
7,291,146 B2	11/2007	Steinke et al.
7,344,533 B2	3/2008	Pearson et al.
7,399,747 B1	7/2008	Clair et al.
7,655,004 B2	2/2010	Long
7,674,249 B2	3/2010	Ivorra et al.
7,680,543 B2	3/2010	Azure
7,718,409 B2	5/2010	Rubinsky et al.
7,742,795 B2	6/2010	Stone et al.
7,937,143 B2	5/2011	Demarais et al.
7,951,582 B2	5/2011	Gazit et al.
7,955,827 B2	6/2011	Rubinsky et al.
8,048,067 B2	11/2011	Davalos et al.
8,114,070 B2	2/2012	Rubinsky et al.
8,162,918 B2	4/2012	Ivorra et al.

(56) References Cited

U.S. PATENT DOCUMENTS

8,221,411 B2	7/2012	Francischelli et al.
8,267,927 B2	9/2012	Dalal et al.
8,282,631 B2	10/2012	Davalos et al.
8,298,222 B2	10/2012	Rubinsky et al.
8,348,921 B2	1/2013	Ivorra et al.
8,425,505 B2*	4/2013	Long 606/37
8,465,484 B2	6/2013	Davalos et al.
8,518,031 B2	8/2013	Boyden et al.
8,603,087 B2	12/2013	Rubinsky et al.
8,835,166 B2	9/2014	Phillips et al.
8,992,517 B2	3/2015	Davalos et al.
2001/0044596 A1	11/2001	Jaafar
2001/0046706 A1	11/2001	Rubinsky et al.
2001/0051366 A1	12/2001	Rubinsky et al.
2002/0010491 A1	1/2002	Schoenbach et al.
2002/0055731 A1	5/2002	Atala et al.
2002/0077676 A1	6/2002	Schroeppel et al.
2002/0082543 A1	6/2002	Park et al.
2002/0099323 A1	7/2002	Dev et al.
2002/0115208 A1	8/2002	Mitchell et al.
2002/0119437 A1	8/2002	Grooms et al.
2002/0137121 A1	9/2002	Rubinsky et al.
2002/0138117 A1	9/2002	Son
2002/0183684 A1	12/2002	Dev et al.
2002/0193831 A1	12/2002	Smith
2003/0009110 A1	1/2003	Tu et al.
2003/0060856 A1*	3/2003	Chornenky et al. 607/40
2003/0088189 A1	5/2003	Tu et al.
2003/0096407 A1	5/2003	Atala et al.
2003/0130711 A1	7/2003	Pearson et al.
2003/0166181 A1	9/2003	Rubinsky et al.
2003/0170898 A1	9/2003	Gundersen et al.
2003/0194808 A1	10/2003	Rubinsky et al.
2003/0199050 A1	10/2003	Mangano et al.
2003/0208200 A1	11/2003	Palanker et al.
2003/0225360 A1	12/2003	Eppstein et al.
2004/0009459 A1*	1/2004	Anderson et al. 434/262
2004/0019371 A1	1/2004	Jaafar et al.
2004/0059389 A1	3/2004	Chornenky et al.
2004/0146877 A1	7/2004	Diss et al.
2004/0153057 A1	8/2004	Davison
2004/0176855 A1	9/2004	Badylak
2004/0193097 A1	9/2004	Hofmann et al.
2004/0236376 A1	11/2004	Miklavcic et al.
2004/0243107 A1	12/2004	Macoviak et al.
2004/0267189 A1	12/2004	Mavor et al.
2005/0013870 A1	1/2005	Freyman et al.
2005/0043726 A1	2/2005	Mchale et al.
2005/0049541 A1	3/2005	Behar et al.
2005/0165393 A1	7/2005	Eppstein
2005/0171523 A1	8/2005	Rubinsky et al.
2005/0171574 A1	8/2005	Rubinsky et al.
2005/0182462 A1	8/2005	Chornenky et al.
2005/0261672 A1	11/2005	Deem et al.
2005/0282284 A1	12/2005	Rubinsky et al.
2005/0288730 A1	12/2005	Deem et al.
2006/0004356 A1	1/2006	Bilski et al.
2006/0015147 A1	1/2006	Persson et al.
2006/0024359 A1	2/2006	Walker et al.
2006/0025760 A1	2/2006	Podhajsky
2006/0079883 A1	4/2006	Elmouelhi et al.
2006/0121610 A1	6/2006	Rubinsky et al.
2006/0142801 A1	6/2006	Demarais et al.
2006/0182684 A1	8/2006	Beliveau
2006/0212078 A1	9/2006	Demarais et al.
2006/0217703 A1	9/2006	Chornenky et al.
2006/0235474 A1	10/2006	Demarais
2006/0264752 A1*	11/2006	Rubinsky et al. 600/439
2006/0264807 A1	11/2006	Westersten et al.
2006/0269531 A1	11/2006	Beebe et al.
2006/0293713 A1	12/2006	Rubinsky et al.
2006/0293725 A1	12/2006	Rubinsky et al.
2006/0293730 A1	12/2006	Rubinsky et al.
2006/0293731 A1	12/2006	Rubinsky et al.
2007/0021803 A1	1/2007	Deem et al.
2007/0025919 A1	2/2007	Deem et al.
2007/0043345 A1	2/2007	Davalos et al.
2007/0060989 A1	3/2007	Deem et al.
2007/0118069 A1	5/2007	Persson et al.
2007/0129711 A1	6/2007	Altshuler et al.
2007/0156135 A1	7/2007	Rubinsky et al.
2007/0230757 A1	10/2007	Trachtenberg et al.
2007/0287950 A1	12/2007	Kjeken et al.
2008/0015571 A1	1/2008	Rubinsky et al.
2008/0021371 A1	1/2008	Rubinsky et al.
2008/0033340 A1	2/2008	Heller et al.
2008/0033417 A1*	2/2008	Nields et al. 606/27
2008/0045880 A1	2/2008	Kjeken et al.
2008/0052786 A1	2/2008	Lin et al.
2008/0071262 A1	3/2008	Azure
2008/0097422 A1*	4/2008	Edwards et al. 606/34
2008/0103529 A1	5/2008	Schoenbach et al.
2008/0132884 A1	6/2008	Rubinsky et al.
2008/0132885 A1	6/2008	Rubinsky et al.
2008/0200912 A1*	8/2008	Long 606/37
2008/0214986 A1	9/2008	Ivorra et al.
2008/0269586 A1	10/2008	Rubinsky et al.
2009/0024075 A1	1/2009	Schroeppel et al.
2009/0029407 A1	1/2009	Gazit et al.
2009/0062788 A1	3/2009	Long et al.
2009/0105703 A1	4/2009	Shadduck
2009/0198231 A1	8/2009	Esser et al.
2009/0247933 A1	10/2009	Maor et al.
2009/0248012 A1	10/2009	Maor et al.
2009/0269317 A1	10/2009	Davalos
2009/0281477 A1	11/2009	Mikus et al.
2009/0292342 A1	11/2009	Rubinsky et al.
2009/0318905 A1	12/2009	Bhargav et al.
2009/0326436 A1	12/2009	Rubinsky et al.
2010/0004623 A1	1/2010	Hamilton et al.
2010/0023004 A1	1/2010	Francischelli et al.
2010/0030211 A1	2/2010	Davalos et al.
2010/0049190 A1	2/2010	Long et al.
2010/0057074 A1	3/2010	Roman et al.
2010/0087813 A1	4/2010	Long
2010/0130975 A1	5/2010	Long
2010/0152725 A1	6/2010	Pearson et al.
2010/0160850 A1	6/2010	Ivorra et al.
2010/0179530 A1	7/2010	Long et al.
2010/0196984 A1	8/2010	Rubinsky et al.
2010/0204560 A1	8/2010	Salahieh et al.
2010/0204638 A1	8/2010	Hobbs et al.
2010/0249771 A1	9/2010	Pearson et al.
2010/0250209 A1	9/2010	Pearson et al.
2010/0255795 A1	10/2010	Rubinsky et al.
2010/0256630 A1	10/2010	Hamilton, Jr. et al.
2010/0261994 A1	10/2010	Davalos et al.
2010/0331758 A1	12/2010	Davalos et al.
2011/0034209 A1	2/2011	Rubinsky et al.
2011/0064671 A1	3/2011	Bynoe
2011/0118732 A1	5/2011	Rubinsky et al.
2011/0217730 A1	9/2011	Gazit et al.
2012/0034131 A1	2/2012	Rubinsky et al.
2012/0071872 A1	3/2012	Rubinsky et al.
2012/0071874 A1	3/2012	Davalos et al.
2012/0085649 A1	4/2012	Sano et al.
2012/0089009 A1	4/2012	Omary et al.
2012/0109122 A1	5/2012	Arena et al.
2012/0179091 A1	7/2012	Ivorra et al.
2012/0226218 A1	9/2012	Phillips et al.
2012/0277741 A1	11/2012	Davalos et al.
2013/0090646 A1*	4/2013	Moss et al. 606/41
2013/0108667 A1	5/2013	Soikum et al.
2013/0184702 A1	7/2013	Neal, II et al.
2013/0196441 A1	8/2013	Rubinsky et al.
2013/0197425 A1	8/2013	Golberg et al.
2013/0202766 A1	8/2013	Rubinsky et al.
2013/0253415 A1	9/2013	Sano et al.
2013/0281968 A1	10/2013	Davalos et al.
2013/0345779 A1	12/2013	Maor et al.
2014/0088578 A1	3/2014	Rubinsky et al.
2014/0163551 A1	6/2014	Maor et al.

(56)   **References Cited**

U.S. PATENT DOCUMENTS

2015/0088120 A1	3/2015	Garcia et al.	
2015/0164584 A1	6/2015	Davalos et al.	
2015/0173824 A1	6/2015	Davalos et al.	

FOREIGN PATENT DOCUMENTS

DE	4000893	A	7/1991
EP	0378132	A	7/1990
EP	0935482	A	8/1999
EP	0528891	B1	7/2000
EP	0935482	B1	5/2005
WO	9104014		4/1991
WO	9639531	A	12/1996
WO	9814238	A	4/1998
WO	0020554	A	4/2000
WO	0107583	A	2/2001
WO	0107584	A	2/2001
WO	0107585	A	2/2001
WO	0110319	A	2/2001
WO	0148153	A	7/2001
WO	0181533	A	11/2001
WO	02078527	A	10/2002
WO	02089686	A	11/2002
WO	02100459	A	12/2002
WO	03099382	A	12/2003
WO	2004037341	A2	5/2004
WO	2005065284	A	7/2005
WO	2007137303		7/2009
WO	2009134876	A	11/2009
WO	2010117806	A1	10/2010
WO	2010118387	A1	10/2010
WO	2010151277	A	12/2010
WO	2011047387	A	4/2011
WO	2012071526	A	5/2012
WO	2012088149	A	6/2012

OTHER PUBLICATIONS

Co-Pending U.S. Appl. No. 12/432,295, Non-Final Rejection dated Nov. 10, 2011, 10 pages.
Co-Pending U.S. Appl. No. 12/432,295, Requirement for Restriction/Election dated Aug. 9, 2011, 7 pages.
Co-Pending U.S. Appl. No. 12/432,295, Response to Non-Final Rejection dated Jan. 23, 2012, 9 pages.
Co-Pending U.S. Appl. No. 12/432,295, Response to Requirement for Restriction/Election dated Sep. 2, 2011, 2 pages.
Co-Pending U.S. Appl. No. 12/491,151, Requirement for Restriction/Election dated Dec. 2, 2011, 6 pages.
Co-Pending U.S. Appl. No. 12/491,151, Response to Requirement for Restriction/Election dated Dec. 13, 2011, 2 pages.
Co-Pending U.S. Appl. No. 12/491,151, Supplemental Amendment dated Dec. 17, 2012, 6 pages.
Co-Pending U.S. Appl. No. 12/609,779, Final Rejection dated Oct. 26, 2012, 20 pages.
Co-Pending U.S. Appl. No. 12/609,779, Non-Final Rejection dated May 23, 2012, 17 pages.
Co-Pending U.S. Appl. No. 12/609,779, Notice of Allowance dated Feb. 12, 2013, 7 pages.
Co-Pending U.S. Appl. No. 12/609,779, Notice of Allowance dated May 23, 2013, 2 pages.
Co-Pending U.S. Appl. No. 12/609,779, Response to Non-Final Rejection dated Sep. 24, 2012, 37 pages.
Co-Pending U.S. Appl. No. 12/609,779, Response with RCE to Final Rejection dated Dec. 18, 2012, 20 pages.
Co-Pending U.S. Appl. No. 12/757,901, filed Apr. 9, 2010.
Co-Pending U.S. Appl. No. 12/757,901, Final Rejection dated Oct. 2, 2013, 11 pages.
Co-Pending U.S. Appl. No. 12/757,901, Non-Final Rejection dated Mar. 11, 2013, 12 pages.
Co-Pending U.S. Appl. No. 12/757,901, Response to Non-Final Rejection dated Aug. 12, 2013, 11 pages.

Co-Pending Application No. PCT/US09/42100, filed Apr. 29, 2009.
Co-Pending Application No. PCT/US09/62806, filed Oct. 30, 2009.
Co-Pending Application No. PCT/US10/30629, filed Apr. 9, 2010.
Co-Pending Application No. PCT/US10/53077, filed Oct. 18, 2010.
Co-Pending Application No. PCT/US11/62067, filed Nov. 23, 2011.
Co-Pending Application No. PCT/US11/66239, filed Dec. 20, 2011.
Co-Pending U.S. Appl. No. 12/491,151, filed Jun. 24, 2009.
Co-Pending U.S. Appl. No. 13/332,133, filed Dec. 20, 2011.
Co-Pending U.S. Appl. No. 13/919,640, filed Jun. 17, 2013.
Co-Pending U.S. Appl. No. 13/958,152, filed Aug. 2, 2013.
Co-Pending U.S. Appl. No. 13/989,175, filed May 23, 2013.
Co-Pending U.S. Appl. No. 14/012,832 , filed Aug. 28, 2013.
Co-Pending U.S. Appl. No. 14/017,210, filed Sep. 3, 2013.
Co-pending European Application No. 10 824 248.8, Invitation Pursuant to rule 62a(1) EPC (Sep. 25, 2013).
Co-Pending U.S. Appl. No. 13/919,640, Notice of Allowance dated Mar. 17, 2014, 6 pages.
Co-Pending U.S. Appl. No. 13/919,640, Response to Notice of Allowance with RCE dated Feb. 21, 2014, 5 pages.
Co-Pending U.S. Appl. No. 12/432,295, Response to Non-Final Office Action, dated Apr. 28, 2014, 14 pages.
Co-Pending U.S. Appl. No. 12/491,151, Non-Final Rejection dated Apr. 4, 2014, 12 pages.
Co-Pending U.S. Appl. No. 13/919,640, Supplemental Notice of Allowance dated Apr. 10, 2014, 5 pages.
Co-pending European Application No. 10 824 248.8, Communication Pursuant to Rule 70(2) dated Feb. 6, 2014, 1 page.
Non-Final Office Action of Co-pending U.S. Appl. No. 12/757,901, mail date of Mar. 11, 2013.
Co-Pending U.S. Appl. No. 12/491,151, Response to Final Rejection dated Aug. 20, 2012, 11 pages.
Co-Pending U.S. Appl. No. 13/550,307, filed Jul. 16, 2012.
Maor, E., A. Ivorra, and B. Rubinsky, Non Thermal Irreversible Electroporation: Novel Technology for Vascular Smooth Muscle Cells Ablation, PLoS One, 2009, 4(3): p. e4757.
Maor, E., A. Ivorra, J. Leor, and B. Rubinsky, Irreversible electroporation attenuates neointimal formation after angioplasty, IEEE Trans Biomed Eng, Sep. 2008, 55(9): p. 2268-74.
Neal II, Robert E. and R.V. Davalos, The Feasibility of Irreversible Electroporation for the Treatment of Breast Cancer and Other Heterogeneous Systems, Ann Biomed Eng, 2009, 37(12): p. 2615-2625.
PCT International Search Report (Aug. 22, 2012), and Written Opinion (Aug. 22, 2012) of PCT/US11/66239.
PCT International Search Report and Written Opinion (Jul. 25, 2012) of PCT/US2011/062067.
Rajagopal, V. and S.G. Rockson, Coronary restenosis: a review of mechanisms and management, The American Journal of Medicine, 2003, 115(7): p. 547-553.
PCT International Search Report, 4 pgs, (Jul. 30, 2010), Written Opinion, 7 pgs, (Jul. 30, 2010), and International Preliminary Report on Patentability, 8 pgs, (Oct. 4, 2011) from PCT/US2010/029243.
Co-Pending U.S. Appl. No. 12/757,901, Response to Final Rejection with RCE, dated Feb. 3, 2014, 11 pages.
Co-Pending U.S. Appl. No. 13/919,640, Notice of Allowance dated Nov. 25, 2013, 15 pages.
Co-pending European Application No. 10 824 248.8, Extended Search Report dated Jan. 20, 2014, 6 pages.
Co-pending European Application No. 10 824 248.8, Response to Invitation Pursuant to rule 62a(1) EPC (Sep. 25, 2013), Response filed Nov. 18, 2013.
Al-Sakere, B. et al., 2007, "Tumor ablation with irreversible electroporation." PLoS One 2.
Amasha, et al., Quantitative Assessment of Impedance Tomography for Temperature Measurements in Microwave Hyperthermia, Clin. Phys. Physiol. Meas., 1998, Suppl. A, 49-53.
Andreason, Electroporation as a Technique for the Transfer of Macromolecules into Mammalian Cell Lines, J. Tiss. Cult. Meth., 15:56-62, 1993.
Baker, et al., Calcium-Dependent Exocytosis in Bovine Adrenal Medullary Cells with Leaky Plasma Membranes, Nature, vol. 276, pp. 620-622, 1978.

(56)   References Cited

OTHER PUBLICATIONS

Barber, Electrical Impedance Tomography Applied Potential Tomography, Advances in Biomedical Engineering, Beneken and Thevenin, eds., IOS Press, 1993.

Beebe, S.J., et al., Nanosecond pulsed electric field (nsPEF) effects on cells and tissues: apoptosis induction and tumor growth inhibition. PPPS-2001 Pulsed Power Plasma Science 2001, 28th IEEE International Conference on Plasma Science and 13th IEEE International Pulsed Power Conference, Digest of Technical Papers (Cat. No. 01CH37251). IEEE, Part vol. 1, 2001, pp. 211-15, vol. I, Piscataway, NJ, USA.

Blad, et al., Impedance Spectra of Tumour Tissue in Comparison with Normal Tissue; a Possible Clinical Application for Electrical Impedance Tomography, Physiol. Meas. 17 (1996) A105-A115.

BPH Management Strategies: Improving Patient Satisfaction, Urology Times, May 2001, vol. 29, Supplement 1.

Brown, et al., Blood Flow Imaging Using Electrical Impedance Tomography, Clin. Phys. Physiol. Meas., 1992, vol. 13, Suppl. A, 175-179.

Brown, S.G., Phototherapy of tumors. World J. Surgery, 1983. 7: p. 700-9.

Chandrasekar, et al., Transurethral Needle Ablation of the Prostate (TUNA)—a Propsective Study, Six Year Follow Up, (Abstract), Presented at 2001 National Meeting, Anaheim, CA, Jun. 5101.

Coates, C.W.,et al., "The Electrical Discharge of the Electric Eel, Electrophorous Electricus," Zoologica, 1937, 22(1), pp. 1-32.

Cook, et al., ACT3: A High-Speed, High-Precision Electrical Impedence Tomograph, IEEE Transacations on Biomedical Engineering, vol. 41, No. 8, Aug. 1994.

Co-pending Application No. PCT/US2010/029243, published as WO 2010/117806.

Cowley, Good News for Boomers, Newsweek, Dec. 30, 1996/Jan. 6, 1997.

Cox, et al., Surgical Treatment of Atrial Fibrillation: A Review, Europace (2004) 5, S20-S-29.

Crowley, Electrical Breakdown of Biomolecular Lipid Membranes as an Electromechanical Instability, Biophysical Journal, vol. 13, pp. 711-724, 1973.

Davalos, et al ., Theoretical Analysis of the Thermal Effects During In Vivo Tissue Electroporation, Bioelectrochemistry, vol. 61, pp. 99-107, 2003.

Davalos, et al., A Feasibility Study for Electrical Impedance Tomography as a Means to Monitor T issue Electroporation for Molecular Medicine, IEEE Transactions on Biomedical Engineering, vol. 49, No. 4, Apr. 2002.

Davalos, et al., Tissue Ablation with Irreversible Electroporation, Annals of Biomedical Engineering, vol. 33, No. 2, Feb. 2005.

Davalos, R.V. et al., 2005, "Tissue ablation with irreversible electroporation." Annals of Biomedical Engineering, 3(2):223-231.

Davalos, Real-Time Imaging for Molecular Medicine through Electrical Impedance Tomography of Electroporation, Dissertation for Ph.D. in Engineering-Mechanical Engineering, Graduate Division of University of California, Berkeley, 2002.

Dean, Nonviral Gene Transfer to Skeletal, Smooth, and Cardiac Muscle in Living Animals, Am J. Physiol Cell Physiol 289: 233-245, 2005.

Dev, et al., Medical Applications of Electroporation, IEEE Transactions of Plasma Science, vol. 28, No. 1, pp. 206-223, Feb. 2000.

Dev, et al., Sustained Local Delivery of Heparin to the Rabbit Arterial Wall with an Electroporation Catheter, Catheterization and Cardiovascular Diagnosis, Nov., 1998, vol. 45, No. 3, pp. 337-343.

Duraiswami, et al., Boundary Element Techniques for Efficient 2-D and 3-D Electrical Impedance Tomography, Chemical Engineering Science, vol. 52, No. 13, pp. 2185-2196, 1997.

Duraiswami, et al., Efficient 2D and 3D Electrical Impedance Tomography Using Dual Reciprocity Boundary Element Techniques, Engineering Analysis with Boundary Elements 22, (1998) 13-31.

Duraiswami, et al., Solution of Electrical Impedance Tomography Equations Using Boundary Element Methods, Boundary Element Technology XII, 1997, pp. 226-237.

Edd, J. et al., In-Vivo Results of a New Focal Tissue Ablation Technique: Irreversible Electroporaton, IEEE Trans. Biomed. Eng. 53 (2006) p. 1409-1415.

Edd, J.F, et al., 2007, "Mathematical modeling of irreversible electroporation for treatment planning.", Technology in Cancer Research and Treatment., 6:275-286.

Erez, et al., Controlled Destruction and Temperature Distributions in Biological Tissues Subjected to Monoactive Electrocoagulation, Transactions of the ASME: Journal of Mechanical Design, vol. 102, Feb. 1980.

Foster, R.S., et al., High-intensity focused ultrasound in the treatment of prostatic disease. Eur. Urol., 1993. 23: 44-7).

Fox, et al., Sampling Conductivity Images via MCMC, Mathematics Department, Auckland University, New Zealand, May 1997.

Garcia et al., "Irreversible electroporation (IRE) to treat brain cancer." ASME Summer Bioengineering Conference, Marco Island, FL, Jun. 25-29, 2008.

Gauger, et al., A Study of Dielectric Membrane Breakdown in the Fucus Egg, J. Membrane Biol., vol. 48, No. 3, pp. 249-264, 1979.

Gehl, et al., In Vivo Electroporation of Skeletal Muscle: Threshold, Efficacy and Relation to Electric Field Distribution, Biochimica et Biphysica Acta 1428, 1999, pp. 233-240.

Gençer, et al., Electrical Impedance Tomography: Induced-Current Imaging Achieved with a Multiple Coil System, IEEE Transactions on Biomedical Engineering, vol. 43, No. 2, Feb. 1996.

Gilbert, et al., Novel Electrode Designs for Electrochemotherapy, Biochimica et Biophysica Acta 1334, 1997, pp. 9-14.

Gilbert, et al., The Use of Ultrasound Imaging for Monitoring Cryosurgery, Proceedings 6th Annual Conference, IEEE Engineering in Medicine and Biology, 107-111, 1984.

Glidewell, et al., The Use of Magnetic Resonance Imaging Data and the Inclusion of Anisotropic Regions in Electrical Impedance Tomography, Biomed, Sci. Instrum. 1993; 29: 251-7.

Gothelf, et al., Electrochemotherapy: Results of Cancer Treatment Using Enhanced Delivery of Bleomycin by Electroporation, Cancer Treatment Reviews 2003: 29: 371-387.

Griffiths, et al., A Dual-Frequency Electrical Impedance Tomography System, Phys. Med. Biol., 1989, vol. 34, No. 10, pp. 1465-1476.

Griffiths, The Importance of Phase Measurement in Electrical Impedance Tomography, Phys. Med. Biol., 1987, vol. 32, No. 11, pp. 1435-1444.

Griffiths, Tissue Spectroscopy with Electrical Impedance Tomography: Computer Simulations, IEEE Transactions on Biomedical Engineering, vol. 42, No. 9, Sep. 1995.

Gumerov, et al., The Dipole Approximation Method and Its Coupling with the Regular Boundary Element Method for Efficient Electrical Impedance Tomography, Boundary Element Technology XIII, 1999.

Hapala, Breaking the Barrier: Methods for Reversible Permeabilization of Cellular Membranes, Critical Reviews in Biotechnology, 17(2): 105-122, 1997.

Heller, et al., Clinical Applications of Electrochemotherapy, Advanced Drug Delivery Reviews, vol. 35, pp. 119-129, 1999.

Ho, et al., Electroporation of Cell Membranes: A Review, Critical Reviews in Biotechnology, 16(4): 349-362, 1996.

Zimmermann, et al., Dielectric Breakdown of Cell Membranes, Biophysical Journal, vol. 14, No. 11, pp. 881-899, 1974.

Zlotta, et al., Long-Term Evaluation of Transurethral Needle Ablation of the Prostate (TUNA) for Treatment of Benign Prostatic Hyperplasia (BPH): Clinical Outcome After 5 Years. (Abstract) Presented at 2001 AUA National Meeting, Anaheim, CA—Jun. 5, 2001.

Zlotta, et al., Possible Mechanisms of Action of Transurethral Needle Ablation of the Prostate on Benign Prostatic Hyperplasia Symptoms: a Neurohistochemical Study, Reprinted from Journal of Urology, vol. 157, No. 3, Mar. 1997, pp. 894-899.

Bolland, F., et al., "Development and characterisation of a full-thickness acellular porcine bladder matrix for tissue engineering", Biomaterials, Elsevier Science Publishers, Barking, GB, vol. 28, No. 6, 28 Nov. 2006, pp. 1061-1070.

(56) **References Cited**

OTHER PUBLICATIONS

Co-Pending U.S. Appl. No. 12/432,295, Final Office Action dated Mar. 21, 2012, 13 pages.

Co-Pending U.S. Appl. No. 12/432,295, Response to Final Office Action dated Jul. 23, 2012, 10 pages.

Co-Pending U.S. Appl. No. 12/491,151, Non-Final Rejection dated Dec. 28, 2011, 7 pages.

Co-Pending U.S. Appl. No. 12/491,151, Response to Non-Final Rejection dated Mar. 28, 2012, 10 pages.

Extended European Search Report. May 11, 2012. PCT/US2009042100.

Gilbert, T. W., et al., "Decellularization of tissues and organs", Biomaterials, Elsevier Science Publishers, Barking, GB, vol. 27, No. 19, Jul. 1, 2006, pp. 3675-3683.

Maor et al., the Effect of Irreversible Electroporation on Blood Vessels, Tech. in Cancer Res. and Treatment, vol. 6, No. 4, Aug. 2007, pp. 307-312.

Ott, H. C., et al., "Perfusion-decellularized matrix: using nature's platform to engineer a bioartificial heart", Nature Medicine, Nature Publishing Group, New York, NY, US, vol. 14, No. 2, Feb. 1, 2008, pp. 213-221.

PCT International Preliminary Report on Patentability for PCT/US09/62806, dated Jan. 4, 2012, 6pgs.

PCT International Search Report (Aug. 2, 2011), Written Opinion (Aug. 2, 2011), and International Preliminary Report on Patentability (Apr. 17, 2012) of PCT/US10/53077.

PCT International Search Report (Jul. 9, 2009), Written Opinion (Jul. 9, 2009), and International Preliminary Report on Patentability (Nov. 2, 2010) of PCT/US2009/042100.

Rubinsky, B., "Irreversible Electroporation in Medicine", Technology in Cancer Research and Treatment, vol. 6, No. 4, Aug. 1, 2007, pp. 255-259.

Sano, M. B., et al., "Towards the creation of decellularized organ constructs using irreversible electroporation and active mechanical perfusion", Biomedical Engineering Online, Biomed Central LTD, London, GB, vol. 9, No. 1, Dec. 10, 2010, p. 83.

Co-Pending U.S. Appl. No. 12/432,295, Final Rejection dated Jun. 16, 2014, 14 pages.

Co-Pending U.S. Appl. No. 13/919,640, Supplemental Notice of Allowance dated Jul. 18, 2014, 2 pages.

Co-Pending International Application No. PCT/US2009/042100, International Preliminary Report on Patentability dated Nov. 2, 2010, 7 pages.

Co-Pending International Application No. PCT/US2009/042100, International Search Report dated Jul. 9, 2009, 6 pages.

Co-Pending International Application No. PCT/US2010/030629, International Preliminary Report on Patentability dated Oct. 11, 2011, 7 pages.

Co-Pending International Application No. PCT/US2011/062067, International Preliminary Report on Patentability dated May 28, 2013, 7 pages.

Co-Pending International Application No. PCT/US2011/062067, International Search Report and Written Opinion dated Jul. 25, 2012, 12 pages.

Co-Pending International Application No. PCT/US2011/066239, International Preliminary Report on Patentability dated Jun. 25, 2013, 7 pages.

PCT International Preliminary Report on Patentability from PCT/US2010/030629 dated Oct. 11, 2011.

PCT International Search Report and Written Opinion from PCT/US2010/053077, dated Aug. 2, 2011.

Agerholm-Larsen, B., et al., "Preclinical Validation of Electrochemotherapy as an Effective Treatment for Brain Tumors", Cancer Research 71: 3753-3762 (2011).

Appelbaum, L., et al., "US Findings after Irreversible Electroporation Ablation: Radiologic-Pathologic Correlation" Radiology 262(1), 117-125 (2012).

Arena, Christopher B., et al., "Towards the development of latent heat storage electrodes for electroporation-based therapies", Applied Physics Letters, 101, 083902 (2012).

Arena, Christopher B., et al., "Phase Change Electrodes for Reducing Joule Heating During Irreversible Electroporation". Proceedings of the ASME 2012 Summer Bioengineering Conference, SBC2012, Jun. 20-23, 2012, Fajardo, Puerto Rico.

Bagla, S. and Papadouris, D., "Percutaneous Irreversible Electroporation of Surgically Unresectable Pancreatic Cancer: A Case Report" J. Vascular Int. Radiol. 23(1), 142-145 (2012.)

Bancroft, et al., Design of a Flow Perfusion Bioreactor System for Bone Tissue-Engineering Applications, Tissue Engineering, vol. 9, No. 3, 2003, p. 549-554.

Ben-David, E.,et al., "Characterizaion of Irreversible Electroporation Ablation in In Vivo Procine Liver" Am. J. Roentgenol. 198(1), W62-W68 (2012).

Cemazer M, Parkins CS, Holder AL., Chaplin DJ, Tozer GM, et al., "Electroporation of human microvascular endothelial cells: evidence for an anti-vascular mechanism of electrochemotherapy", Br J Cancer 84: 565-570 (2001).

Corovic, S. et al., "Analytical and numerical quantification and comparison of the local electric field in the tissue for different electrode configurations," Biomed Eng Online, 6, 2007.

Co-Pending U.S. Appl. No. 12/432,295, Non-Final Office Action dated Nov. 26, 2013, 15 pages.

Daud, A.I., et al., "Phase I Trial of Interleukin-12 Plasmid Electroporation in Patients With Metastatic Melanoma," Journal of Clinical Oncology, 26, 5896-5903, Dec. 20, 2008.

Davalos, R.V., et al., "Electrical Impedance tomography for imaging tissue electroporation," IEEE Transactions on Biomedical Engineering, 51, 761-767, 2004.

Demirbas, M. F., "Thermal Energy Storage and Phase Change Materials: An Overview" Energy Sources Part B 1(1), 85-95 (2006).

Ellis TL, Garcia PA, Rossmeisl JH, Jr., Henao-Guerrero N, Robertson J, et al., "Nonthermal irreversible electroporation for intracranial surgical applications. Laboratory investigation", J Neurosurg 114: 681-688 (2011).

Faroja, M., et al., "Irreversible Electroporation Ablation: Is the entire Damage Nonthermal?", Radiology, 266(2), 462-470 (2013).

Foster RS, "High-intensity focused ultrasound in the treatment of prostatic disease", European Urology, 1993, vol. 23 Suppl 1, pp. 29-33.

Garcia P.A., et al., "7.0-T Magnetic Resonance Imaging Characterization of Acute Blood-Brain-Barrier Disruption Achieved with Intracranial Irreversible Electroporation", Plos One, Nov. 2012, 7:11, e50482.

Garcia P.A., et al., "Pilot study of irreversible electroporation for intracranial surgery", Conf Proc IEEE Eng Med Biol Soc, 2009:6513-6516, 2009.

Garcia PA, Rossmeisl JH, Jr., Neal RE, 2nd, Ellis TL, Davalos RV, "A Parametric Study Delineating Irreversible Electroporation from Thermal Damage Based on a Minimally Invasive Intracranial Procedure", Biomed Eng Online 10: 34 (2011).

Garcia, P. A., et al., "Towards a predictive model of electroporation-based therapies using pre-pulse electrical measurements," Conf Proc IEEE Eng Med Biol Soc, vol. 2012, pp. 2575-2578, 2012.

Garcia, P. A., et al., "Non-thermal Irreversible Electroporation (N-TIRE) and Adjuvant Fractioned Radiotherapeutic Multimodal Therapy for Intracranial Malignant Glioma in a Canine Patient" Technol. Cancer Res. Treatment 10(1), 73-83 (2011).

Hjouj, M., et al., "Electroporation-Induced BBB Disruption and Tissue Damage Depicted by MRI", Neuro-Oncology 13: Issue suppl 3, abstract ET-32 (2011).

Hjouj, M., et al., "MRI Study on Reversible and Irreversible Electroporation Induced Blood Brain Barrier Disruption", Plos One, Aug. 2012, 7:8, e42817.

Lee, E.W., et al., "Imaging guided percutaneous irreversible electroporation: ultrasound and immunohistological correlation", Technol Cancer Res Treat 6: 287-294 (2007).

Li, W., et al., "The Effects of Irreversible Electroporation (IRE) on Nerves" PloS One, Apr. 2011, 6(4), e18831.

Mahmood, F., et al., "Diffusion-Weighted MRI for Verification of Electroporation-Based Treatments", Journal of Membrane Biology 240: 131-138 (2011).

(56)   **References Cited**

OTHER PUBLICATIONS

Mahnic-Kalamiza, S., et al., "Educational application for visualization and analysis of electric field strength in multiple electrode electroporation," BMC Med Educ, vol. 12, p. 102, 2012.

Marty, M., et al., "Electrochemotherapy—An easy, highly effective and safe treatment of cutaneous and subcutaneous metastases: Results of ESOPE (European Standard Operating Procedures of Electrochemotherapy) study," European Journal of Cancer Supplements, 4, 3-13, 2006.

Neal II, R. E., et al., "Experimental characterization and numerical modeling of tissue electrical conductivity during pulsed electric fields for irreversible electroporation treatment planning," IEEE Trans Biomed Eng., vol. 59:4, pp. 1076-1085. Epub 2012 Jan 6, 2012.

Neal II, R. E., et al., "Successful Treatment of a Large Soft Tissue Sarcoma with Irreversible Electroporation", Journal of Clinical Oncology, 29:13, e372-e377 (2011).

Rubinsky, B., et al., "Irreversible Electroporation: A New Ablation Modality—Clinical Implications" Technol. Cancer Res. Treatment 6(1), 37-48 (2007).

Salford, L.G., et al., "A new brain tumour therapy combining bleomycin with in vivo electropermeabilization", Biochem. Biophys. Res. Commun., 194(2): 938-943 (1993).

Sharma, A. , et al., "Review on Thermal Energy Storage with Phase Change Materials and Applications", Renewable Sustainable Energy Rev. 13(2), 318-345 (2009).

Thomson, K. R., et al., "Investigation of the Safety of Irreversible Electroporation in Humans" J. Vascular Int. Radiol. 22 (5), 611-621 (2011).

Co-Pending U.S. Appl. No. 12/491,151, Response to Apr. 4, 2014 Non-Final Rejection dated Aug. 22, 2014, 12 pages.

Boone, K., Barber, D. & Brown, B. Review—Imaging with electricity: report of the European Concerted Action on Impedance Tomography. J. Med. Eng. Technol. 21, 201-232 (1997).

Davalos, R. V. & Rubinsky, B. Temperature considerations during irreversible electroporation. International Journal of Heat and Mass Transfer 51, 5617-5622, doi:10.1016/j.ijheatmasstransfer.2008.04.046 (2008).

Garcia, P. et al. Intracranial nonthermal irreversible electroporation: in vivo analysis. J Membr Biol 236, 127-136 (2010).

International Preliminary Report on Patentability of Corresponding International Application No. PCT/2011/066239, dated Jun. 25, 2013.

Jossinet et al., Electrical Impedance Endo-Tomography: Imaging Tissue From Inside, IEEE Transactions on Medical Imaging, Vol. 21, No. 6, Jun. 2002, pp. 560-565.

Lee, E. W. et al. Advanced Hepatic Ablation Technique for Creating Complete Cell Death : Irreversible Electroporation. Radiology 255, 426-433, doi:10.1148/radiol.10090337 (2010).

Payselj, N. et al. The course of tissue permeabilization studied on a mathematical model of a subcutaneous tumor in small animals. IEEE Trans Biomed Eng 52, 1373-1381 (2005).

Phillips, M., Maor, E. & Rubinsky, B. Non-Thermal Irreversible Electroporation for Tissue Decellularization. J. Biomech. Eng, doi:10.1115/1.4001882 (2010).

Sel, D. et al. Sequential finite element model of tissue electropermeabilization. IEEE Transactions on Biomedical Engineering 52, 816-827, doi:10.1109/tbme.2005.845212 (2005).

Sel, D., Lebar, A. M. & Miklavcic, D. Feasibility of employing model-based optimization of pulse amplitude and electrode distance for effective tumor electropermeabilization. IEEE Trans Biomed Eng 54, 773-781 (2007).

Weaver, J. C., Electroporation of biological membranes from multicellular to nano scales, IEEE Trns. Dielectr. Electr. Insul. 10, 754-768 (2003).

Holder, et al., Assessment and Calibration of a Low-Frequency System for Electrical Impedance Tomography (EIT), Optimized for Use in Imaging Brain Function in Ambulant Human Subjects, Annals of the New York Academy of Science, vol. 873, Issue 1, Electrical BI, pp. 512-519, 1999.

Huang, et al., Micro-Electroporation: Improving the Efficiency and Understanding of Electrical Permeabilization of Cells, Biomedical Microdevices, vol. 2, pp. 145-150, 1999.

Hughes, et al., An Analysis of Studies Comparing Electrical Impedance Tomography with X-Ray Videofluoroscopy in the Assessment of Swallowing, Physiol. Meas. 15, 1994, pp. A199-A209.

Issa, et al., The TUNA Procedure for BPH: Review of the Technology: The TUNA Procedure for BPH: Basic Procedure and Clinical Results, Reprinted from Infections in Urology, Jul./Aug. 1998 and Sep./Oct. 1998.

Ivanuša, et al., MRI Macromolecular Contrast Agents as Indicators of Changed Tumor Blood Flow, Radiol. Oncol. 2001; 35(2): 139-47.

Jaroszeski, et al., In Vivo Gene Delivery by Electroporation, Advanced Drug Delivery Review, vol. 35, pp. 131-137, 1999.

Kinosita, et al., Hemolysis of Human Erythrocytes by a Transient Electric Field, Proc. Natl. Acad. Sci. USA, vol. 74, No. 5, pp. 1923-1927, 1977.

Liu, et al., Measurement of Pharyngeal Transit Time by Electrical Impedance Tomography, Clin. Phys. Physiol. Meas., 1992, vol. 13, Suppl. A, pp. 197-200.

Lundqvist, et al., Altering the Biochemical State of Individual Cultured Cells and Organelles with Ultramicroelectrodes, Proc. Natl. Acad. Sci. USA, vol. 95, pp. 10356-10360, Sep. 1998.

Lurquin, Gene Transfer by Electroporation, Molecular Biotechnology, vol. 7, 1997.

Lynn, et al., A New Method for the Generation and Use of Focused Ultrasound in Experimental Biology, The Journal of General Physiology, vol. 26, 179-193, 1942.

Miklavčič et al., A Validated Model of an in Vivo Electric Field Distribution in Tissues for Electrochemotherapy and for DNA Electrotransfer for Gene Therapy, Biochimica et Biophysica Acta 1523 (2000), pp. 73-83.

Miklavčič et al., The Importance of Electric Field Distribution for Effective in Vivo Electroporation of Tissues, Biophysical Journal, vol. 74, May 1998, pp. 2152-2158.

Miller, L., et al., Cancer cells ablation with irreversible electroporation, Technology in Cancer Research and Treatment 4 (2005) 699-706.

Mir, et al., Effective Treatment of Cutaneous and Subcutaneous Malignant Tumours by Electrochemotherapy, British Journal of Cancer, vol. 77, No. 12, pp. 2336-2342, 1998.

Mir, et al., Electrochemotherapy Potentiation of Antitumour Effect of Bleomycin by Local Electric Pulses, European Journal of Cancer, vol. 27, No. 1, pp. 68-72, 1991.

Mir, et al., Electrochemotherapy, a Novel Antitumor Treatment: First Clinical Trial, C.R. Acad. Sci. Paris, Ser. III, vol. 313, pp. 613-618, 1991.

Mir, L.M. and Orlowski, S., The basis of electrochemotherapy, in Electrochemotherapy, electrogenetherapy, and transdermal drug delivery: electrically mediated delivery of molecules to cells, M.J. Jaroszeski, R. Heller, R. Gilbert, Editors, 2000, Humana Press, p. 99-118.

Mir, L.M., et al., Electric Pulse-Mediated Gene Delivery to Various Animal Tissues, in Advances in Genetics, Academic Press, 2005, p. 83-114.

Mir, Therapeutic Perspectives of In Vivo Cell Electropermeabilization, Bioelectrochemistry, vol. 53, pp. 1-10, 2000.

Narayan, et al., Establishment and Characterization of a Human Primary Prostatic Adenocarcinoma Cell Line (ND-1), The Journal of Urology, vol. 148, 1600-1604, Nov. 1992.

Naslund, Cost-Effectiveness of Minimally Invasive Treatments and Transurethral Resection (TURP) in Benign Prostatic Hyperplasia (BPH), (Abstract), Presented at 2001 AUA National Meeting Anaheim, CA, Jun. 5, 2001.

Naslund, Michael J., Transurethral Needle Ablation of the Prostate, Urology, vol. 50, No. 2, Aug. 1997.

Neumann, et al., Gene Transfer into Mouse Lyoma Cells by Electroporation in High Electric Fields, J. Embo., vol. 1, No. 7, pp. 841-845, 1982.

Neumann, et al., Permeability Changes Induced by Electric Impulses in Vesicular Membranes, J. Membrane Biol., vol. 10, pp. 279-290, 1972.

(56)   References Cited

OTHER PUBLICATIONS

Okino, et al., Effects of High-Voltage Electrical Impulse and an Anticancer Drug on In Vivo Growing Tumors, Japanese Journal of Cancer Research, vol. 78, pp. 1319-1321, 1987.

Onik, et al., Sonographic Monitoring of Hepatic Cryosurgery in an Experimental Animal Model, AJR American J. of Roentgenology, vol. 144, pp. 1043-1047, May 1985.

Onik, et al., Ultrasonic Characteristics of Frozen Liver, Cryobiology, vol. 21, pp. 321-328, 1984.

Organ, L.W., Electrophysiological principles of radiofrequency lesion making, Apply. Neurophysiol., 1976. 39: p. 69-76.

PCT International Preliminary Report on Patentability for PCT/US2009/042100, dated Nov. 2, 2010 (7 pages).

PCT International Search Report for PCT/US10/29243 (WO 2010/117806) dated Jul. 30, 2010.

PCT International Search Report for PCT/US2009/042100, dated Jul. 9, 2009 (1 page).

PCT International Search Report for PCT/US2009/062806, dated Jan. 19, 2010.

PCT International Search Report for PCT/US2010/030629 (WO 2010/118387), dated Jul. 15, 2010.

Piñero, et al., Apoptotic and Necrotic Cell Death Are Both Induced by Electroporation in HL60 Human Promyeloid Leukaemia Cells, Apoptosis, vol. 2, No. 3, 330-336, Aug. 1997.

Precision Office TUNA System, When Patient Satisfaction is Your Goal.

Rols, M.P., et al., Highly Efficient Transfection of Mammalian Cells by Electric Field Pulses: Application to Large Volumes of Cell Culture by Using a Flow System, Eur. J. Biochem. 1992, 206, pp. 115-121.

Rubinsky, B., ed, Cryosurgery. Annu Rev. Biomed. Eng. vol. 2 2000. 157-187.

Schmukler, Impedance Spectroscopy of Biological Cells, downloaded from IEEE Xplore website.

Sersa, et al., Reduced Blood Flow and Oxygenation in SA-1 Tumours after Electrochemotherapy with Cisplatin, British Journal of Cancer, 87, 1047-1054, 2002.

Sersa, et al., Tumour Blood Flow Modifying Effects of Electrochemotherapy: a Potential Vascular Targeted Mechanism, Radiol. Oncol., 37(1): 43-8, 2003.

Sharma, et al., Poloxamer 188 Decreases Susceptibility of Artificial Lipid Membranes to Electroporation, Biophysical Journal, vol. 71, No. 6, pp. 3229-3241, Dec. 1996.

Shiina, S., et al, Percutaneous ethanol injection therapy for hepatocellular carcinoma: results in 146 patients. AJR, 1993, 160: p. 1023-8.

Tekle, Ephrem, R. Dean Astumian, and P. Boon Chock, "Electroporation by using bipolar oscillating electric field: An improved method for DNA transfection of NIH 3T3 cells, Proc. Natl. Acad. Sci., vol. 88, pp. 4230-4234, May 1991, Biochemistry.

Thompson, et al., To determine whether the temperature of 2% lignocaine gel affects the initial discomfort which may be associated with its instillation into the male urethra, BJU International (1999), 84, 1035-1037.

TUNA—Suggested Local Anesthesia Guidelines.

Vidamed, Inc., Transurethral Needle Ablation (TUNA): Highlights from Worldwide Clinical Studies, Vidamed's Office TUNA System.

Weaver, Electroporation: A General Phenomenon for Manipulating Cells and Tissues, Journal of Cellular Biochemistry, 51: 426-435, 1993.

Weaver, et al., Theory of Electroporation: A Review, Bioelectrochemistry and Bioenergetics, vol. 41, pp. 136-160, 1996.

Weisstein: Cassini Ovals. From MathWorld—A. Wolfram Web Resource; Apr. 30, 2010; http://mathworld.wolfram.com/ (updated May 18, 2011).

International Preliminary Report on Patentability of Corresponding International Application No. PCT/2011/062067, dated May 28, 2013.

A.I. Daud et al., "Phase I Trial of Interleukin-12 Plasmid Electroporation in Patients With Metastatic Melanoma," Journal of Clinical Oncology, 26, pp. 5896-5903, 2008.

Co-Pending U.S. Appl. No. 12/432,295, Response to Jun. 16, 2014 Final Rejection filed Oct. 16, 2014, 13 pages.

Co-Pending U.S. Appl. No. 12/491,151, Final Rejection dated Apr. 20, 2012, 8 pages.

Co-Pending U.S. Appl. No. 12/609,779, filed Oct. 30, 2009.

Co-Pending Application No. PCT/US04/43477, filed Dec. 21, 2004.

Co-Pending U.S. Appl. No. 12/432,295, Supplemental Response After RCE, filed Nov. 17, 2014, 9 pages.

Co-Pending U.S. Appl. No. 14/627,046, filed Feb. 20, 2015.

Co-Pending U.S. Appl. No. 14/686,380, filed Apr. 14, 2015.

Golberg, A. and Rubinsky, B., "A statistical model for multidimensional irreversible electroporation cell death in tissue." Biomed Eng Online, 9, 13 pages, 2010.

Mir et al., "Mechanisms of Electrochemotherapy" Advanced Drug Delivery Reviews 35:107-118 (1999).

Neal II et al., "A Case Report on the Successful Treatment of a Large Soft-Tissue Sarcoma with Irreversible Electroporation," Journal of Clinical Oncology, 29, pp. 1-6, 2011.

Co-Pending U.S. Appl. No. 12/491,151, Official Notice of Allowance dated Nov. 6, 2014, 15 pages.

Co-Pending U.S. Appl. No. 12/757,901, Issued as Patent No. 8,926,606 on Jan. 6, 2015, 42 pages.

Co-Pending U.S. Appl. No. 12/757,901, Official Notice of Allowance dated Nov. 4, 2014, 10 pages.

Co-Pending U.S. Appl. No. 14/558,631, filed Dec. 2, 2014.

Co-Pending Application No. PCT/US15/30429, filed May 12, 2015.

Co-Pending U.S. Appl. No. 12/432,295, Non-Final Office Action dated Jun. 23, 2015, 12 pages.

Ball, C., K.R. Thomson, and H. Kavnoudias, "Irreversible electroporation: a new challenge in "out of-operating theater" anesthesia." Anesth Analg, 2010. 110(5): p. 1305-9.

Carpenter A.E. et al., "CellProfiler: image analysis software for identifying and quantifying cell phenotypes." Genome Biol. 2006; 7(10): R100. Published online Oct. 31, 2006, 11 pages.

Charpentier, K.P., et al., "Irreversible electroporation of the pancreas in swine: a pilot study." HPB: the official journal of the International Hepato Pancreato Biliary Association, 2010. 12(5): pp. 348-351.

Clark et al., "The electrical properties of resting and secreting pancreas." The Journal of Physiology, vol. 189, pp. 247-260 (1967).

Dahl et al., "Nuclear shape, mechanics, and mechanotransduction." Circulation Research vol. 102, pp. 1307-1318 (2008).

Flanagan et al., "Unique dielectric properties distinguish stem cells and their differentiated progeny." Stem Cells, vol. 26, pp. 656-665 (2008).

Gascoyne et al., "Membrane changes accompanying the induced differentiation of Friend murine erythroleukemia cells studied by dielectrophoresis." Biochimica et Biophysica Acta (BBA)-Biomembranes, vol. 1149, pp. 119-126 (1993).

Gimsa et al., "Dielectric spectroscopy of single human erythrocytes at physiological ionic strength: dispersion of the cytoplasm." Biophysical Journal, vol. 71, pp. 495-506 (1996).

Helczynska et al., "Hypoxia promotes a dedifferentiated phenotype in ductal breast carcinoma in situ." Cancer Research, vol. 63, pp. 1441-1444 (2003).

Ibey et al., "Selective cytotoxicity of intense nanosecond-duration electric pulses in mammalian cells." Biochimica Et Blophysica Acta-General Subjects, vol. 1800, pp. 1210-1219 (2010).

Jarm et al., "Antivascular effects of electrochemotherapy: implications in treatment of bleeding metastases." Expert Rev Anticancer Ther. vol. 10, pp. 729-746 (2010).

Jensen et al., "Tumor volume in subcutaneous mouse xenografts measured by microCT is more accurate and reproducible than determined by 18FFDG-microPET or external caliper." BMC medical Imaging vol. 8:16, 9 Pages (2008).

Kinosita et al., "Electroporation of cell membrane visualized under a pulsed-laser fluorescence microscope." Biophysical Journal, vol. 53, pp. 1015-1019 (1988).

Kirson et al., "Alternating electric fields arrest cell proliferation in animal tumor models and human brain tumors." Proceedings of the National Academy of Sciences vol. 104, pp. 10152-10157 (2007).

Kotnik and Miklavcic, "Theoretical evaluation of voltage inducement on internal membranes of biological cells exposed to electric fields." Biophysical Journal, vol. 90(2), pp. 480-491 (2006).

(56)   **References Cited**

OTHER PUBLICATIONS

Labeed et al., "Differences in the biophysical properties of membrane and cytoplasm of apoptotic cells revealed using dielectrophoresis." Biochimica et Biophysica Acta (BBA)-General Subjects, vol. 1760, pp. 922-929 (2006).

Maček Lebar and Miklavčič, "Cell electropermeabilization to small molecules in vitro: control by pulse parameters." Radiology and Oncology, vol. 35(3), pp. 193-202 (2001).

Malpica et al., "Grading ovarian serous carcinoma using a two-tier system." The American Journal of Surgical Pathology, vol. 28, pp. 496-504 (2004).

Marszalek et al., "Schwan equation and transmembrane potential induced by alternating electric field." Biophysical Journal, vol. 58, pp. 1053-1058 (1990).

Neal II, R.E., et al., "Treatment of breast cancer through the application of irreversible electroporation using a novel minimally invasive single needle electrode." Breast Cancer Research and Treatment, 2010. 123(1): pp. 295-301.

O'Brien et al., "Investigation of the Alamar Blue (resazurin) fluorescent dye for the assessment of mammalian cell cytotoxicity." European Journal of Biochemistry, vol. 267, pp. 5421-5426 (2000).

Onik, G. and B. Rubinsky, eds. "Irreversible Electroporation: First Patient Experience Focal Therapy of Prostate Cancer. Irreversible Electroporation", ed. B. Rubinsky 2010, Springer Berlin Heidelberg, pp. 235-247.

Onik, G., P. Mikus, and B. Rubinsky, "Irreversible electroporation: implications for prostate ablation." Technol Cancer Res Treat, 2007. 6(4): pp. 295-300.

Paszek et al., "Tensional homeostasis and the malignant phenotype." Cancer Cell, vol. 8, pp. 241-254 (2005).

Pucihar et al., "Numerical determination of transmembrane voltage induced on irregularly shaped cells." Annals of Biomedical Engineering, vol. 34, pp. 642-652 (2006).

Sabuncu et al., "Dielectrophoretic separation of mouse melanoma clones." Biomicrofluidics, vol. 4, 7 pages (2010).

Saur et al., "CXCR4 expression increases liver and lung metastasis in a mouse model of pancreatic cancer." Gastroenterology, vol. 129, pp. 1237-1250 (2005).

Seibert et al., "Clonal variation of MCF-7 breast cancer cells in vitro and in athymic nude mice." Cancer Research, vol. 43, pp. 2223-2239 (1983).

Seidler et al., "A Cre-loxP-based mouse model for conditional somatic gene expression and knockdown in vivo by using avian retroviral vectors." Proceedings of the National Academy of Sciences, vol. 105, pp. 10137-10142 (2008).

Verbridge et al., "Oxygen-Controlled Three-Dimensional Cultures to Analyze Tumor Angiogenesis." Tissue Engineering, Part A vol. 16, pp. 2133-2141 (2010).

Yang et al., "Dielectric properties of human leukocyte subpopulations determined by electrorotation as a cell separation criterion." Biophysical Journal, vol. 76, pp. 3307-3314 (1999).

Zhang, Y. et al., MR imaging to assess immediate response to irreversible electroporation for targeted ablation of liver tissues: preclinical feasibility studies in a rodent model. Radiology, 2010. 256(2): p. 424-32.

Alberts et al., "Molecular Biology of the Cell," 3rd edition, Garland Science, New York, 1994, 1 page, summary in Biochemical Education 22(3) 1994, p. 164.

Asami et al., "Dielectric properties of mouse lymphocytes and erythrocytes." Biochimica et Biophysica Acta (BBA)-Molecular Cell Research, 1010 (1989) pp. 49-55.

Bower et al., "Irreversible electroporation of the pancreas: definitive local therapy without systemic effects." Journal of surgical oncology, 2011. 104(1): pp. 22-28.

Eppich et al., "Pulsed electric fields for selection of hematopoietic cells and depletion of tumor cell contaminants." Nature Biotechnology 18, pp. 882-887 (2000).

Ermolina et al., "Study of normal and malignant white blood cells by time domain dielectric spectroscopy." IEEE Transactions on Dielectrics and Electrical Insulation, 8 (2001) pp. 253-261.

Fischbach et al., "Engineering tumors with 3D scaffolds." Nat Meth 4, pp. 855-860 (2007).

Ibey et al., "Selective cytotoxicity of intense nanosecond-duration electric pulses in mammalian cells." Biochimica Et Biophysica Acta-General Subjects, vol. 1800, pp. 1210-1219 (2010).

Kingham et al., "Ablation of perivascular hepatic malignant tumors with irreversible electroporation." Journal of the American College of Surgeons, 2012. 215(3), pp. 379-387.

Kinosita and Tsong, "Formation and resealing of pores of controlled sizes in human erythrocyte membrane." Nature, vol. 268 (1977) pp. 438-441.

Kinosita and Tsong, "Voltage-induced pore formation and hemolysis of human erythrocytes." Biochimica et Biophysica Acta (BBA)-Biomembranes, 471 (1977) pp. 227-242.

Lebar et al., "Inter-pulse interval between rectangular voltage pulses affects electroporation threshold of artificial lipid bilayers." IEEE Transactions on NanoBioscience, vol. 1 (2002) pp. 116-120.

Ron et al., "Cell-based screening for membranal and cytoplasmatic markers using dielectric spectroscopy." Biophysical chemistry, 135 (2008) pp. 59-68.

Rossmeisl, "New Treatment Modalities for Brain Tumors in Dogs and Cats." Veterinary Clinics of North America: Small Animal Practice 44, pp. 1013-1038 (2014).

Rubinsky et al., "Optimal Parameters for the Destruction of Prostate Cancer Using Irreversible Electroporation." The Journal of Urology, 180 (2008) pp. 2668-2674.

Sano et al., "Contactless Dielectrophoretic Spectroscopy: Examination of the Dielectric Properties of Cells Found in Blood." Electrophoresis, 32, pp. 3164-3171, 2011.

Schoenbach et al., "Intracellular effect of ultrashort electrical pulses." Bioelectromagnetics, 22 (2001) pp. 440-448.

Yao et al., "Study of transmembrane potentials of inner and outer membranes induced by pulsed-electric-field model and simulation." IEEE Trans Plasma Sci, 2007. 35(5): pp. 1541-1549.

Zhang, Y., et al., MR imaging to assess immediate response to irreversible electroporation for targeted ablation of liver tissues: preclinical feasibility studies in a rodent model. Radiology, 2010. 256(2): p. 424-32.
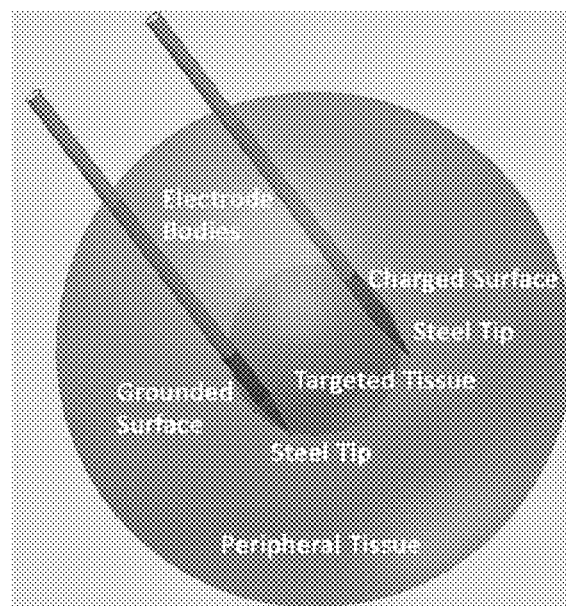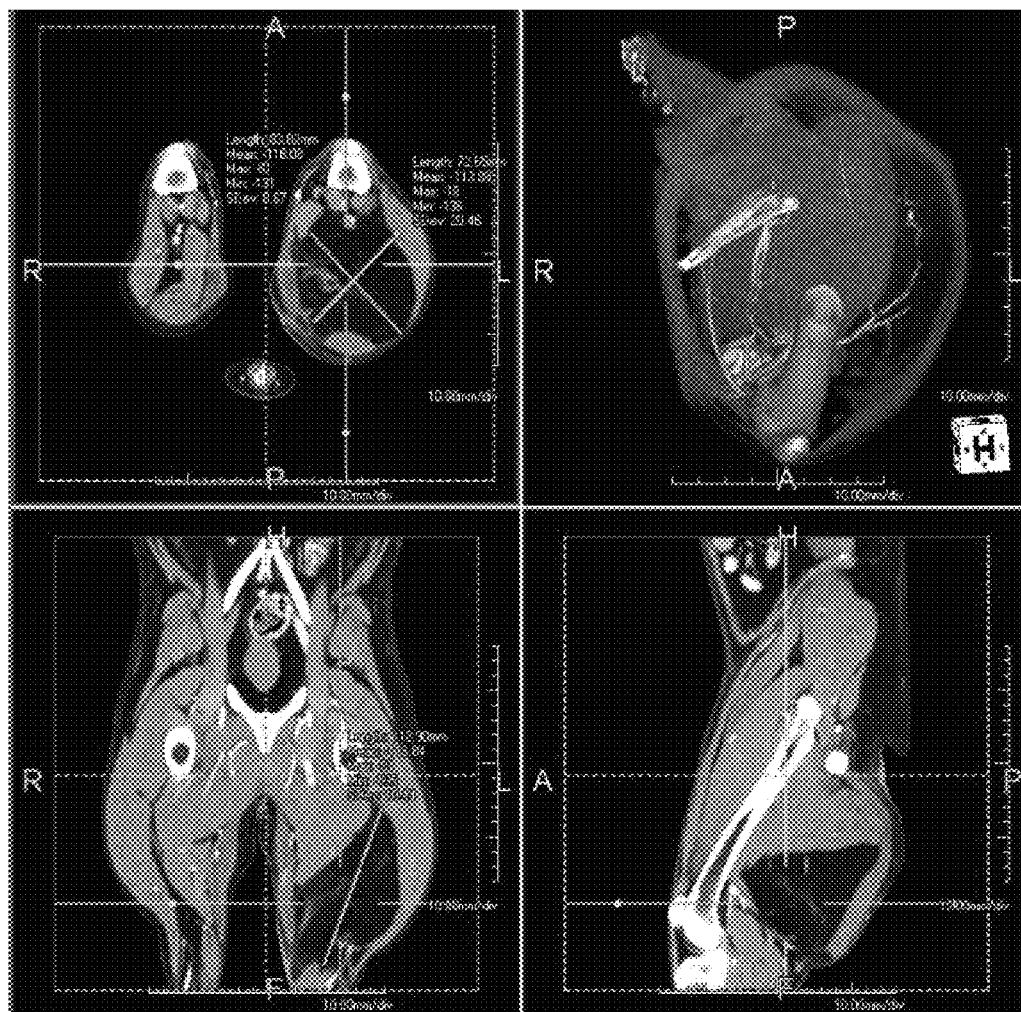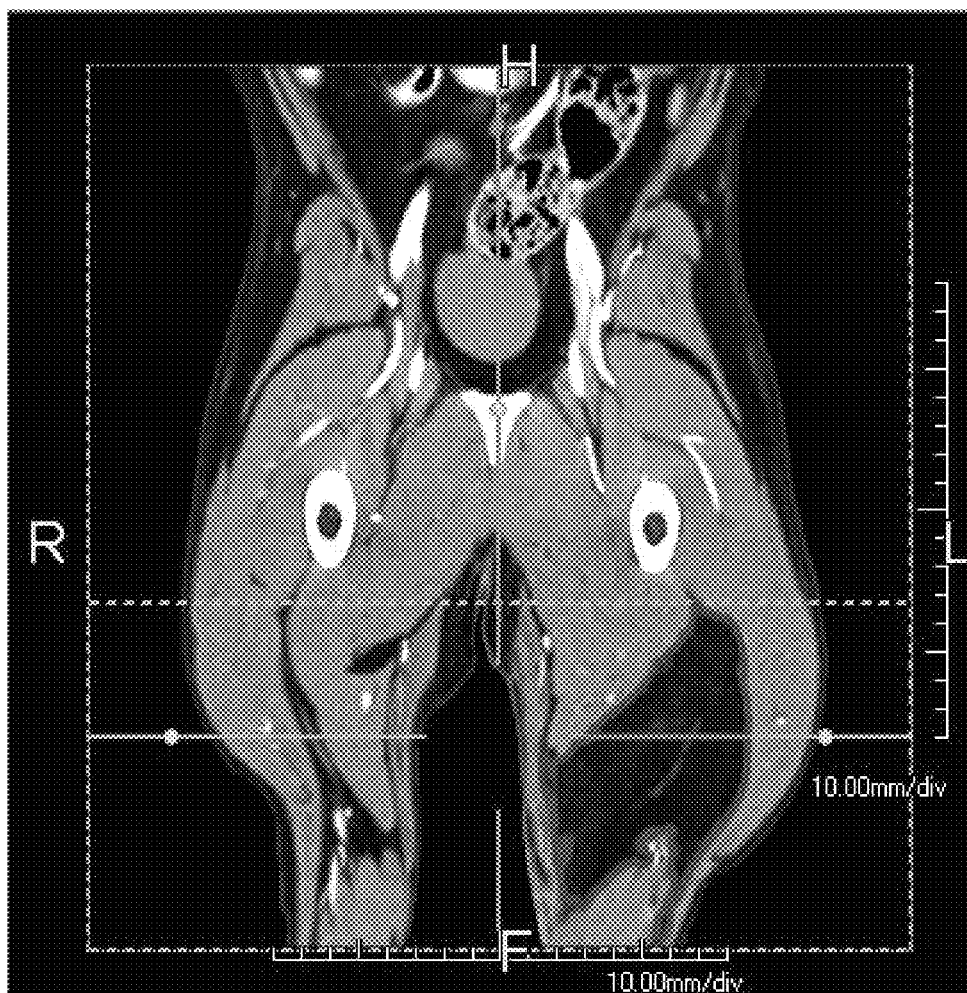
* cited by examiner
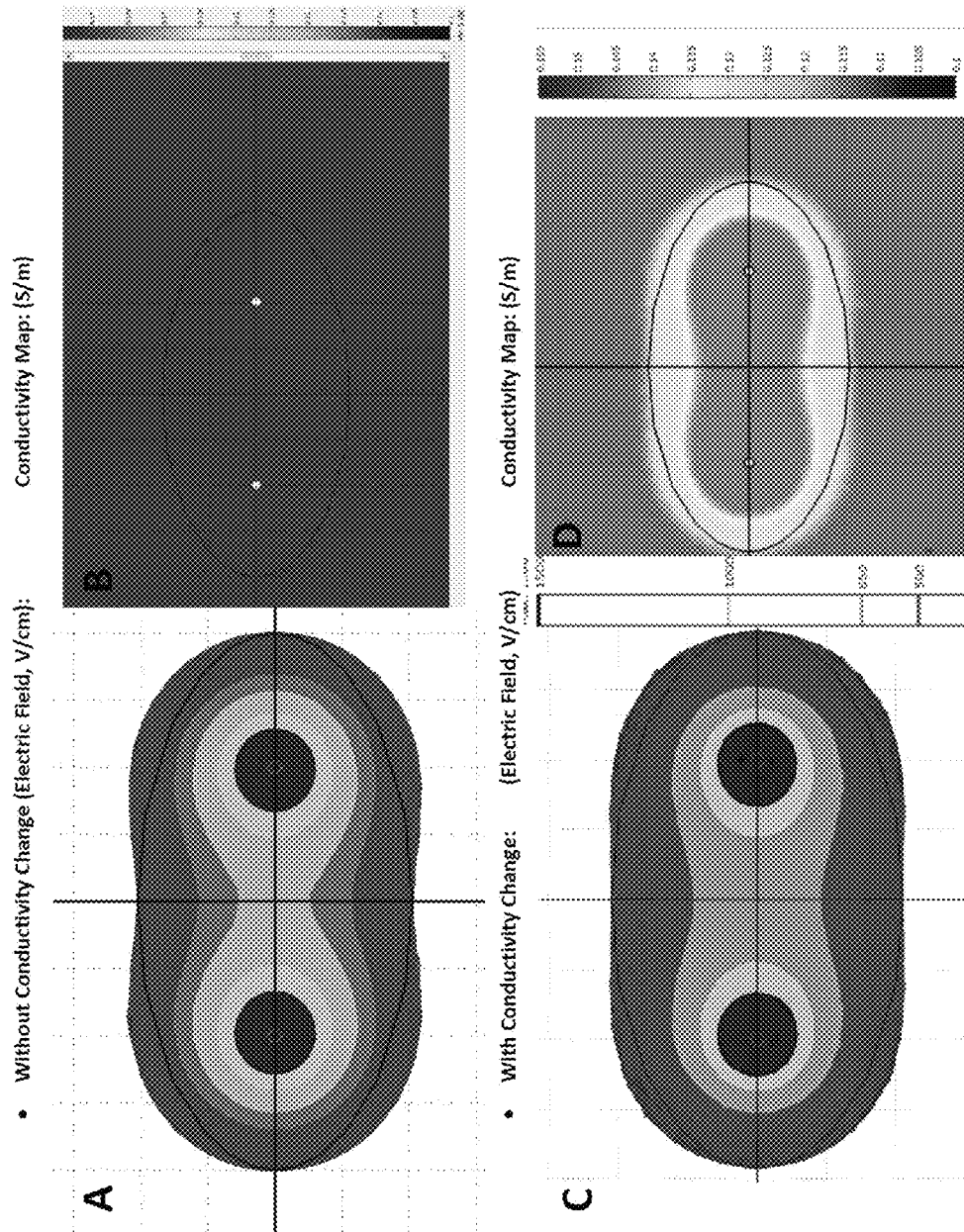
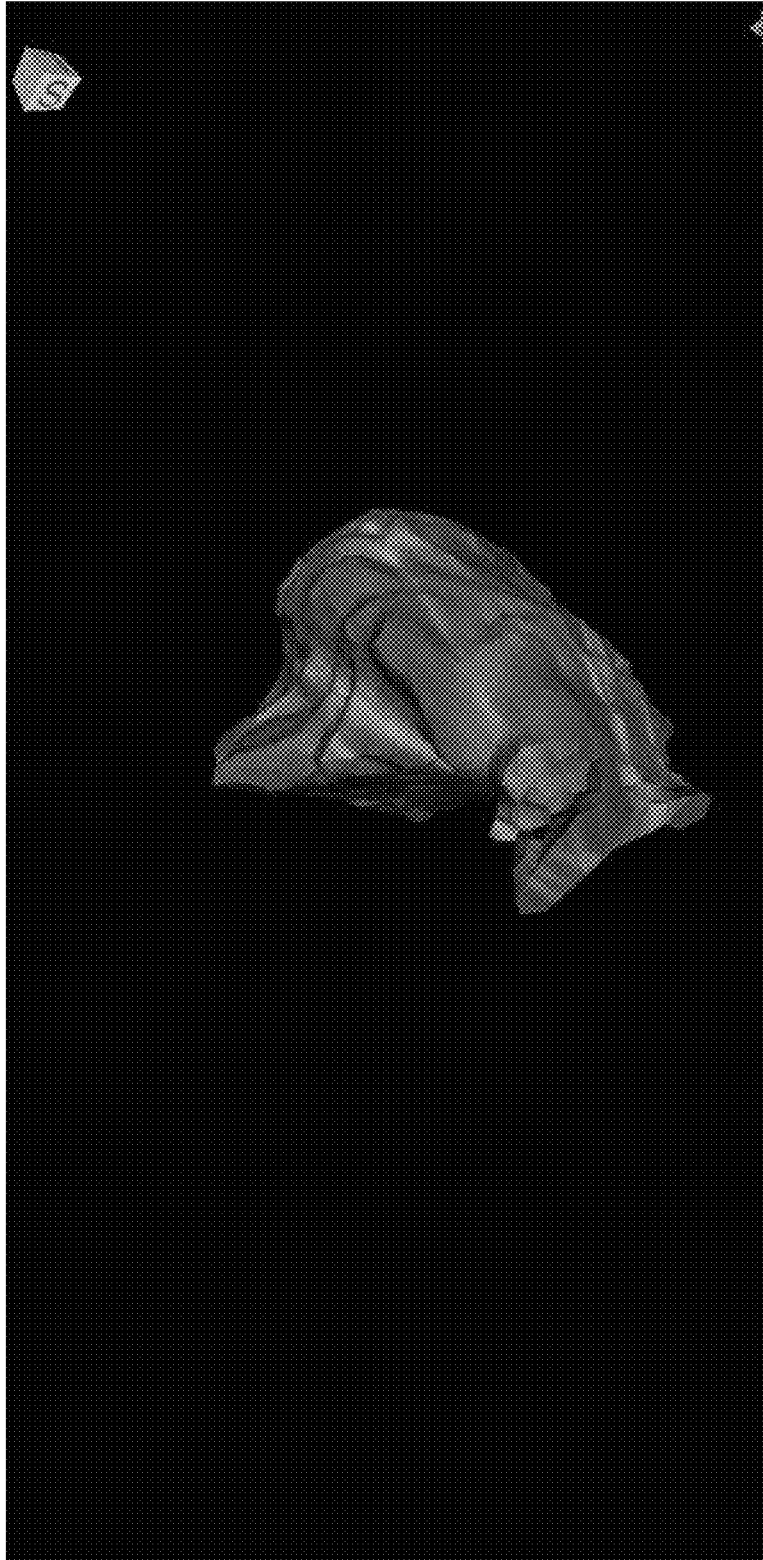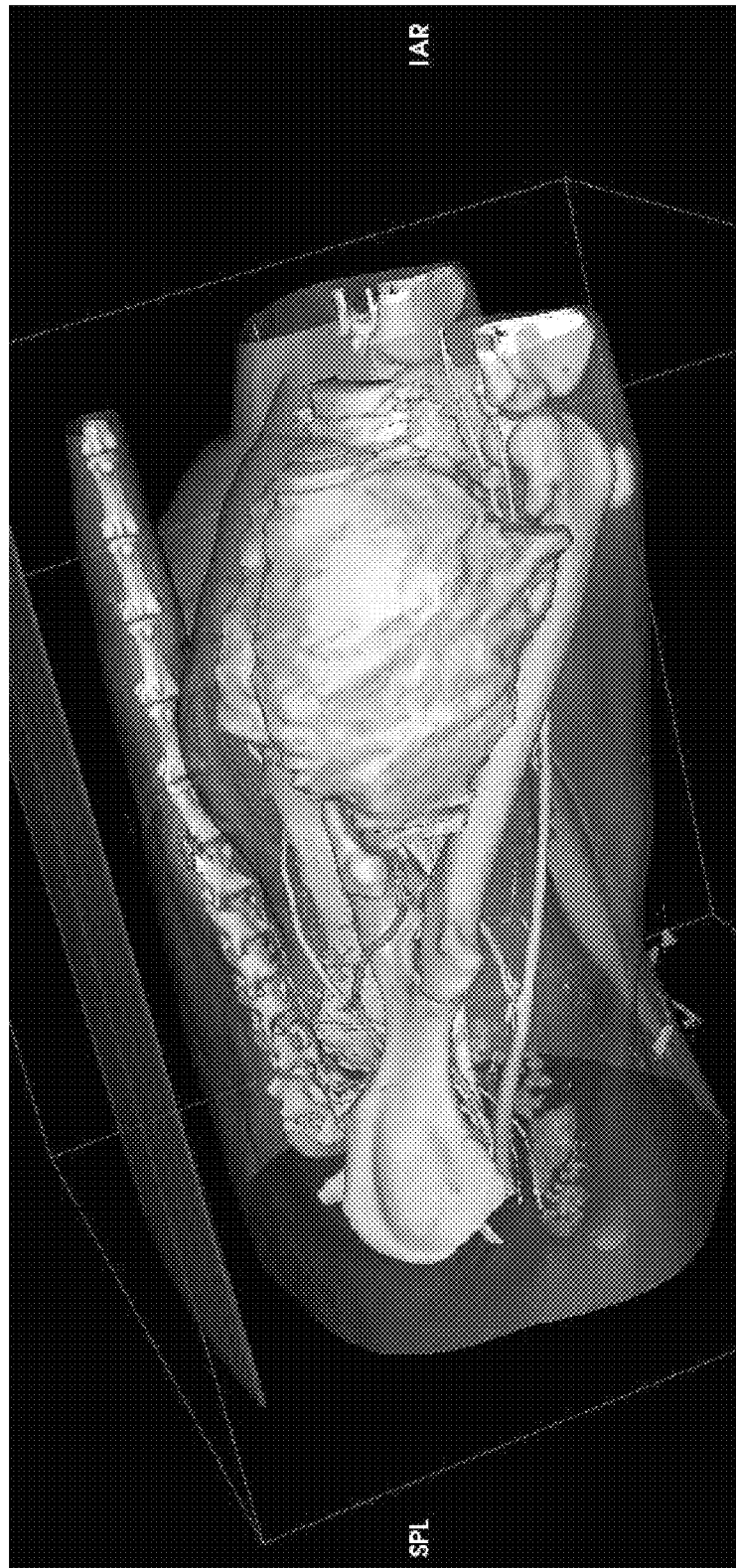FIGS. 1A-D
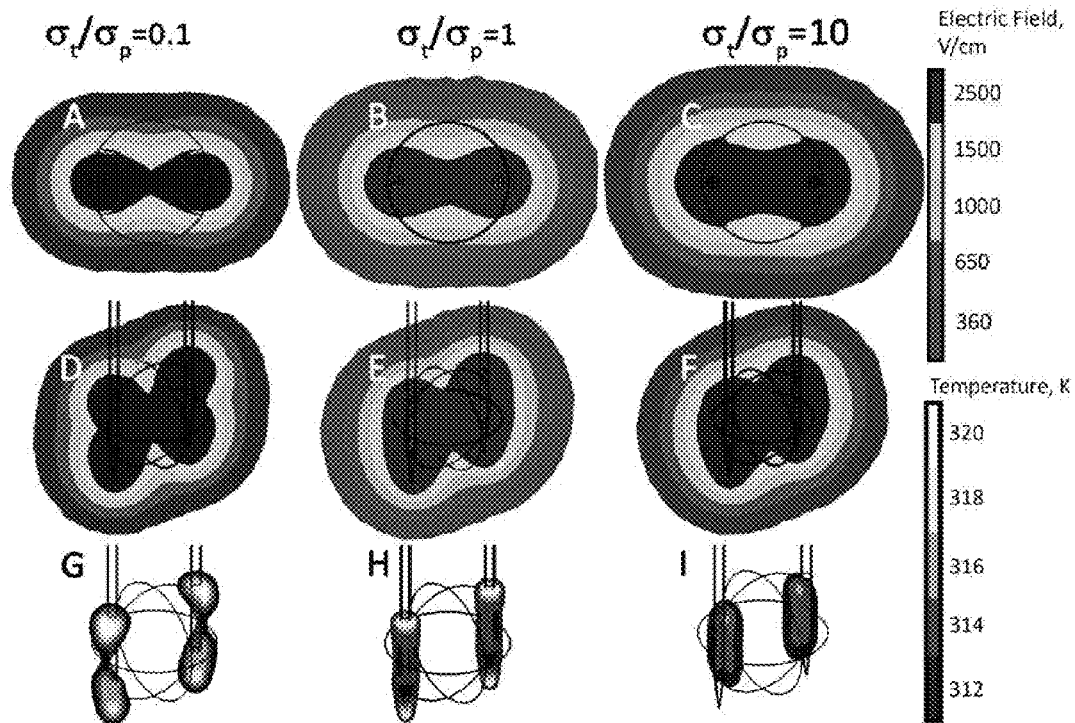
FIGS. 2A-I

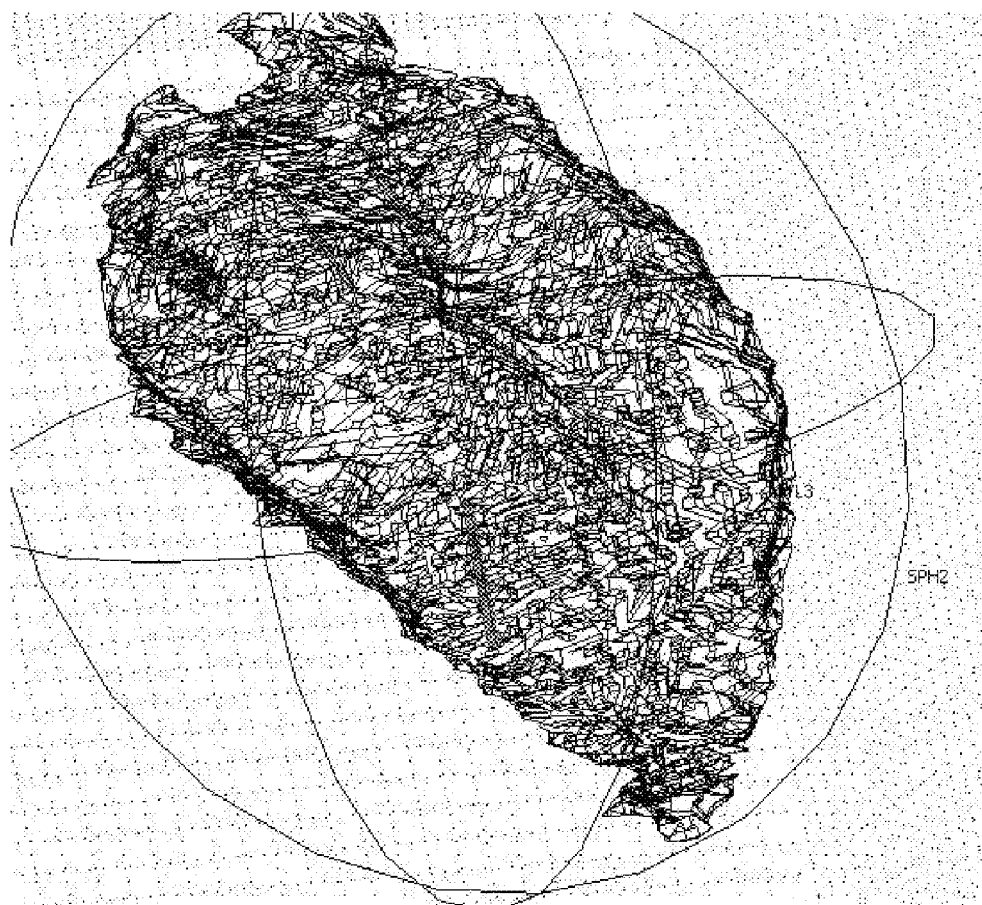

FIG. 2J

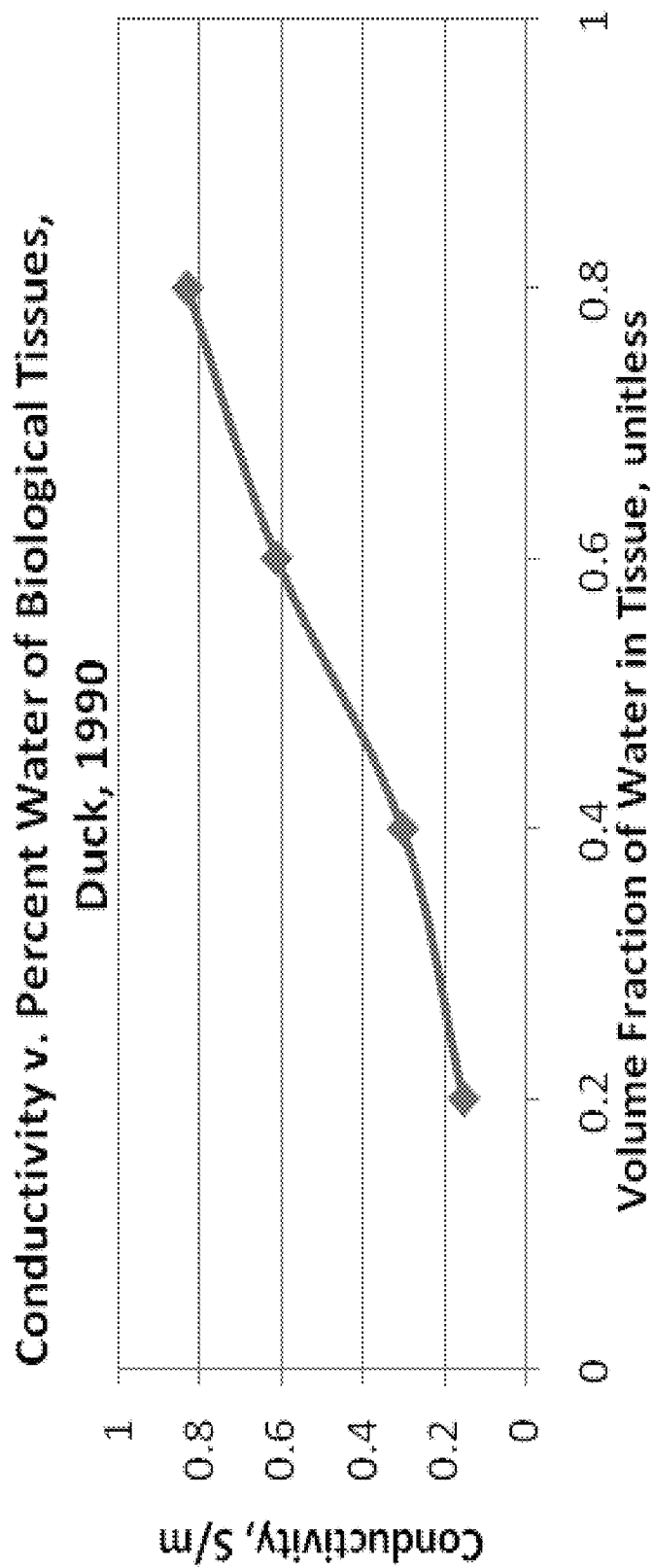FIG. 3

FIG. 4

FIG. 5

FIG. 6

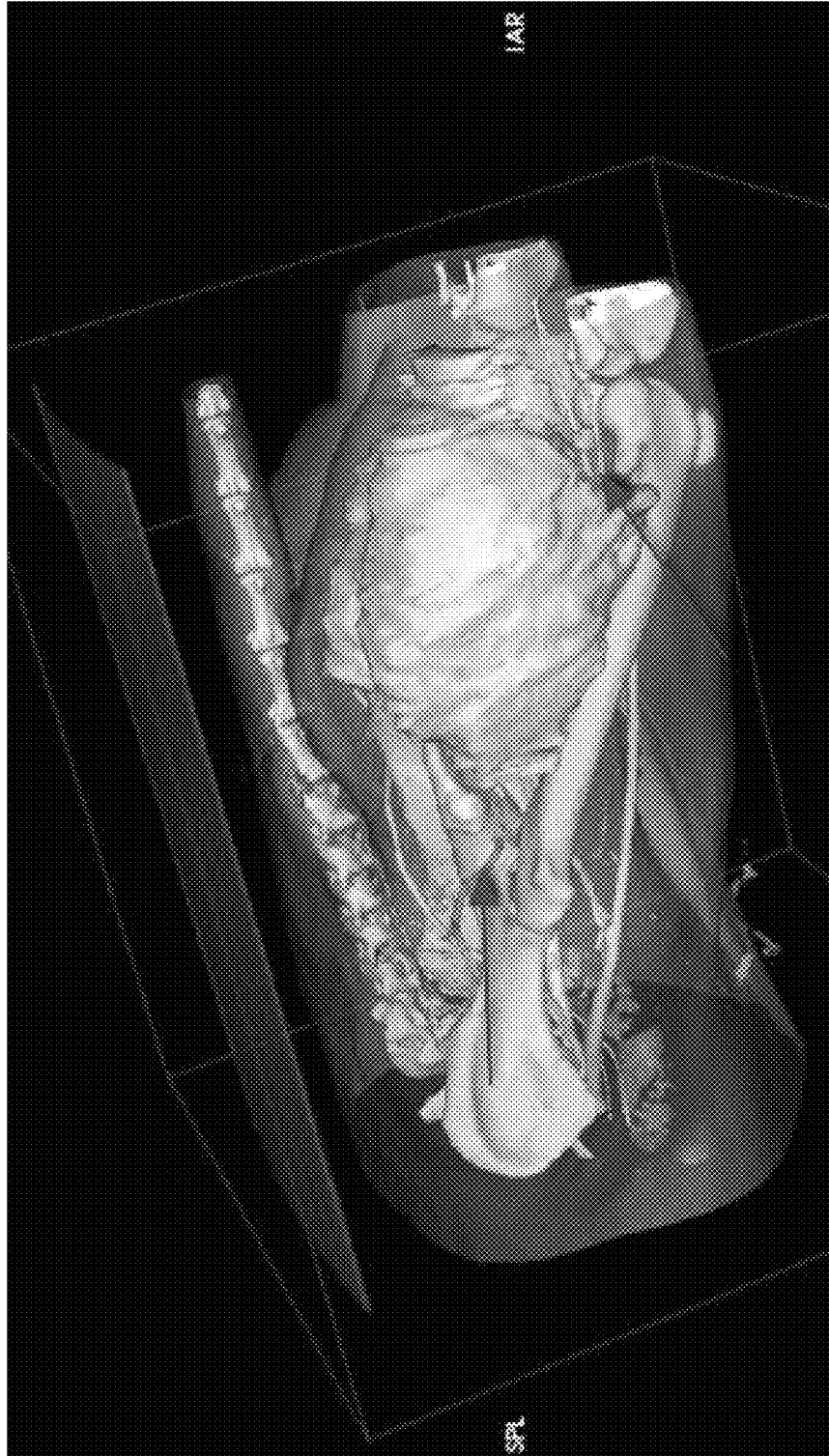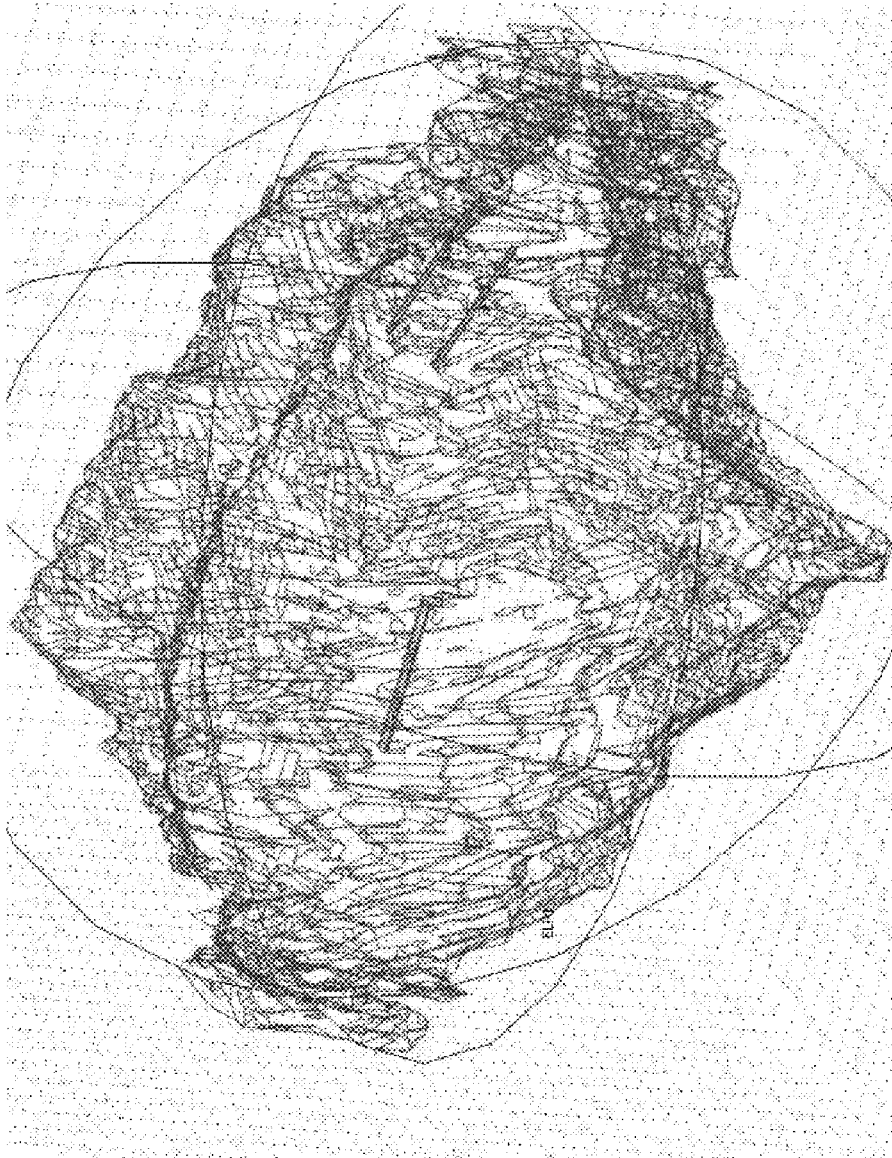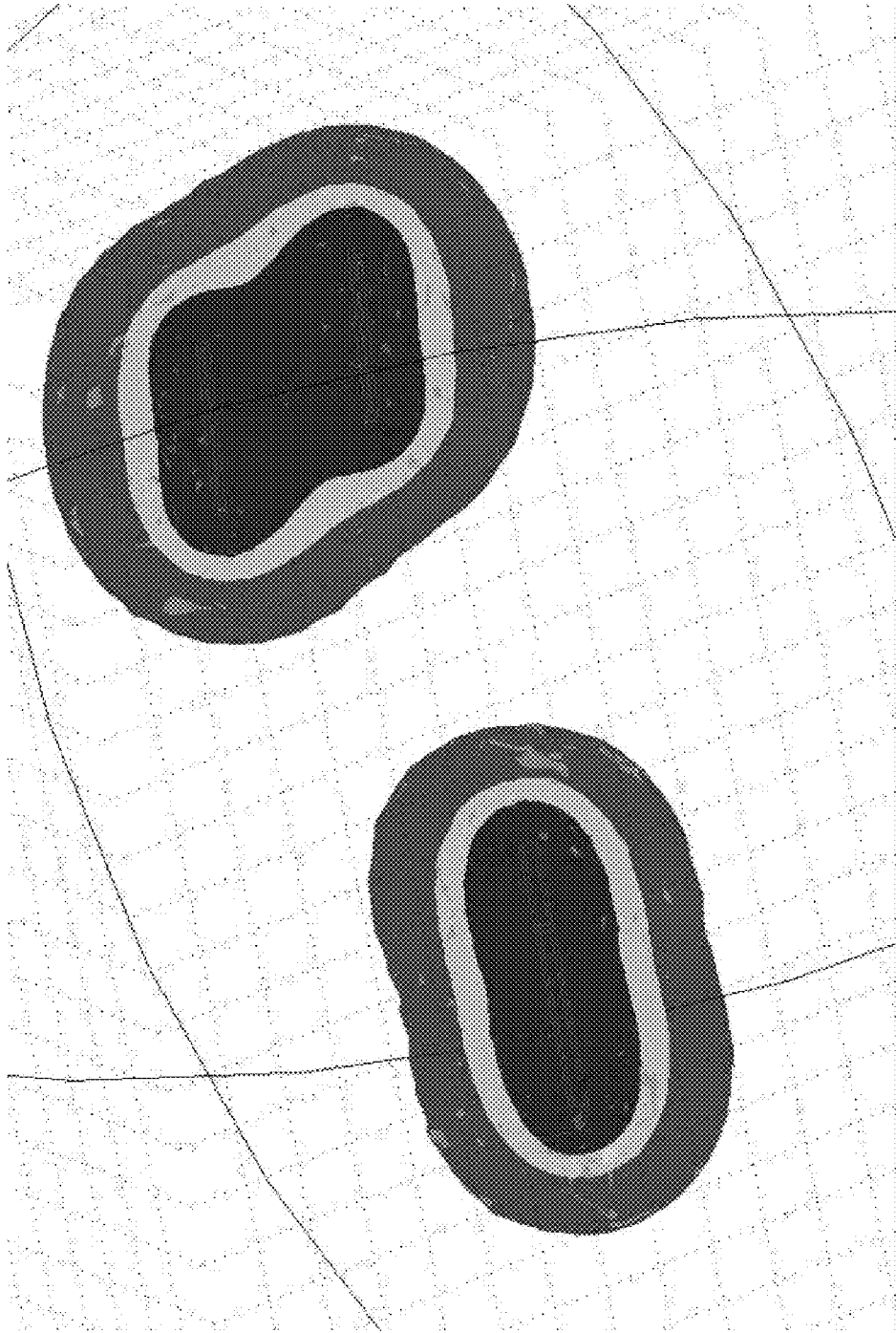FIG. 7

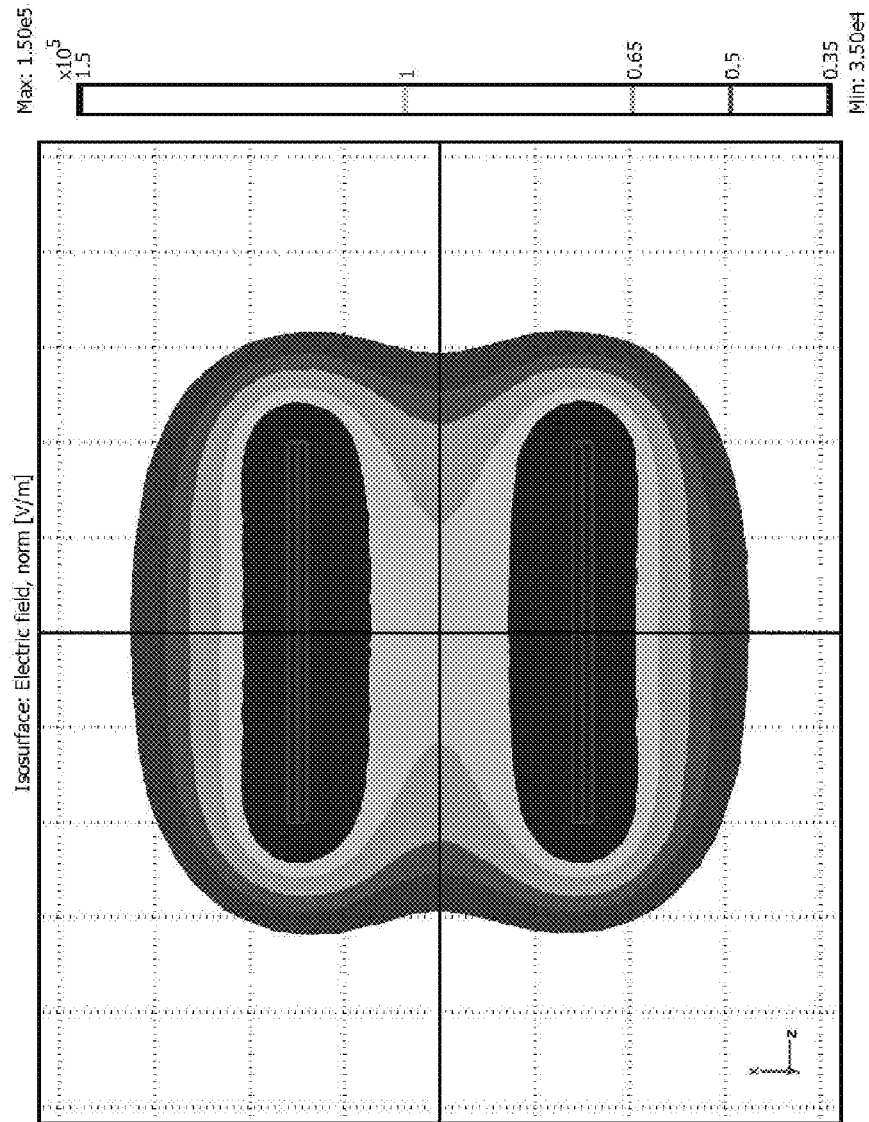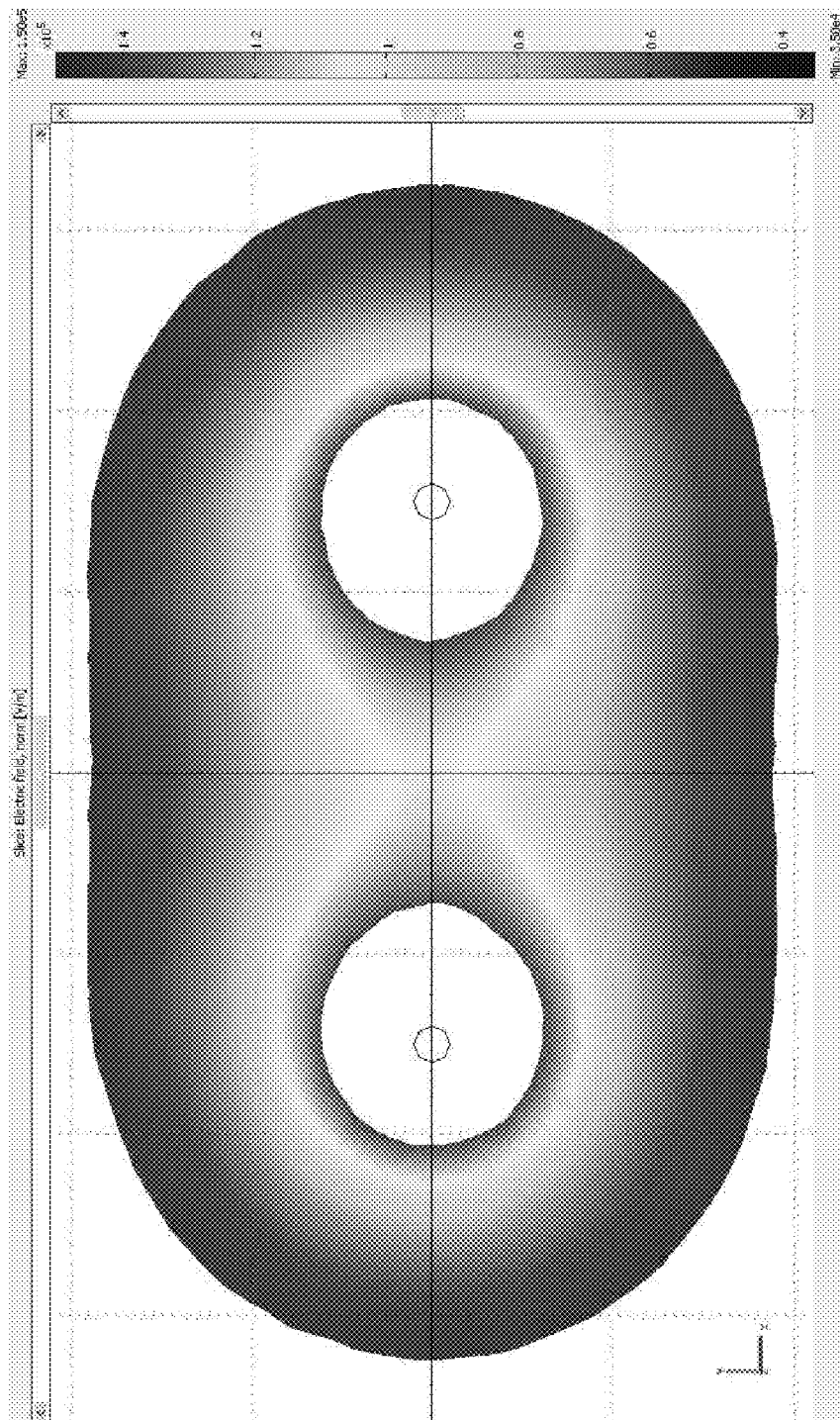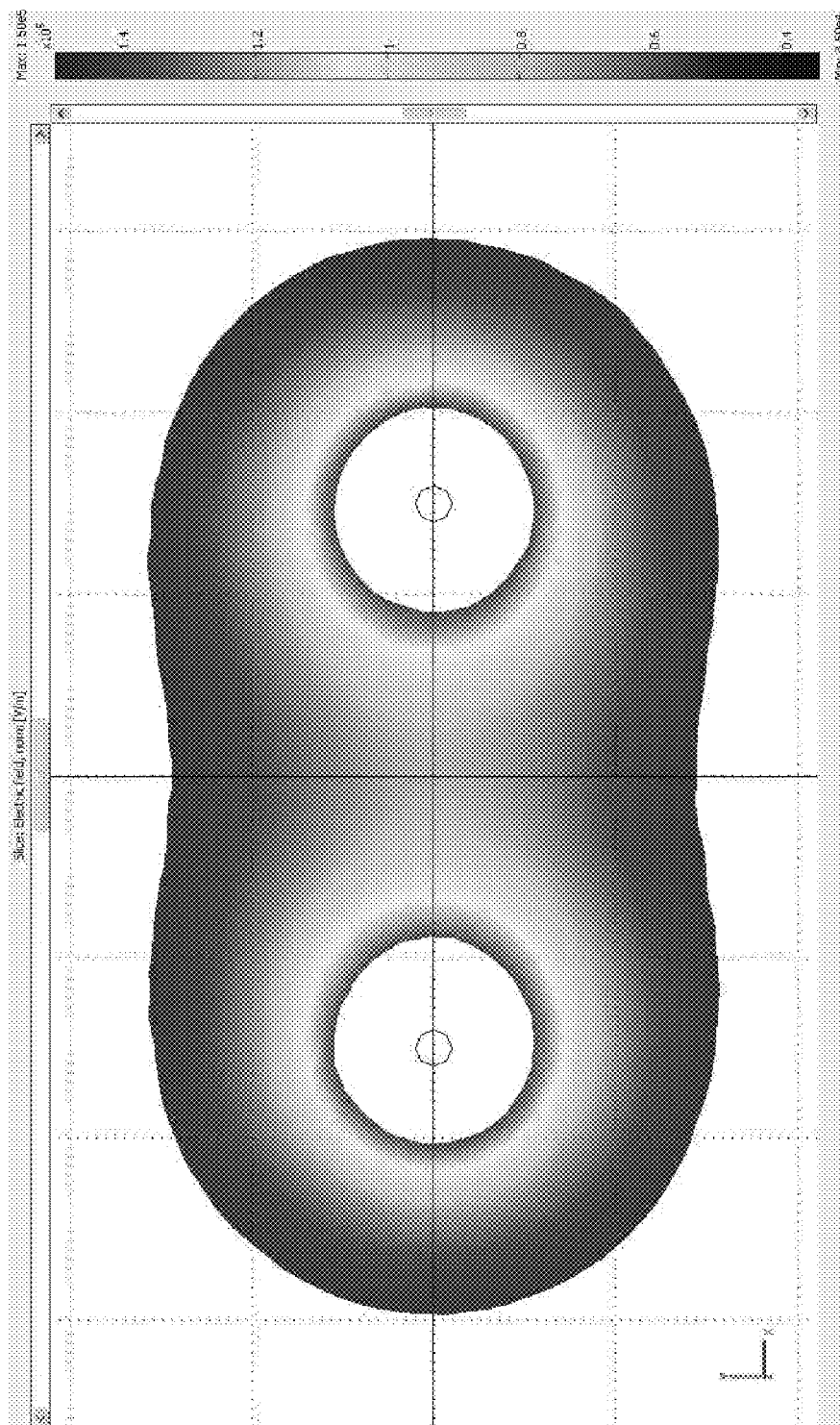Conductivity v. Percent Water of Biological Tissues, Duck, 1990
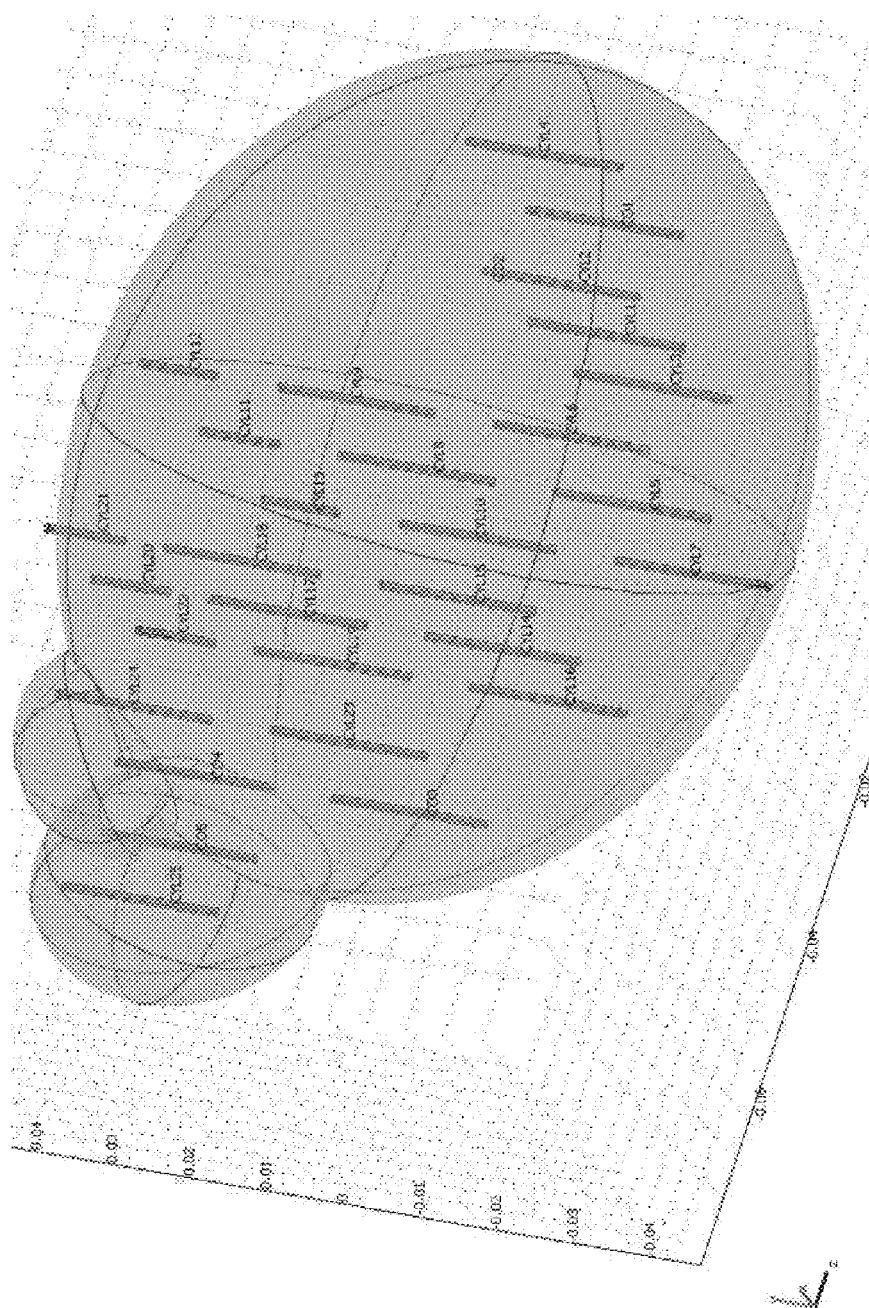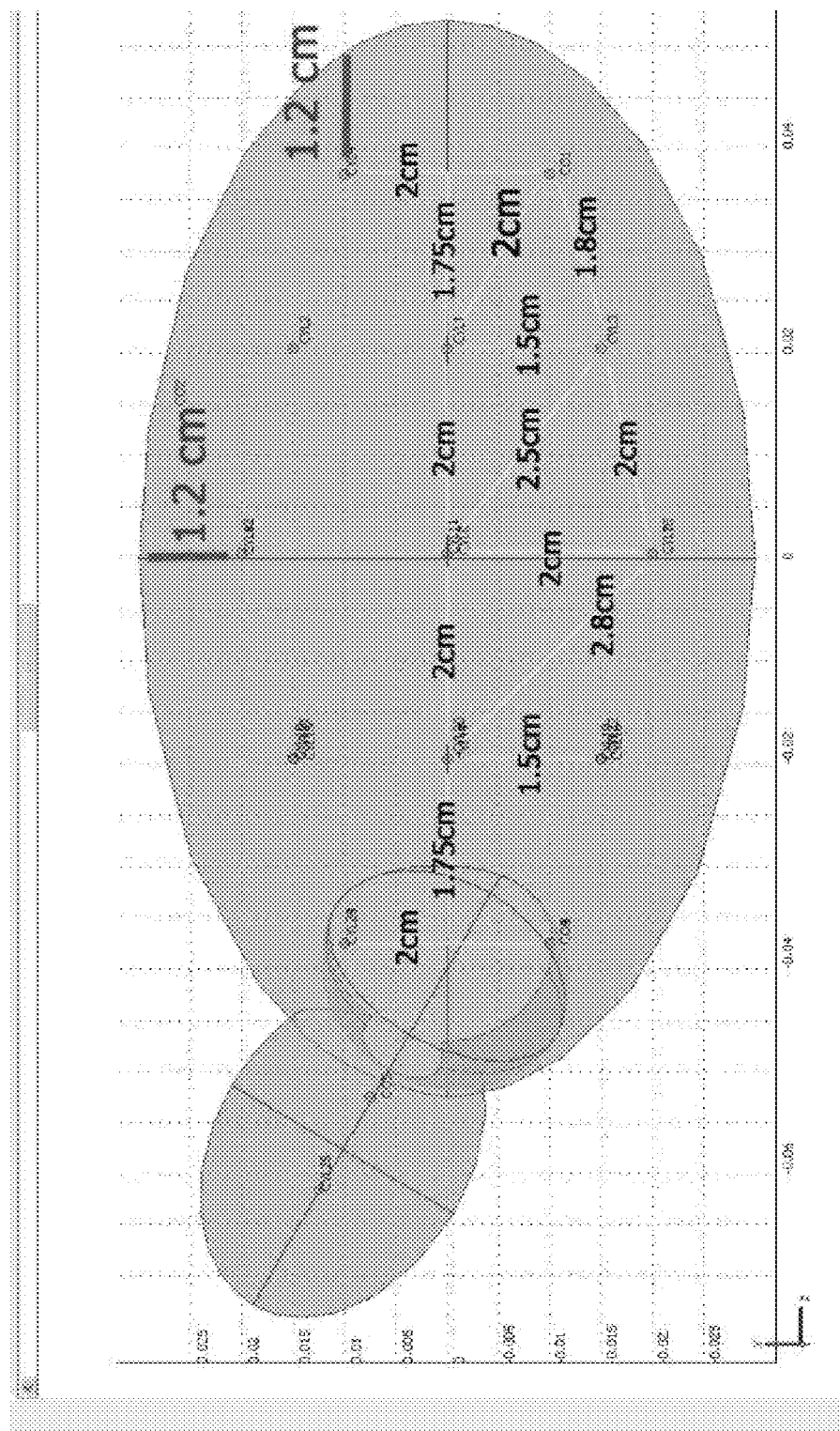
FIG. 8

FIG. 9

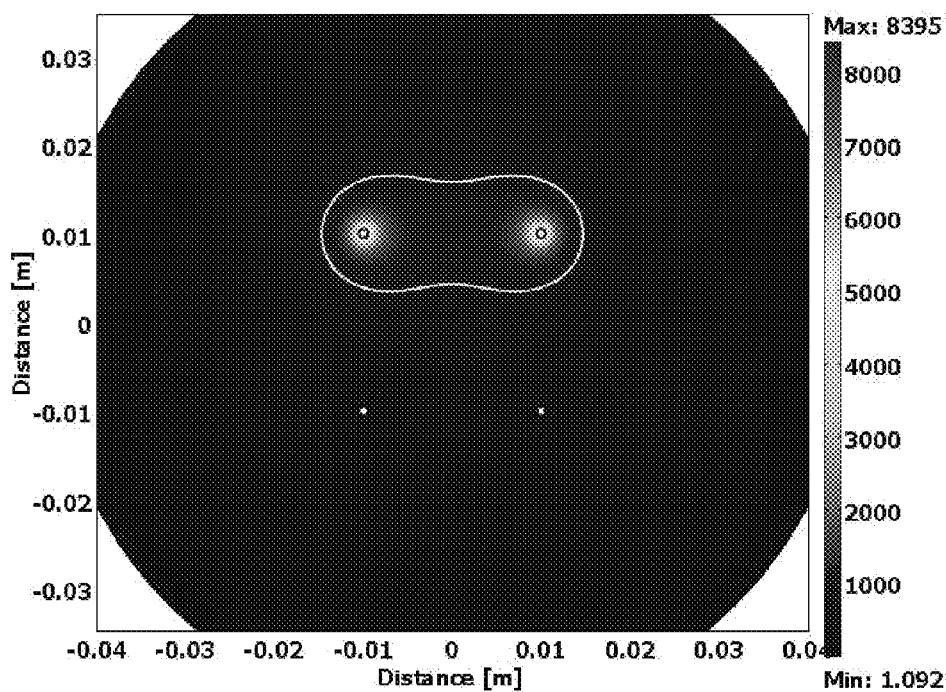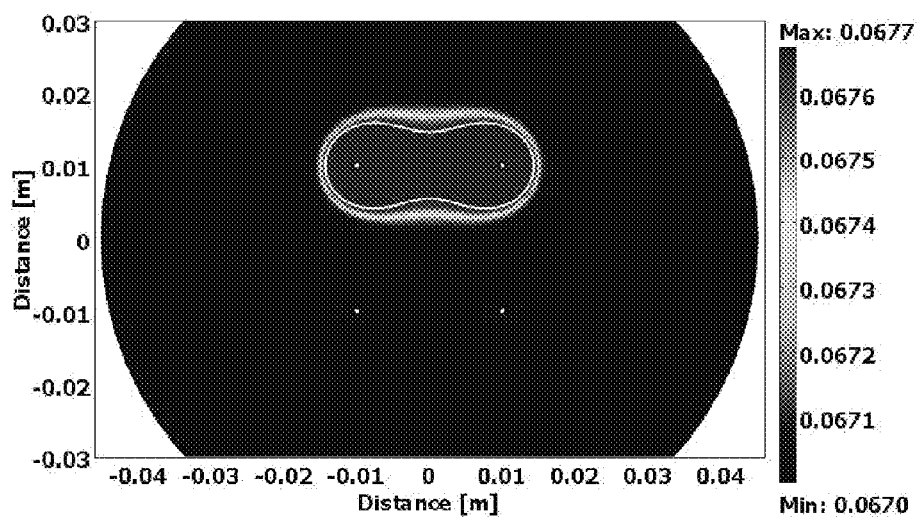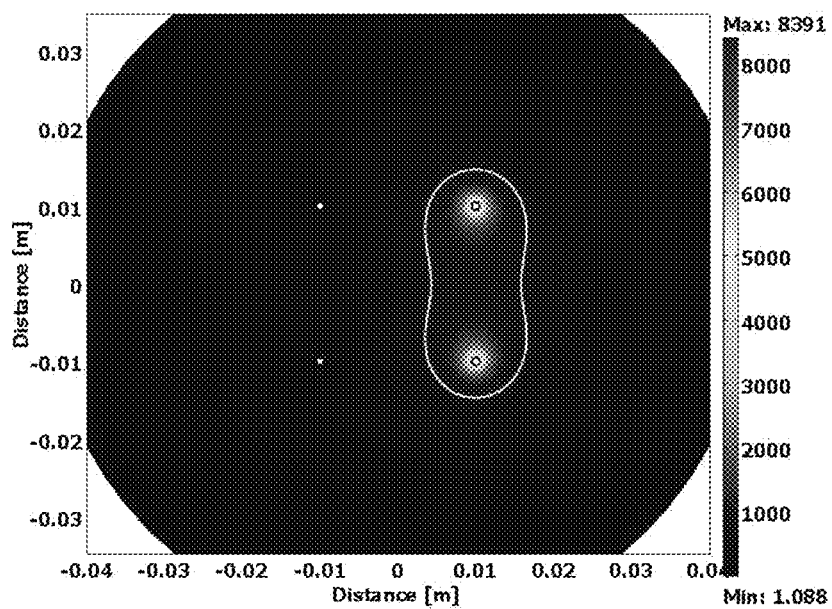FIG. 10

FIG. 11A

FIG. 11B

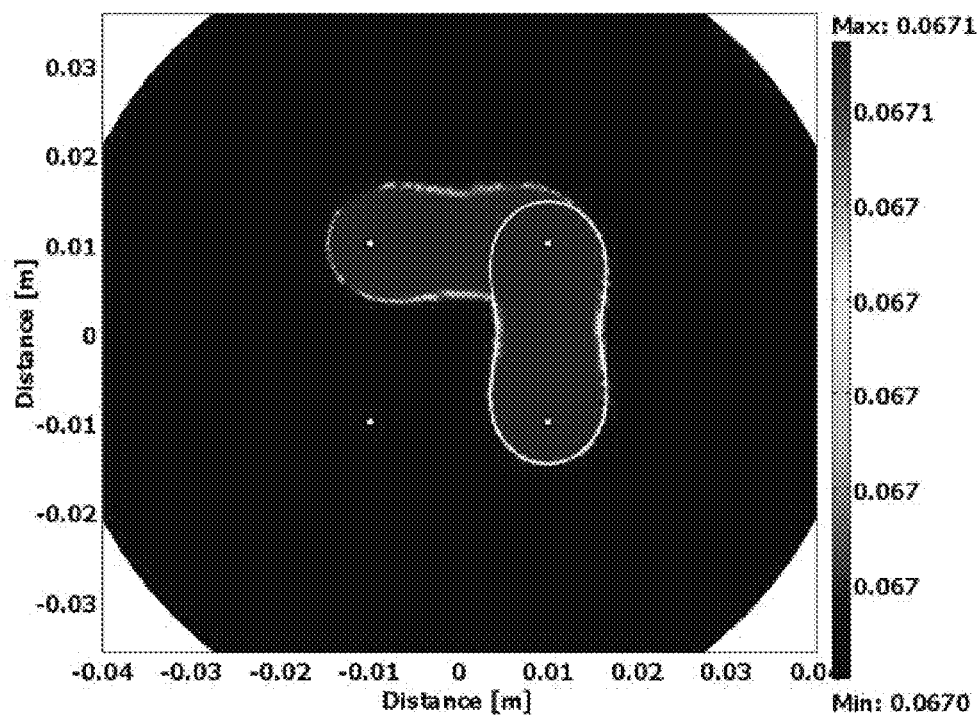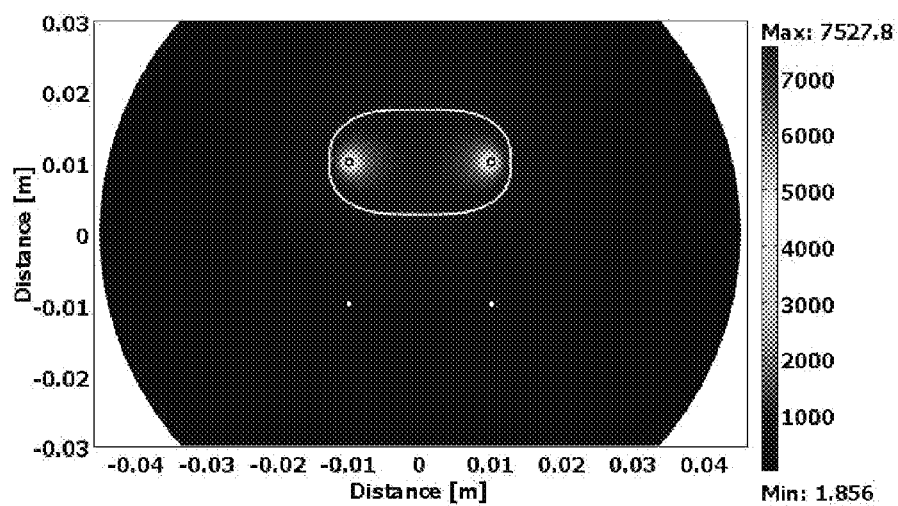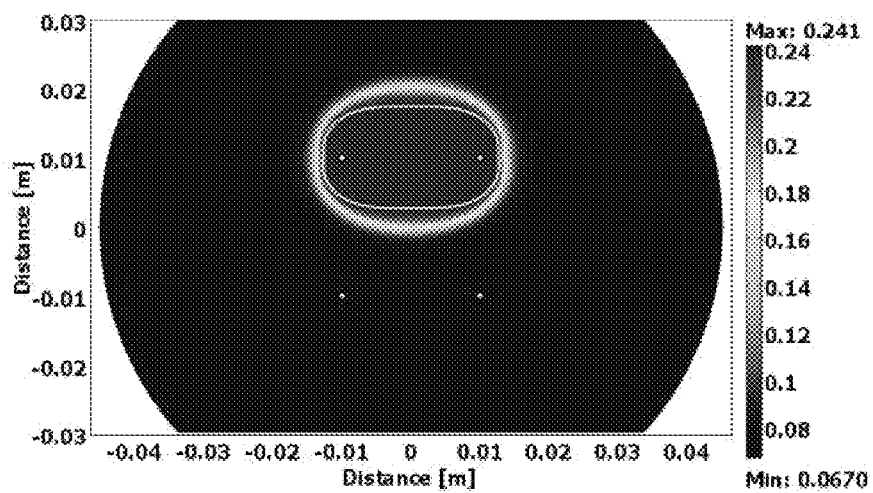FIG. 11C

FIG. 11D

FIG. 12A
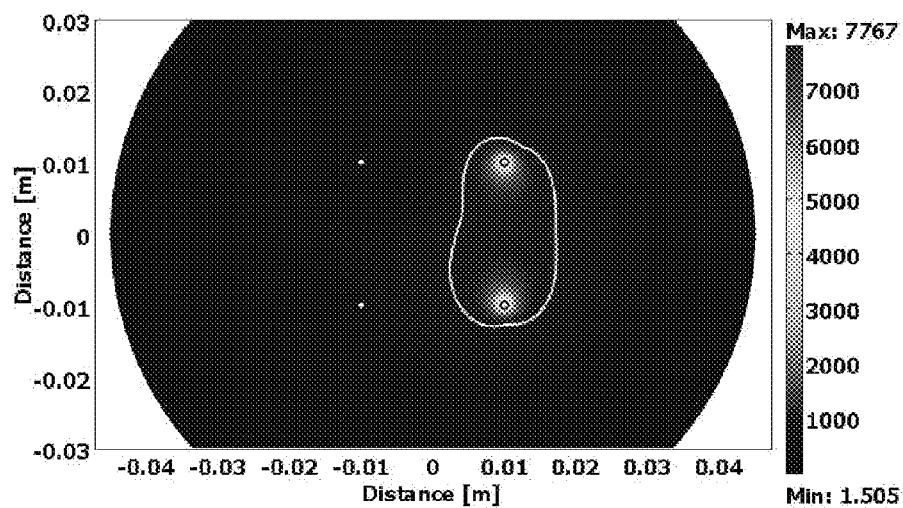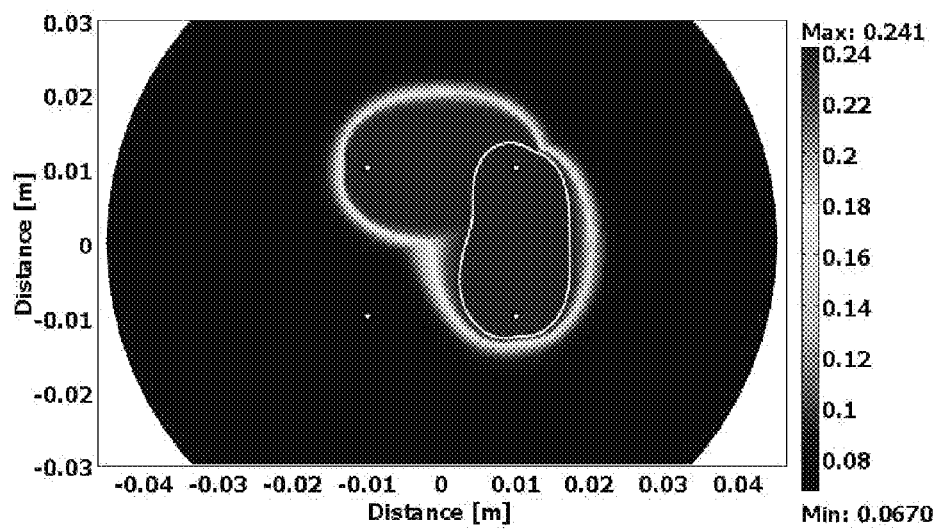
FIG. 12B

FIG. 13A

FIG. 13B
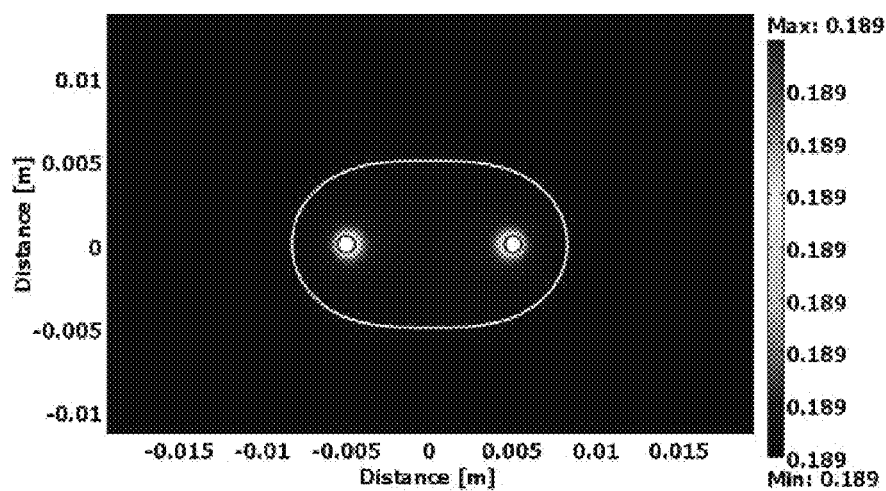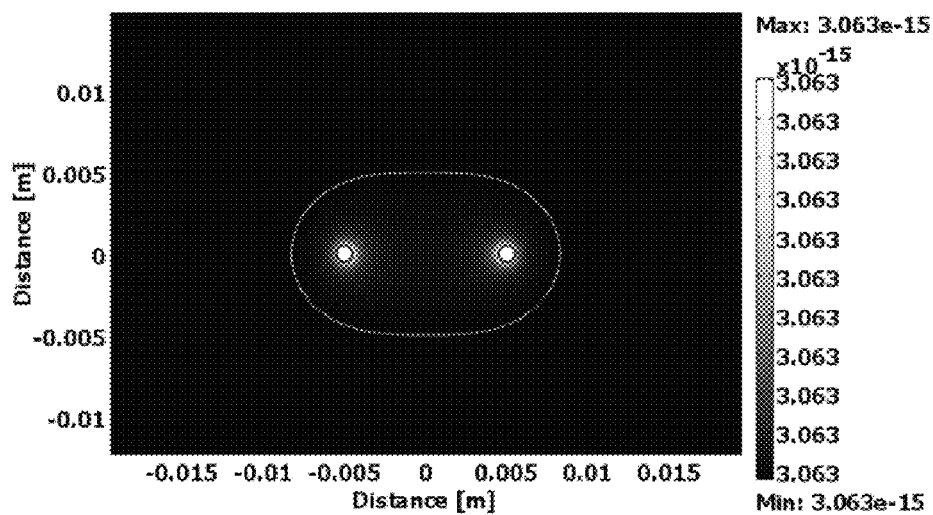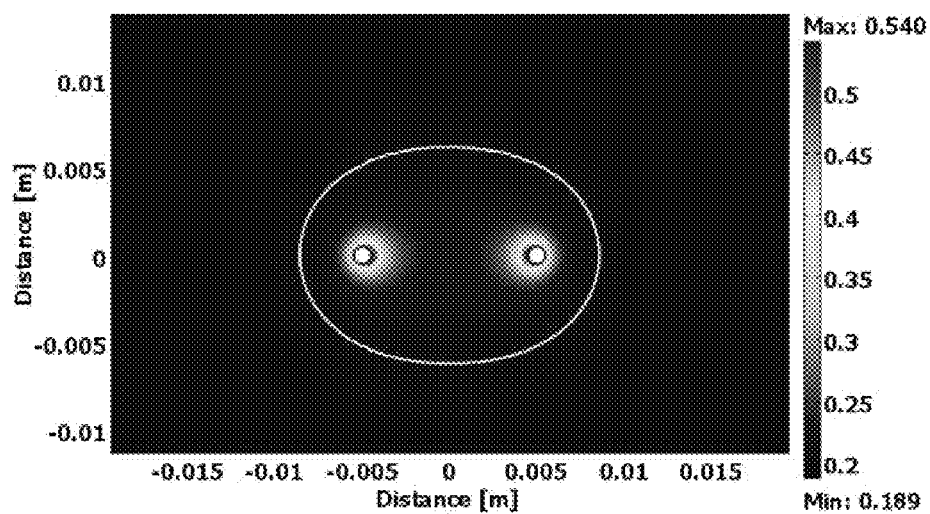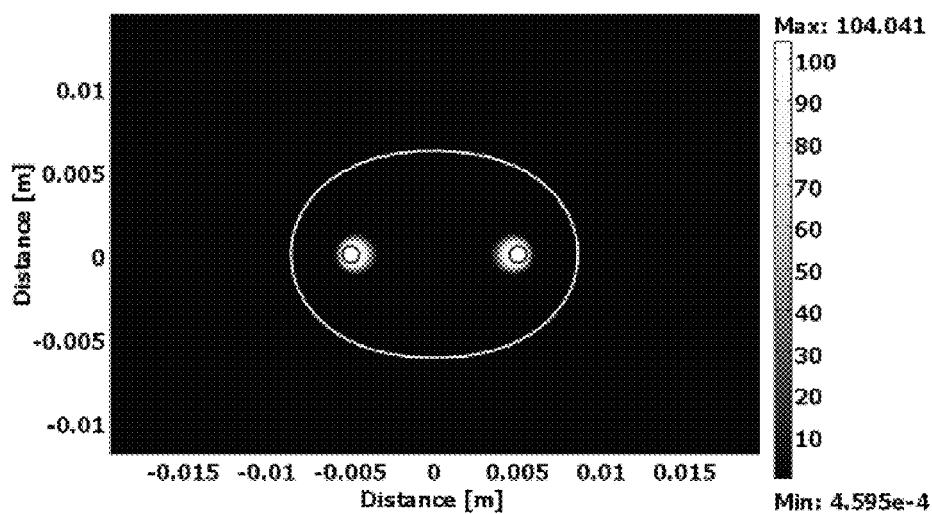
FIG. 14A

FIG. 14B

FIG. 15A
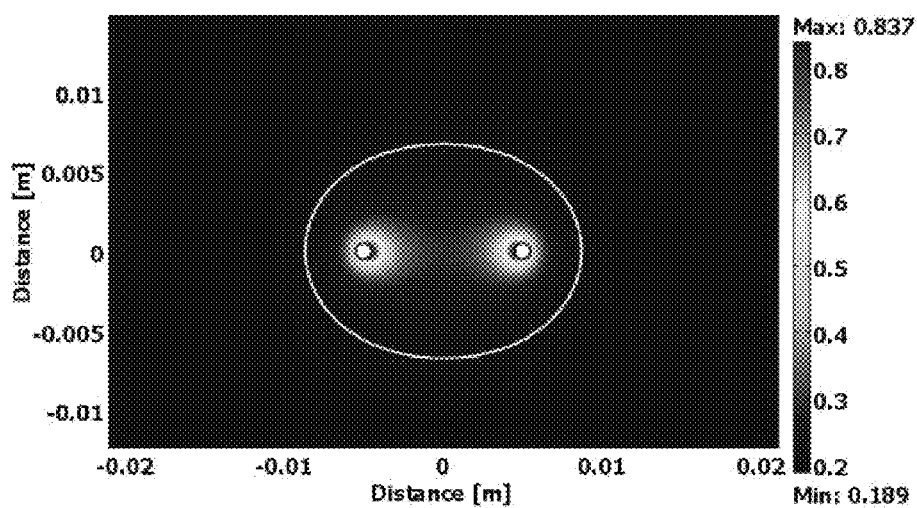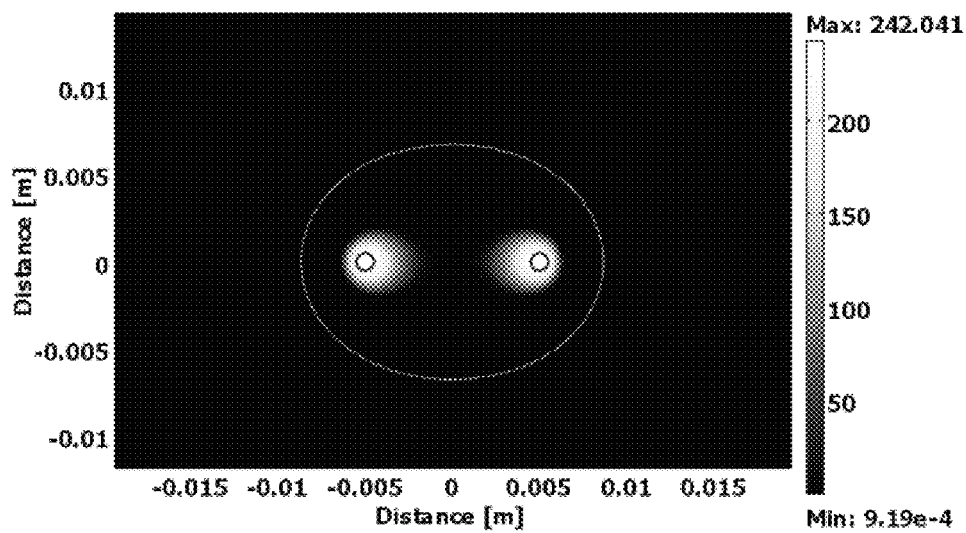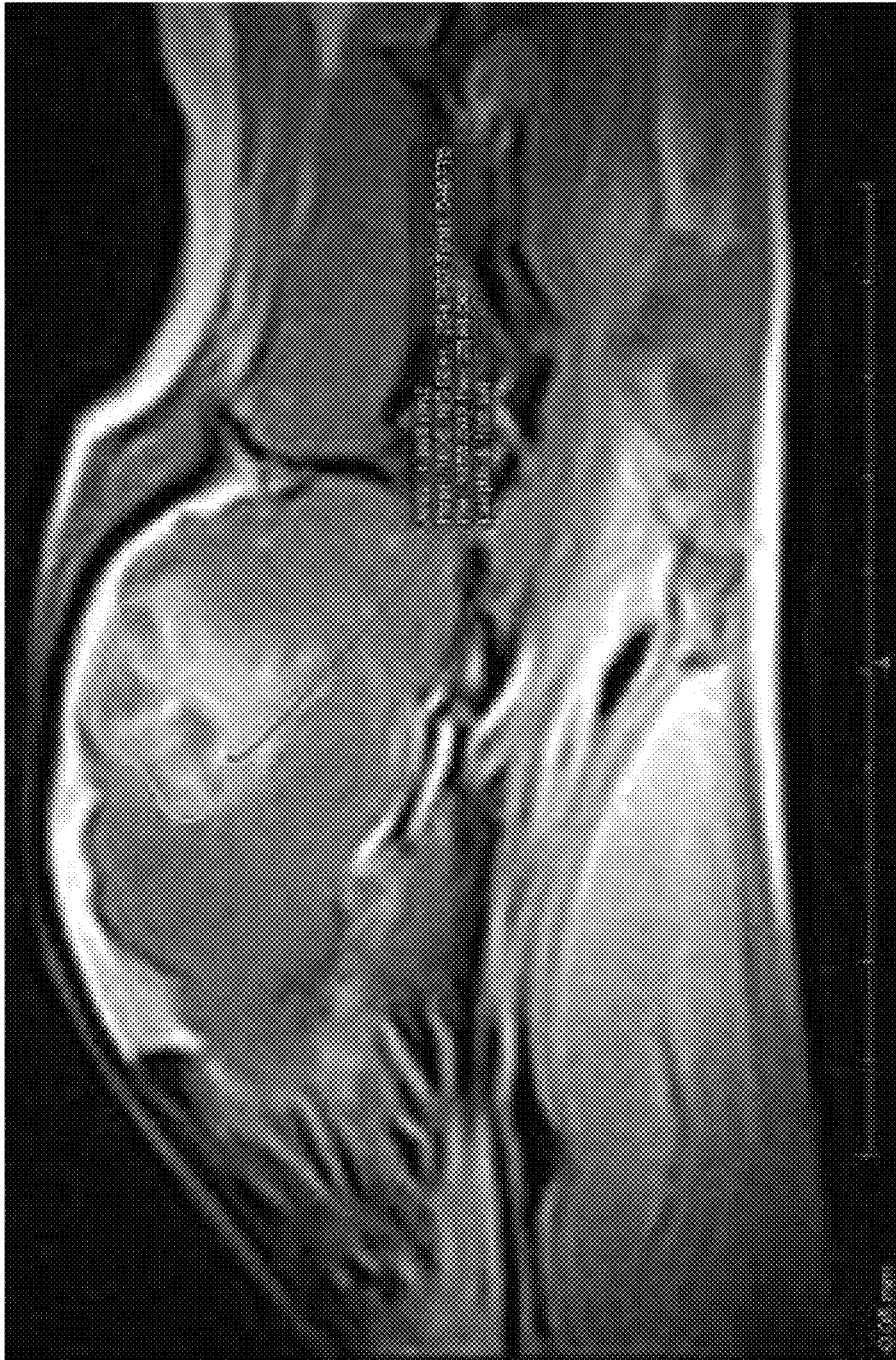

FIG. 15B

FIG. 16A
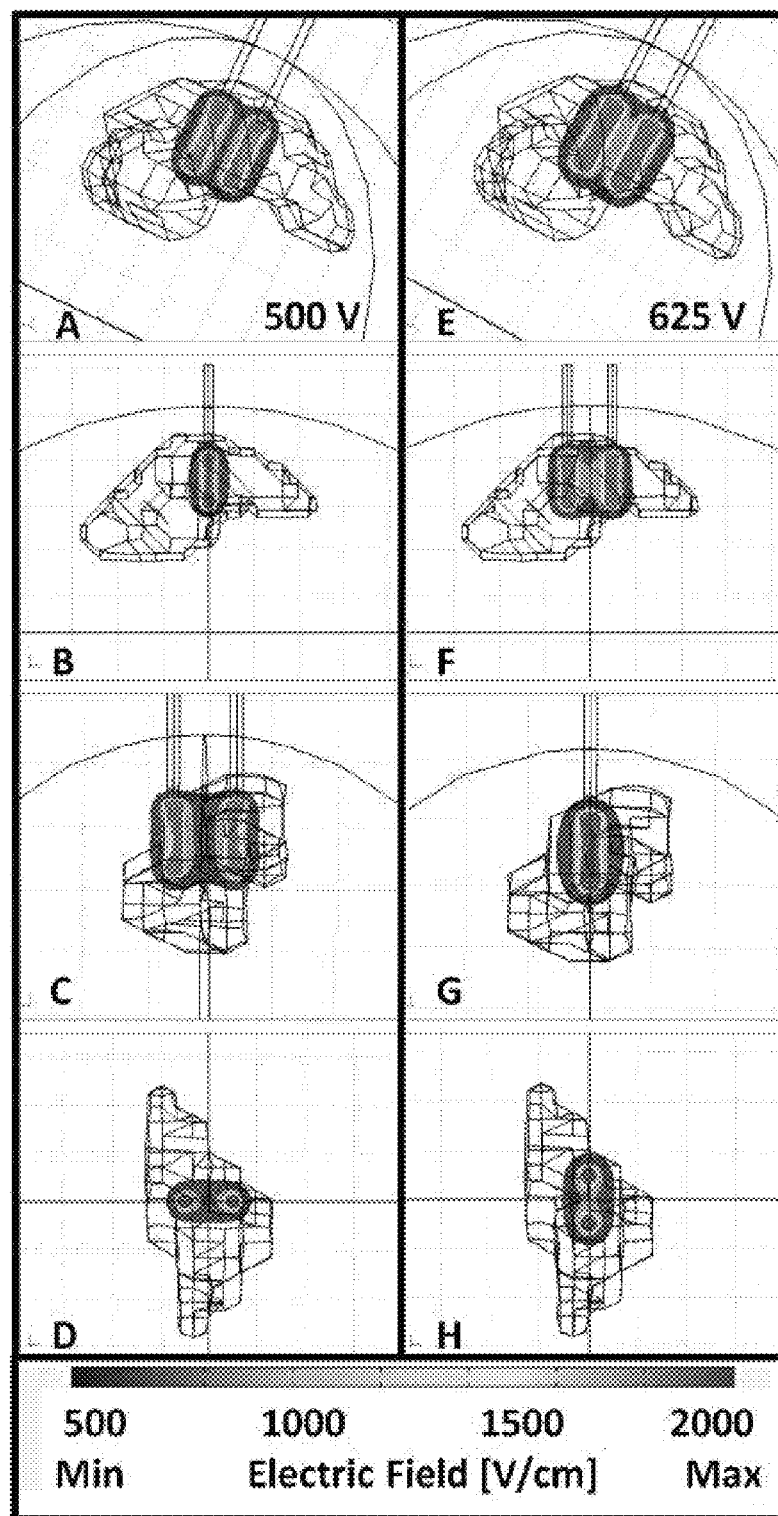

FIG. 16B

FIG. 17A

FIG. 17B

FIG. 18A

FIG. 18B

FIG. 19A

FIG. 19B

FIG. 20A

FIG. 20B

FIGS. 21A-H

FIG. 22

FIG. 23A
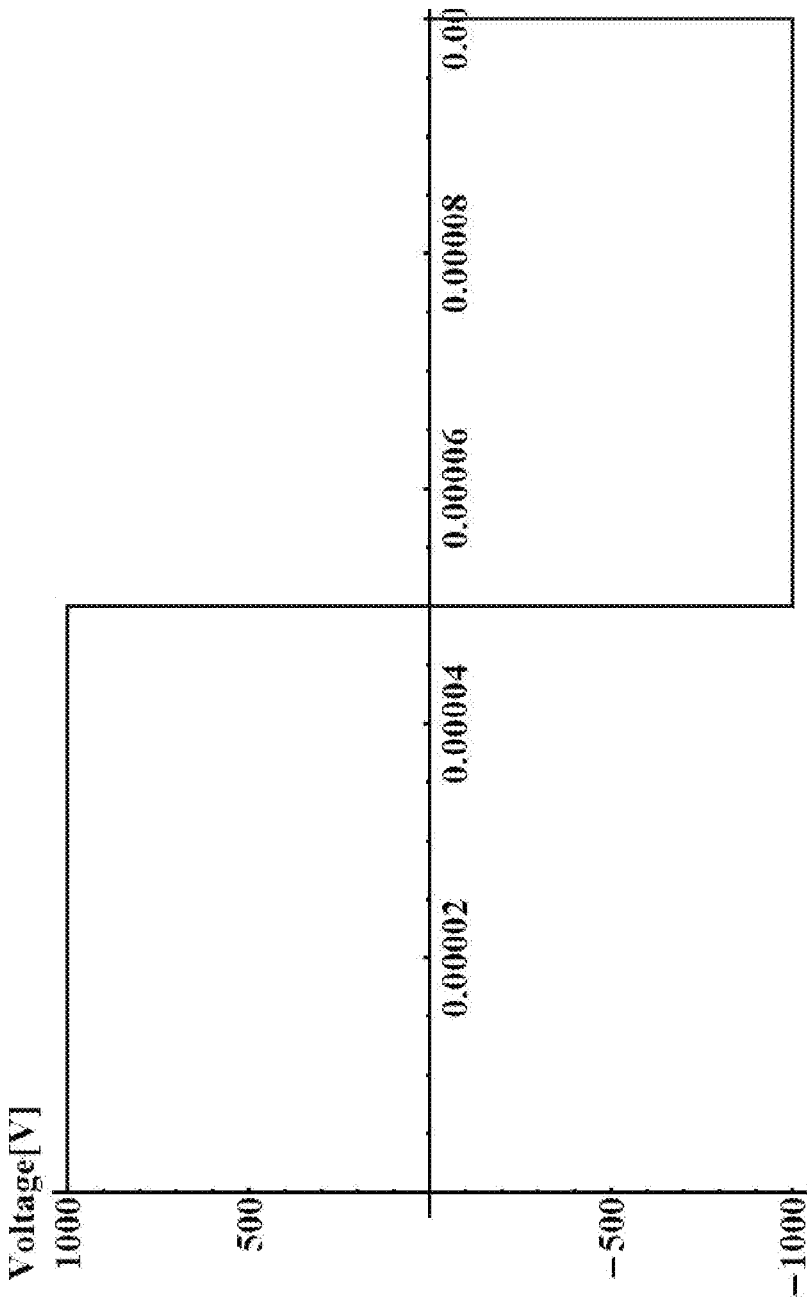
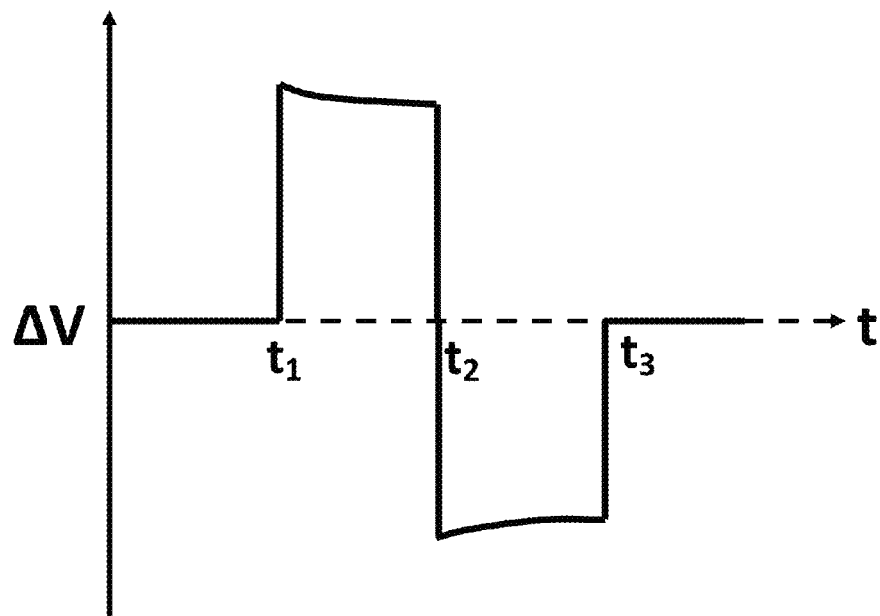(1) (0) (2)   (1) (0) (2)
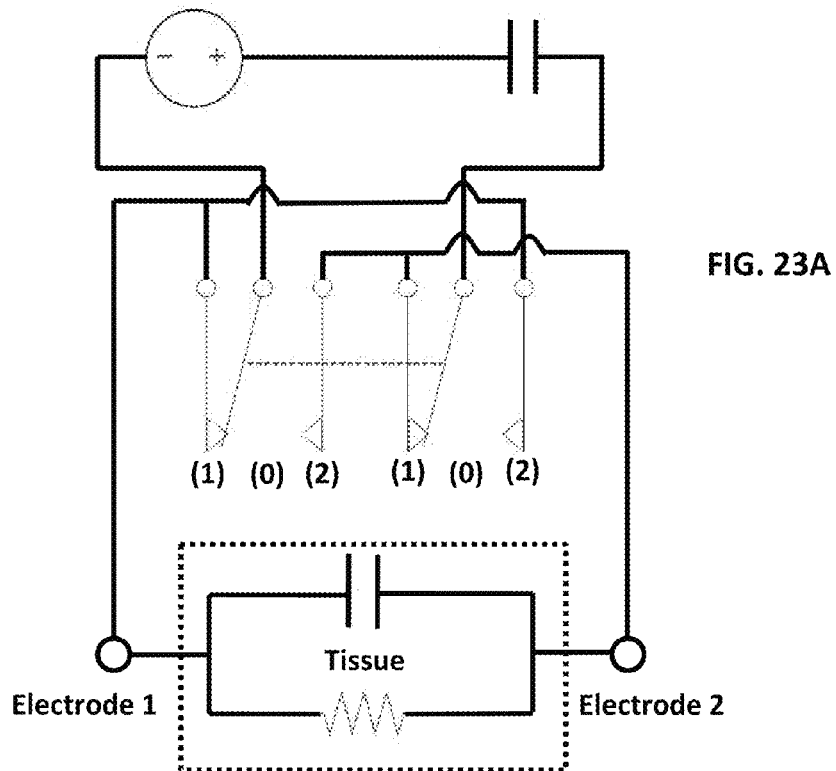
Tissue

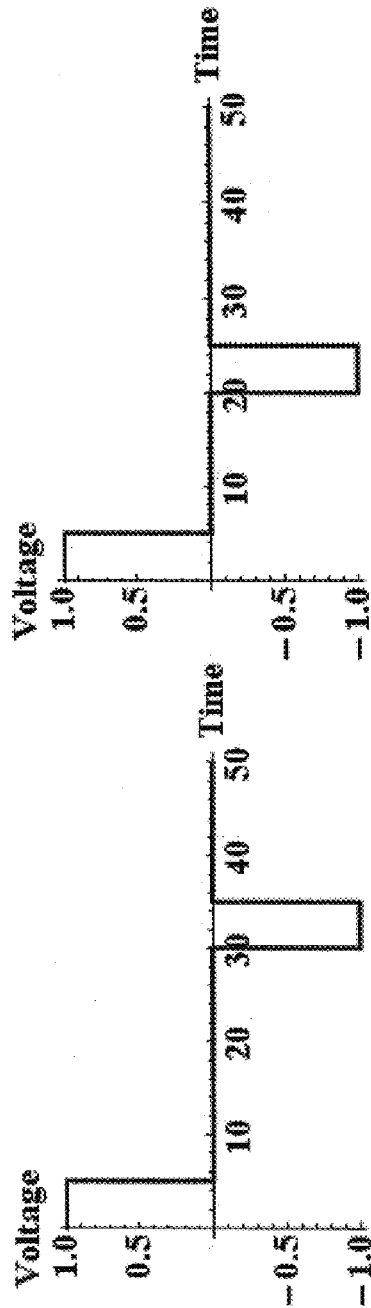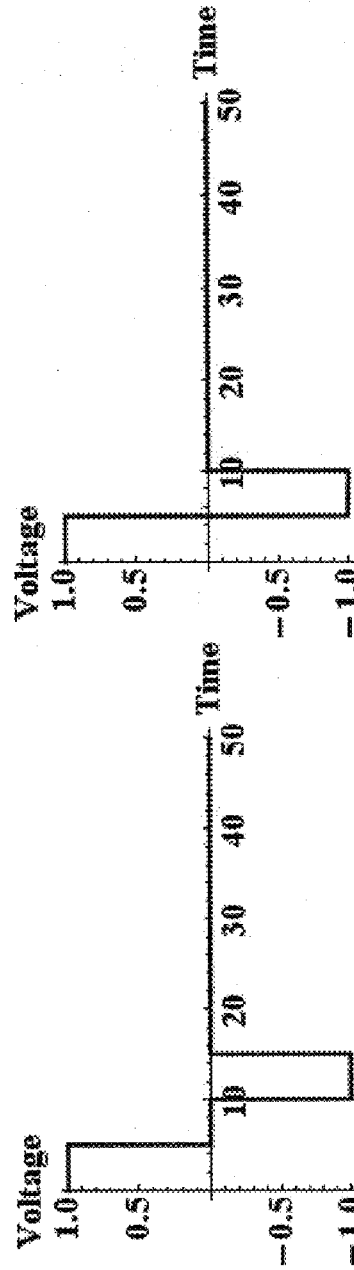Electrode 1   Electrode 2

FIG. 23B

FIG. 24A
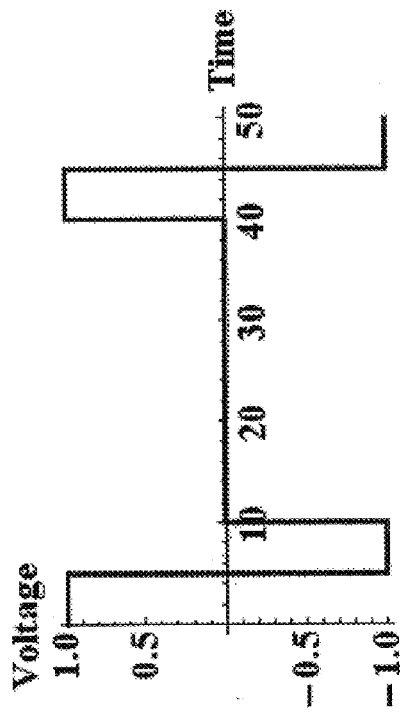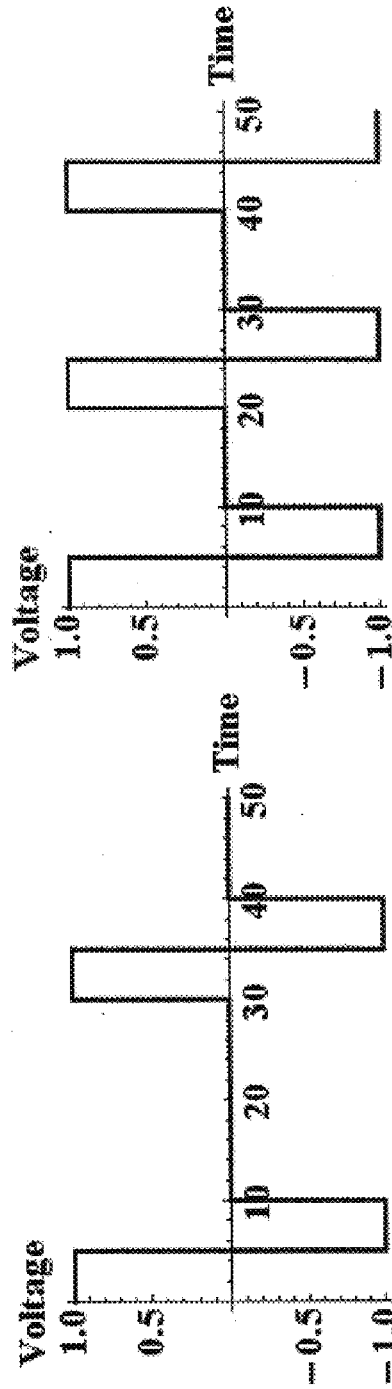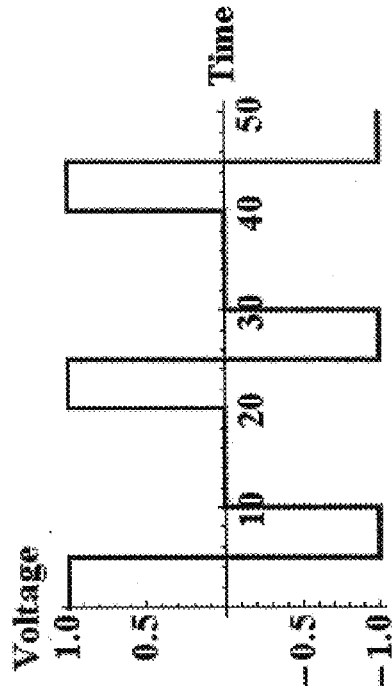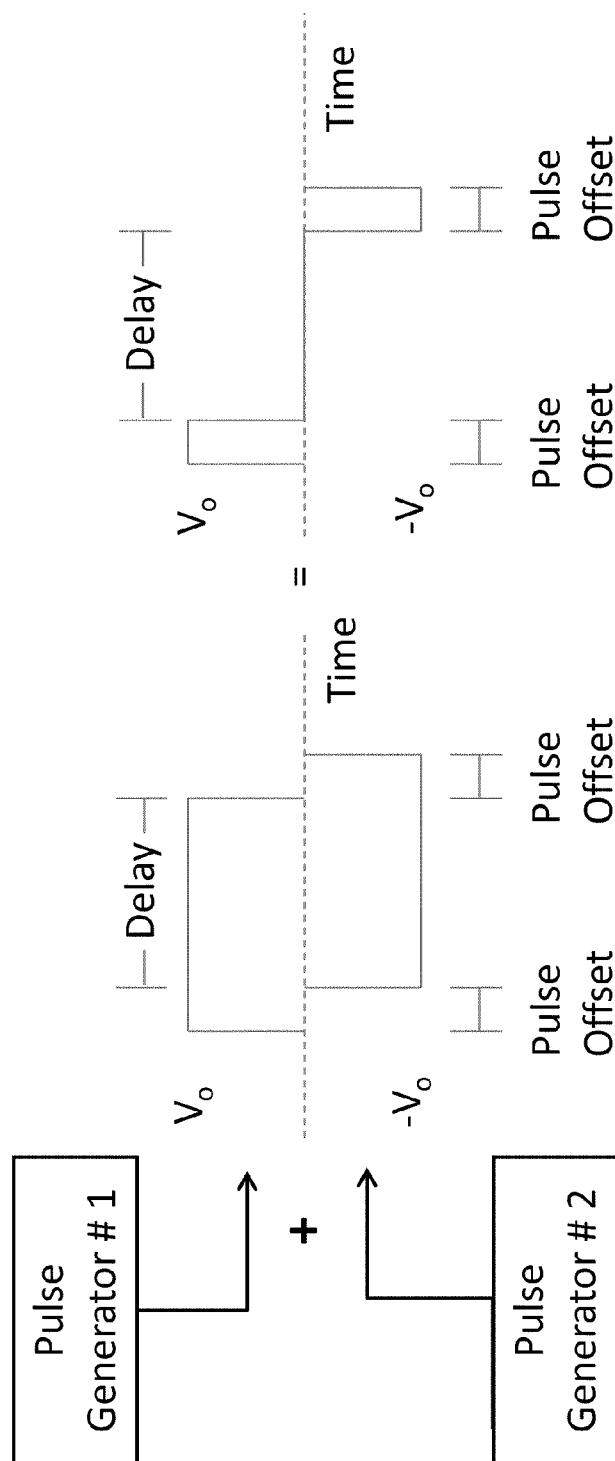
FIG. 24B

FIG. 24C

FIG. 24D

FIG. 24E

FIG. 24F

FIG. 24G

Delay: 100 µs – 1000 s
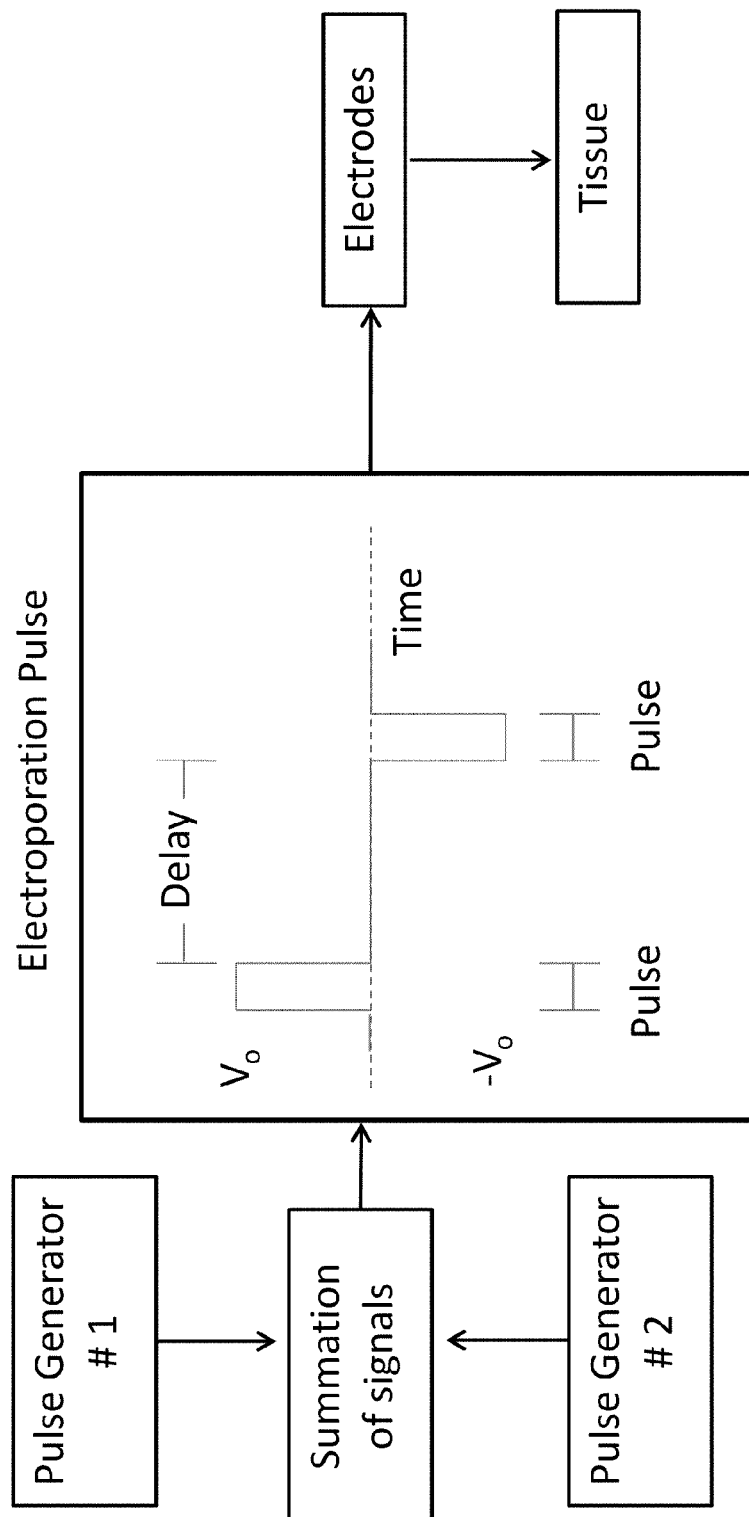Pulse: 10 ns – 10 ms
V_o: Applied Voltage

FIG. 25A

FIG. 25B

Monopolar and/or Bipolar Electroporation Pulses Generated Continuously

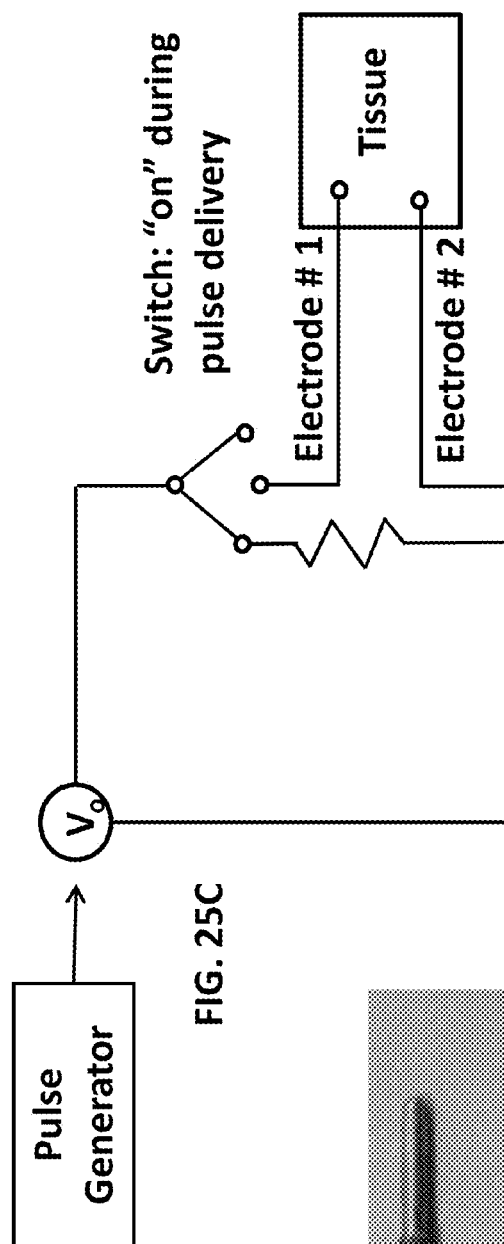Switch: "on" during pulse delivery

FIG. 25C

FIG. 26B

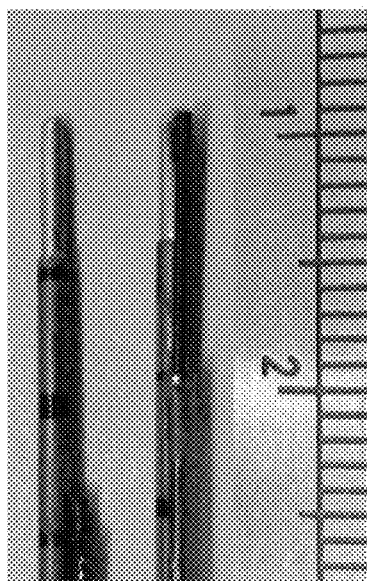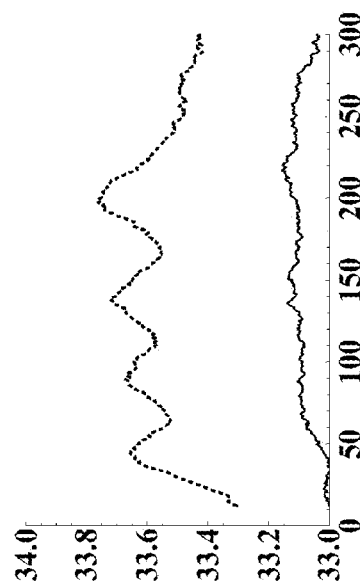FIG. 26A

TREATMENT PLANNING FOR ELECTROPORATION-BASED THERAPIES

CROSS-REFERENCE TO RELATED APPLICATIONS

This application claims priority to and the benefit of the filing date of U.S. Provisional Application No. 61/252,445, filed Oct. 16, 2009; and this application is a Continuation-in-Part (CIP) of U.S. patent application Ser. No. 12/757,901, filed Apr. 9, 2010, which claims priority to U.S. Provisional Application Nos. 61/167,997, filed Apr. 9, 2009, and 61/285, 618, filed Dec. 11, 2009; and this application is a CIP of U.S. patent application Ser. No. 12/609,779, which was filed Oct. 30, 2009 and which claims priority to U.S. Provisional Application No. 61/157,670, filed Mar. 5, 2009, and which is a CIP of U.S. application Ser. No. 12/491,151, filed Jun. 24, 2009, which claims priority to U.S. Provisional Application Nos. 61/075,216, filed Jun. 24, 2008, 61/171,564, filed Apr. 22, 2009, and 61/167,997, filed Apr. 9, 2009, and which is a CIP of U.S. patent application Ser. No. 12/432,295, which was filed Apr. 29, 2009, which claims priority to U.S. Provisional Application No. 61/125,840, filed Apr. 29, 2008, each of which is hereby incorporated by reference herein in its entirety.

BACKGROUND OF THE INVENTION

1. Field of the Invention

The present invention provides systems, methods, and devices for electroporation-based therapies (EBTs). Embodiments provide patient-specific treatment protocols derived by the numerical modeling of 3D reconstructions of target tissue from images taken of the tissue, and optionally accounting for one or more of physical constraints and/or dynamic tissue properties. The present invention further relates to systems, methods, and devices for delivering bipolar electric pulses for irreversible electroporation without damage to tissue typically associated with an EBT-induced excessive charge delivered to the tissue and mitigate electrochemical effects that may distort the treatment region.

2. Description of Related Art

Irreversible electroporation (IRE) and other electroporation-based therapies (EBTs), such as electrogenetransfer or electrochemotherapy, may often be administered in a minimally invasive fashion. There are, however, several considerations that may lead to an increase in the difficulty of administering such treatments. This includes typical applications where deep targeted regions are treated by placing needle or other electrodes deep into the tissue, where one can no longer directly visualize the affected area. There is some evidence that changes in the tissue's permeability, and therefore also its electrical conductivity, allow one to visualize and monitor affected regions in real-time. These changes are most pronounced in homogeneous and image-dense tissues, such as hyperechoic ultrasound tissues, where increased permeability decreases the electroporated echogenicity. However, many tumors and other tissues are far too heterogeneous or exhibit properties that do not allow for simple visualization of the electroporated areas. In addition, these changes for real-time imaging typically only designate electroporated regions, not necessarily those killed for IRE therapies.

In applying EBTs, ensuring adequate coverage of the targeted region (e.g., any mass or lesion or undesirable tissue to be affected, including margins beyond the lesion itself), while sparing healthy tissues is vital to therapeutic success. Due to the limitations inherent in treating deep tissues without

exposing them, it is critical for practitioners to develop and implement treatment protocols capable of achieving their clinical objectives.

Furthermore, typical electrodes and pulsing parameters (number of pulses, pulse polarity, pulse length, repetition rate, pulse shape, applied voltage, electrode geometry and orientation, etc.) will have a large impact on the affected areas. Typical therapeutic geometries dictated by current electrode setups will be ellipsoidal in general shape. However, many tumors do not distinctly fit the shapes created by a single setup of an electrode. Therefore, successful implementation of EBTs typically requires a complex array of electrodes and pulse parameters arranged in a specific manner to ensure complete treatment of the targeted area while minimizing effects to healthy tissue and sparing vital structures. Such predictions of superimposing treatment regions for complex protocols can be cumbersome. Therefore, treatment planning techniques that aid or allow a practitioner to develop general treatment protocols for most clinical tumors are typically used to effectively capitalize on the great therapeutic potential for IRE and other EBTs.

Current treatment planning techniques from systems such as the NanoKnife® utilize interpolations and analytical techniques to aid practitioner treatment region predictions. The interpolation techniques provide the physician with diagrams of 3D numerical model solution predicted treatment areas from very specific settings, including an exact number of pulses, pulse length, voltage, and electrode setup (e.g., separation distance, exposure length, and diameter) with dimensions provided for the treatment areas in 2 planes and the general shape. The predicted treatment dimensions are taken from the experimental results of applying that specific set of conditions in experimental subjects, typically in healthy, homogeneous environments. It is from this diagram of expected region, that the physician would set up their electrodes the same way and use the same pulses and arrange multiple applications to the point where they anticipate they will have treated the entire volume.

There is room, however, for improvement in such systems. If the targeted volume is smaller than the dimensions in the diagram, the practitioner has no information about how much to change the physical setup (exposure length, separation distance, etc.), or pulse parameters (voltage, number of pulses, etc.) in order to prevent damaging the surrounding tissue. In another example, if the shape does not fit that of the diagram, the practitioner will not be able to adjust the protocol to minimize damage beyond the targeted margin while still treating the targeted area.

In another solution to facilitating practitioner treatment planning, software is provided that uses a lookup table of treatment dimensions or uses a calibrated analytical solution to mimic the shape of numerical simulations. The lookup table may be taken from a large compilation of simulations run at varying physical and pulse parameters, where dimensions of interest for predicted treatment regions are taken based on a calibrated electric field threshold found to represent the affected margin of interest observed in experiments on healthy tissue (IRE, reversible electroporation, no electroporation, thermal damage).

Although the lookup table would allow a practitioner to manipulate the above variables and receive real-time feedback on predicted dimensions, the geometry of the affected region is often more complex than can be summarized with a few dimensions. Therefore, analytical solutions for the shape of the electric field distribution have been developed and are the current state-of-the-art on the NanoKnife® system. These solutions are able to mimic the shape of the electric field

distribution from typical numerical simulations. The value of electric field contour is then matched to that seen from the numerical solution so that they both respond to their physical and pulse conditions in approximately the same manner. A calibration can then be used to adjust the size, and therefore various electric field thresholds (IRE, reversible, no electroporation, thermal damage) depicted to provide predicted affected regions. The practitioner may then adjust the variables such as voltage and separation distance (currently the only two that account for changes in predicted margins in the NanoKnife® embodiment), and see how the predicted affected margins vary in real-time. This provides the practitioner a much better method to find and place an appropriate electrode array with variable voltages to treat the entire region. There is also an optimization autoset probes function that places the probes and sets the voltage based on the number of probes selected and three dimensions input for the targeted region (assuming it to be a perfect ellipsoid).

The current state-of-the-art provides a very basic, fundamental explanation to practitioners about predicted treatment regions. Application of the current techniques in real-life clinical and experimental scenarios in which EBTs will typically be used provides to the practitioner helpful but inflexible tools.

For example, the analytical embodiment is a simple cross-sectional view of predicted margins at the center of the electrodes. This means that it cannot account for the falloff of electric field distribution (and therefore affected margins) at the tips of the electrodes. Although use of this approach can mimic the shape and size of these regions in 2D, it is not possible to accurately depict 3D scenario shapes in detail. Further, the lookup table cannot easily provide an accurate 3D shape, nor can the analytical solution be adapted.

True electroporation applications will increase the conductivity of the affected regions, which will in turn change the size and shape of the electric field distribution. A comparison of the electric field distribution (A,C) and conductivity map (B,D) of two identical numerical models without (A,B) and with (C,D) changing conductivity is shown in FIGS. 1A-D. From these figures, one can see how the conductivity increases from 0.1 S/m (the baseline level for the entire tissue domain, constant in part B) up to 0.155 S/m, an increase of 55%, for regions experiencing predicted IRE (deep red in part D), with regions experiencing varying extents of predicted reversible electroporation filling in between this (cyan through bright red). This change in conductivity in response to electroporation effects results in an altered electric field distribution, which may be seen in part C, where the distribution is larger, especially at the region between the electrodes. Changes in conductivity have been observed to reach several times higher than the baseline conductivity in the literature. These changes can be simulated in numerical solutions, and the general size changes can be accounted for with some accuracy in the analytical solutions by recalibrating them, but their shape is fixed, and cannot accurately reflect the predicted affected region's shape when considering changing conductivity.

Tumors will often have different electrical and physical properties than their neighboring tissues or even from their native tissues of origin (e.g., cancerous astrocytes which may not behave the same as normal ones). In addition, surrounding tissues of different tissue types will also have different properties from each other (bone, muscle, fat, blood). These differences in electrical properties will alter the electric field distribution for a given application of EBTs. Because the electric field to which the tissue is exposed is the primary determinant in the effect on the cell, these changes will

change the shape and size of the affected regions. Numerical simulations are capable of modeling the electric field distribution in such heterogeneous systems. However, the rigid analytical solutions cannot be adjusted to account for such differences, and therefore could not as accurately predict affected regions for the different environments in clinical cases. The analytical solution, e.g., could not predict the differences between a tumor situated adjacent to the skull, the quadriceps muscle, or the heart. Although lookup tables could theoretically be developed for the dimensions of the affected regions in a number of environments, the great variability between the anatomy of each patient, each specific tumor, and each exact tumor location relative to its environment is impractical and futile.

FIGS. 2A-J demonstrate the effect of heterogeneous systems on electric field distribution. These figures show the electric field and temperature distribution for a three-dimensional numerical model. More particularly, FIG. 2J shows the model setup, where two needle electrodes (1 mm in diameter) are placed within the outer borders of a targeted region of tissue, surrounded by a peripheral region. The red and black regions on the electrodes represent the energized surfaces, where 4200 V was applied to one electrode and the other was set to ground. The thermal properties were set to represent a targeted region of a tumor within fat. The electrical conductivity for the targeted (σt) and peripheral (σp) tissues was manipulated between 0.025 and 0.25 S/m to establish conductivity ratios (σt/σp; relative conductivities of the targeted/peripheral region) of 0.1, 1, and 10. FIGS. 2A-I show the numerical model outputs for conductivity ratios (σt/σp) of 0.1 (A,D,G), 1 (B,E,H), and 10 (C,F,I) showing electric field (A-F) during the pulse and temperature (G-I) distributions 1 second after the first pulse. The higher conductivity ratios show progressively more area treated by IRE with less thermal effects. Targeted tissue boundary may be seen as the solid black line. Observing the electric field distribution at the boundary shows that the shape is also changing (not just size) as a result of the heterogeneous environment. Existing treatment planning systems are not capable of accounting for such dynamic tissue properties in real time.

The current embodiment of the treatment planning software still leaves it up to the practitioner to select a desired number of probes, but provides no simple method of showing how the optimized distributions will be shaped if the user wants to directly compare using different numbers of probes for a given lesion. The current system therefore also does not select the optimal number of probes for the user, a question that may be difficult to answer for more complex electrode geometries.

Temperature changes associated with Joule-type resistive heating of the tissue will also affect local regions conductivity based on its temperature (typically increases by approximately 3%/° C.). This will also change the size and shape of the electric field distribution based on the parameters used; including the number of pulses, pulse length, and repetition rate for an entire protocol (more pulses of longer length with higher repetition rates will all increase the thermally-associated conductivity changes, increasing this variation). Because the current treatment planning tools are based on simulations from the electric field distribution of a single application of a pulse, these dynamic conductivity behaviors also cannot be taken into account. Something that does would have to be able to simulate the changes that occur as a result of thermal effects on conductivity.

The current state of the art does allow the practitioner to describe the size/shape of the lesion in very basic dimensional terms (length, width, depth). This shape is then superimposed

to scale with the predicted treatment regions, allowing a practitioner to ensure appropriate distribution and coverage. Although we have already pointed out the insufficiencies in handling this third dimension, it should also be pointed out that the basic ellipsoidal shape assumed by this system is wholly inadequate at describing the complex, often irregular, asymmetric geometries that tumors may take in clinical settings. The practitioner is thus left currently with assessing treatment protocol adequacy in 2D terms.

What is needed is a technique and system (or a series of independent systems) that allows a practitioner to accurately plan and implement in real time patient-specific treatment protocols which are capable of accounting for dynamic tissue properties and which can be used with accuracy and reliability in the clinical or experimental setting for EBTs.

SUMMARY OF THE INVENTION

The numerous limitations inherent in the planning system described above provide great incentive for a new, better system capable of accounting for one or more of these issues. If EBTs are to be seen as an accurate, reliable therapeutic method, then treatment planning methods and packages should be developed that can more accurately predict treatment outcomes with these considerations taken into account in a patient-to-patient basis.

The primary limitation to the above-mentioned, state-of-the-art treatment planning system is its need to provide treatment predictions in real-time, where a practitioner would be capable of changing the voltage or geometry parameters of a treatment protocol and immediately see how that impacts the entire treatment region. However, as more complex tumor shapes, sizes, and environments are encountered, real-time evaluation of superimposed treatment regions is cumbersome at best and inadequate to develop reliable therapies. Therefore, a more advanced system that allows treatment planning in advance of applying the therapy would be ideal to handling these detailed procedures. This allows for the adaptation of numerical solutions to provide treatment regions.

Accordingly, embodiments of the invention provide treatment planning systems, methods, and devices for determining a patient-specific electroporation-based treatment protocol comprising: a) a module operably configured to receive and process information from medical images of a target structure to prepare a 3-D reconstruction model of the target structure; and b) a module operably configured to perform a numerical model analysis using as inputs in the analysis the 3-D reconstruction and information from one or more of physical constraints, tissue heterogeneities, dynamic effects of electropermeabilization, dynamic thermal effects, or effects resulting from multiple treatments; and c) a module operably configured to construct one or more electrical protocols defining a treatment region and treatment parameters for effectively treating the target structure.

Further included in embodiments of the invention are treatment planning systems for determining a patient-specific electroporation-based treatment protocol comprising: a) a processing module operably configured for performing the following stages: 1) receiving and processing information from medical images of a target structure and preparing a 3-D reconstruction model of the target structure; 2) performing a numerical model analysis using as inputs in the analysis the 3-D reconstruction and information from one or more of physical constraints, tissue heterogeneities, dynamic effects of electropermeabilization, dynamic thermal effects, or effects resulting from multiple treatments; and 3) constructing one or more protocols each providing a treatment region

with parameters for electroporating the target structure; and b) a processor for executing the stages of the processing module.

Such treatment planning systems can comprise a processing module capable of performing one or more of the stages in real time.

Information from medical images to be analyzed in treatment systems according to embodiments of the invention can be extracted from one or an array of images obtained from pathologic specimens or one or more imaging modalities chosen from radiographs, tomograms, nuclear scintigraphic scans, CT, MRI, PET, or US. The information from one or more of these sources can be compiled to prepare a 3D reconstruction of the target area, which is represented by a surface or a solid volume. The treatment planning systems according to embodiments of the invention can have as a target structure a) a targeted region or mass; or b) a targeted region or mass with neighboring regions; or c) a 3D map of voxels to be treated as independent elements in the finite modeling software.

Preferred numerical model analysis for treatment systems of the invention comprise finite element modeling (FEM). Even more preferred as treatment planning systems, wherein the numerical model analysis involves accounting for physical constraints, tissue heterogeneities, dynamic effects of electropermeabilization, dynamic thermal effects, and multiple treatment effects.

Even further, self-optimization algorithms for constructing the treatment protocols can also be incorporated into the inventive methods, systems, and devices. For example, the treatment planning systems can comprise a self-optimization algorithm which is capable of repeatedly evaluating one or more of physical constraints, placement of electrodes, electric field distribution simulations, and evaluation of outcome success until one or more effective protocol is constructed. It can also generate a predicted treatment time that will aid the physician in determining the optimal protocol.

According to some embodiments of the invention, the treatment planning systems can involve automatically, interactively, or automatically and interactively with or without user input determining the treatment region and parameters for electroporating.

Such treatment planning systems can also be capable of constructing protocols for an initial patient treatment or retreatment with or without additional medical images.

Treatment systems according to embodiments of the invention can also be adapted to instruct an electrical waveform generator to perform the protocol.

Such systems can further comprise an electrical waveform generator in operable communication with the processing module and capable of receiving and executing the treatment protocol.

Instructions for implementing the treatment protocols can comprise specifying a number of bipolar pulses to be delivered, a length of pulse duration, and a length of any delay between pulses. Additionally, the generators of such treatment systems can be operably configured for delivering a bipolar pulse train.

Methods and devices incorporating one or more of the features of the treatment planning systems according to the invention are also considered embodiments.

In particular, treatment planning methods can comprise: a) receiving and processing information from medical images of a target structure and preparing a 3-D reconstruction model of the target structure; b) performing a numerical model analysis using as inputs in the analysis the 3-D reconstruction and information from one or more of physical constraints, tissue

7

heterogeneities, dynamic effects of electropermeabilization, dynamic thermal effects, or effects resulting from multiple treatments; and c) constructing an electroporation protocol based on results of the analyzing; wherein the receiving, processing, analyzing, and constructing is performed in real time.

Other methods may comprise method steps for reducing adverse effects of irreversible electroporation of tissue comprising administering electrical pulses through electrodes to tissue in a manner which causes irreversible electroporation of the tissue but minimizes electrical charge build up on the electrodes, or minimizes charge delivered to the tissue, or both. Adverse effects to be avoided may include, to name a few, one or more of thermal damage of the tissue, deleterious electrochemical effects, or electrolysis.

Preferred methods according to the invention may comprise electrical pulses comprising a series of unipolar and bipolar pulses with a net charge of zero. More particularly, the net charge of zero can be achieved by a change in potential direction for each pulse, or a change in potential direction within each pulse.

Further, electrical pulses generated in the methods can together comprise a pulse protocol comprising a train of unipolar pulses followed by a train of unipolar pulses of opposite polarity, or a train of bipolar pulses, or simultaneous unipolar pulses of opposite polarity which are offset from one another by a desired amount, or a combination of protocols.

Electrical pulses used in the methods, systems, and devices of the invention can have a waveform which is square, triangular, trapezoidal, exponential decay, sawtooth, sinusoidal, or of alternating polarity, or comprise a combination of one or more waveforms.

Control systems for electroporation devices are also considered embodiments of the present invention. Such systems can be configured to comprise: a) a processor in operable communication with a control module; b) a control module executable by the processor and in operable communication with an electrical circuit, wherein the control module is operably configured for initiating switching of the circuit at a rate of between 10 ms to 1 ns; and c) an electrical circuit operably configured to enable delivery of a voltage to an electrode and switching of the voltage to a second electrode to cause reversing of the polarity of the electric potential between the two electrodes.

Similarly, electroporation system embodiments of the invention can comprise: a) an electroporation device capable of delivering a first unipolar electrical pulse; b) the electroporation device further capable of, or a second electroporation device capable of, delivering a second unipolar electrical pulse which is opposite in polarity to the first unipolar pulse; c) a processor in operable communication with a control module; d) a control module executable by the processor and in operable communication with the electroporation device(s), wherein the control module is operably configured for initiating delivery of the first unipolar electrical pulse at a time 1 and for initiating delivery of the second unipolar electrical pulse at time 2 offset from time 1 by 1 second to 1 nanosecond.

Electroporation devices can also be operably configured to enable delivery of an electrical pulse to a first electrode, switching of the pulse to a second electrode to cause reversing of the polarity of the electric potential between the two electrodes, and switching of the pulse back to the first electrode or to zero, wherein a cycle of switching is established which cycle is capable of being performed at a rate of between 10 milliseconds to 1 nanosecond.

8

Such devices, systems, and methods can be configured to provide for switching to occur between or within the electrical pulse. Devices, for example, can be configured such that the electrical pulses together comprise a pulse protocol comprising a train of unipolar pulses followed by a train of unipolar pulses of opposite polarity or a train of bipolar pulses.

BRIEF DESCRIPTION OF THE DRAWINGS

FIGS. 1A-D are schematic diagrams comparing the electric field distribution (A,C) and conductivity map (B,D) of two identical numerical models without (A,B) and with (C,D) changing conductivity.

FIGS. 2A-I are schematic diagrams showing the numerical model outputs for conductivity ratios (τ_t/σ_p) of 0.1 (A,D,G), 1 (B,E,H), and 10 (C,F,I); showing electric field (A-F) during the pulse and temperature (G-I) distributions 1 second after the first pulse.

FIG. 2J is a schematic diagram showing placement of the electrodes in the targeted tissue for the set up illustrated in FIGS. 2A-I.

FIG. 3 is a series of CT images showing the presence of a tumor in the left thigh of the canine patient of Example I.

FIG. 4 is a CT image from FIG. 3, within which the region of interest is traced.

FIG. 5 is a drawing of a 3D reconstruction of the target region of Example I, which was reconstructed by compiling a series of axial traces to create a representative shape of the targeted region in three dimensions.

FIG. 6 is the drawing of the 3D reconstructed geometry shown in FIG. 5 visualized relative to the rest of the patient.

FIG. 7 is a graphic representation of the 3D reconstruction of FIG. 5 as imported into and converted within Comsol Multiphysics.

FIG. 8 is a graph from Duck, 1990, showing the relationship between conductivity and %-water, which may also be used to estimate a tissue's electrical properties.

FIG. 9 is the drawing of the 3D reconstruction of the target tumor of FIG. 5 visualized in relation to surrounding structures within the body, which is a tool useful for developing treatment constraints.

FIG. 10 is a graphic representation of the 3D reconstruction of FIG. 5 as imported into and converted within Comsol Multiphysics and further including a demonstrative electrode placement for an exemplary treatment protocol.

FIG. 11A is a schematic representation of an electric field distribution map, showing a top view of the electrodes of FIG. 10 in an energized state.

FIGS. 11B-D are schematic diagrams demonstrating falloff of the electric field distribution in the third dimension, showing an exemplary electric field distribution in the xz-plane (FIG. 11B), in the xy-plane at the midpoint of the electrodes, and in the xy-plane at the tips of the electrodes.

FIG. 12A is a schematic drawing showing a representative geometry of the treatment area in which compiled ellipsoids (shown in pink) illustrate the electroporation protocol developed to attain the desired treatment objectives.

FIG. 12B is a schematic drawing showing a top view of the treatment area geometry shown in FIG. 12A, and further demonstrating the electrode insertion paths.

FIGS. 13A-B are respectively schematic diagrams of an electric field distribution and a corresponding conductivity map demonstrating a homogeneous distribution that only changes by 0.1% for visualization purposes when irreversible electroporation is accomplished.

FIGS. 14A-B are respectively schematic diagrams of an electric field distribution and a corresponding cumulative

conductivity map demonstrating a treatment region where more than two electrode pairs are energized and homogeneous distribution only changes by 0.1% for visualization purposes when irreversible electroporation is accomplished.

FIGS. **15**A-B are respectively schematic diagrams of an electric field distribution and a corresponding conductivity map demonstrating a heterogeneous distribution that changes from 0.67 S/m to 0.241 due to electropermeabilization caused by electroporation.

FIGS. **16**A-B are respectively schematic diagrams of an electric field distribution and a corresponding conductivity map demonstrating a heterogeneous distribution that changes from 0.67 S/m to 0.241 S/m due to electropermeabilization.

FIGS. **17**A-B are respectively schematic diagrams of an electric conductivity map and corresponding potential thermal damage resulting from electroporation at t=0 s.

FIGS. **18**A-B are respectively schematic diagrams of an electric conductivity map and corresponding potential thermal damage resulting from the electroporation at t=30 s.

FIGS. **19**A-B are respectively schematic diagrams of an electric conductivity map and corresponding potential thermal damage resulting from the electroporation at t=60 s.

FIGS. **20**A-B are two-dimensional (2-D) diagnostic T1 post-contrast MRI scans in which the tumor was traced.

FIGS. **21**A-H is a graphic representation of a three-dimensional (3-D) solid representing a tumor volume and displaying the voltage configurations that would mainly affect tumor tissue in this particular situation.

FIG. **22** is a graph showing a Bipolar IRE pulse (100 µs duration) with alternating polarity in the middle of the pulse.

FIG. **23**A is a schematic diagram of a representative circuit model for switching polarity between pulses and multipolar pulses.

FIG. **23**B is a graph showing the shape of a bipolar pulse that can be created using the electrical circuit of FIG. **23**A.

FIGS. **24**A-G are graphs showing various pulsing protocols according to the invention, demonstrating exemplary frequencies, pulse length, and time delay between pulses.

FIGS. **25**A-B are schematic diagrams showing variations in techniques for generating bipolar electrical pulses in accordance with embodiments of the invention.

FIG. **25**C is a schematic diagram of a representative circuit model for generating and administering simultaneous, continuous, but offset pulses as shown in FIG. **25**A.

FIG. **26**A is a photograph showing the N-TIRE electrodes with attached fiber optic probes, which were used in this intracranial treatment of white matter to measure temperature during pulse delivery.

FIG. **26**B is a graph showing temperature [° C.] distribution during an N-TIRE treatment in the white matter of a canine subject.

DETAILED DESCRIPTION OF VARIOUS EMBODIMENTS OF THE INVENTION

Irreversible electroporation (IRE) is a new focal tissue ablation technique. The treatments are capable of sparing major blood vessels, extracellular matrix and other sensitive or critical structures. The procedure involves the delivery of low-energy electric pulses through minimally invasive electrodes inserted within the tissue. The target tissue is exposed to external electric field distributions around the electrodes, which alter the resting transmembrane potential of the cells. The degree of tissue electroporation (i.e., no effect, reversible electroporation and/or irreversible electroporation) depends on the magnitude of the induced transmembrane potential.

Numerical models for electric field optimization are available and typically include the physical properties of the tissue and treatment parameters including electrode geometry and pulse parameters (e.g., duration, number, amplitude, polarity, and repetition rate). These models can also incorporate the dynamic changes in tissue electric conductivity due to electroporation and thermal effects.

In embodiments of the invention there is provided a numerical model to visualize the IRE treated regions using sequential independent combinations of multiple energized and grounded electrodes. Specifically, in such models electric conductivity changes due to electroporation and thermal effects from an IRE pulse sequence are capable of being incorporated into the analysis for developing and constructing more effective treatment protocols. A particular embodiment involves setting the resulting conductivity distribution as the initial condition for the next pulse sequence, then repeating this procedure sequentially until all the pulse sequences are completed. In this manner, electric conductivity dependencies from previous pulses are incorporated and more accurate electric field distributions are presented. It is important to note that it is assumed that once a tissue is irreversibly electroporated, the tissue conductivity would not revert back. Consequently, a comprehensive IRE distribution can be presented in which the conductivity changes due to the previous pulses are considered. Such methods are most useful when using three or more electrodes with electrode-pairs being energized independently.

The electric conductivity map in certain circumstances can be crucial in the treatment planning of irreversible electroporation and other pulsed electric field therapeutic applications. The conductivity map is what determines how the current generated by the applied voltages/potentials will flow and the magnitude of the electric field. Several factors affect this distribution before, during and after the treatment including tissue heterogeneities, electropermeabilization, thermal effects and multiple treatments.

First, each tissue has its own "resting/unique" electric conductivity before the application of the electric pulses. Thus, in any particular organ or system there could be a mixture of conductivities that need to be accounted for in the treatment planning as in the case of white matter, gray matter and tumor tissue in the brain for example. Also, due to the permeabilization of the cells in the tissue that are exposed to an electric field threshold capable of altering the membrane structure, there is an increase in conductivity as well (electroporation effect). In addition, each of the tissue's conductivity will vary with changes in temperature as is the case for brain (3.2% C^{-1}) or liver (2% C^{-1}).

The main region treated by irreversible electroporation does not have sufficient increase in temperature to generate thermal damage, however, at the electrode tissue interface (where the electric field is highest) there is a significant increase in temperature and thus the conductivity map is altered. Capturing these and other dynamic effects can be crucial since they represent more accurate/realistic treatment geometries and pulse parameters that are not captured elsewhere. Accounting for these effects in treatment planning software is expected to lead to the optimization of pulse parameters and minimize damage to surrounding healthy tissue.

Numerical modeling methods, such as finite element modeling (FEM), are more accurate and are actually where the previous treatment planning systems derive their solutions (the lookup table and analytical solutions are calibrated to mimic the numerical solutions).

The reason numerical solutions were not implemented previously is that software packages to do so can be expensive, can take extensive periods to come up with a solution (inhibiting real-time feedback as was the goal above), and require familiarity with complex software in order to develop protocols (practically requiring an engineer to develop the plans). Because the direction of EBTs is toward application in more complex settings where more accurate solutions are desirable and take priority over time for development, the system described in this disclosure is one that can be performed with numerical solutions by developing the treatment plan well in advance (hours, days, weeks, or months) of its implementation.

Example I

General Stages of Planning Electroporation-Based Treatments

A canine patient with a 360 cm³ tumor in the left thigh was treated according to a treatment planning embodiment of the invention. This treatment plan serves to demonstrate the complexity and numerous steps typically involved in developing and implementing a comprehensive treatment plan for electroporation-based therapies. This description is intended to provide guidance as to the formulation of a basic treatment planning system, which can be operably configured to include one or more of the following stages:

Image Acquisition.

Images of the target lesion or of a portion of the body to be treated can be acquired by taking an array of medical images using one or more imaging modalities, including CT, MRI, PET, or US to name a few.

As shown in FIG. 3, in preparation for isolating and reconstructing a target region, an imaging modality such as computed tomography CT can be used to determine the presence of a tumor. Using an image or series of images, information about or relating to the region of interest can be collected and used to determine a targeted region, its location, its position, any important or relevant nearby structures that must be accounted for (such as blood vessels, nerves, collecting ducts, etc.), and any relative basic dimensions (such as depth within tissue, basic cross-sectional sizes, distance from other structures, etc.). The CT images shown in FIG. 3 have used axial slices with TeraRecon software to compile the pixels into voxels and develop other sectional slices as well as an overall 3D reconstruction of the scans based on radiodensity (though individual regions of interest have not been isolated). Other imaging modalities such as ultrasound or MRI may also be used to assess the lesion.

Regions of Interest (ROI) Tracing.

The target ROI can be outlined in the images used to identify the tumor, whether manually or by way of a computer program, to identify a potential treatment area. For example, a computer program capable of detecting anomalies, such as the OsiriX open-source image analysis software (Geneva, Switzerland), could be used to outline the targeted region (e.g., a tumor, site for electrogenetransfer, etc.). As shown in FIG. 4, one of the CT scans from FIG. 3 is shown with the region of interest traced. Tracing the region of interest in each of a series of CT images compiling the 2D traces of each slice would allow for compilation of 3D geometry for the target region.

Visualizing and Reconstructing 3D Geometry.

The traced regions of interest from a series of axial CT slices can be compiled and interpolated between the steps to create a three-dimensional geometry that the practitioner

could use to gain an understanding of the basic shape of the target mass and/or its location relative to other tissues.

FIG. 5 shows a series of axial traces having been compiled to create a representative shape of the targeted region in three dimensions. This reconstruction may be maneuvered to assess its general shape and thus allow determination of potentially efficient electrode insertion approaches.

If desired, the reconstructed geometry can also be visualized relative to the rest of the patient. This allows one to assess (in greater detail than the initial FIG. 3 images) physical constraints such as bones preventing electrode insertion, relative location of sensitive structures, and orientation of the lesion relative to the body, allowing a practitioner to evaluate optimal electrode insertion approaches. For example, in FIG. 6, the long axis of the tumor is roughly parallel to the length leg and femur, so a user may consider reducing the number of electrodes and insertions used by orienting the electrodes along this axis, or they may go with more electrodes perpendicular to the top of the leg (since the femur prevents access from the bottom of the leg).

Geometry Modeling.

The 3D geometry can then be imported into finite element modeling software (FEM). Indeed, several geometries can be imported using software such as Comsol Multiphysics (Comsol, Stockholm, Sweden), including: a) just the targeted region or mass; b) the targeted region and other traced neighboring regions (muscle, fat, bone, etc); or a 3D Map of all the voxels to be treated as independent elements in the finite modeling software. The coordinate system from the medical images can also be matched.

FIG. 7 shows a model of the 3D target geometry as imported into numerical modeling software. More particularly, the geometry developed and shown in FIG. 5 may be converted to a surface or a solid and imported into numerical modeling software. Here, the black shape is a converted geometry within Comsol Multiphysics for the targeted region reconstructed above. Its dimensions and volume have been normalized to ensure its size matches that of the reconstructed volume.

Assign Model Properties.

Any physical and/or thermal properties and/or electrical properties can be assigned in numerous ways. For example, the properties can be assigned arbitrarily; deduced by designating which of the target region or the other traced neighboring regions are of what tissue type and using properties of these tissue types from the literature; experimentally measured with a "pre-pulse" (e.g., as described in U.S. patent application Ser. No. 12/491,151, "Irreversible Electroporation to Treat Aberrant Cell Masses;" or the properties can be derived from an algorithm or coordination scheme based on voxel or pixel value imported from the 3D map.

The assignment of properties to the model can be performed within software and manually accounted for in placements. If such properties are either assigned arbitrarily or are deduced as described above, the different shapes depicted in the model (e.g., FIG. 7) may each be assigned a different set of properties to best represent the tissue or material used (such as 0.025 S/m for the fatty tumor, and 0.5 S/m for the surrounding tissue).

In a preferred embodiment, the tissue properties are derived from medical images. Due to the properties of tissue and how the tissues are assessed by modern imaging techniques, it may be possible to derive accurate estimations of a tissue's properties based on its response to the various imaging modalities.

For example, for computed tomography, pixel values are based on the radiodensity of the tissue at that point in the

image (its attenuation). It is common practice to scale these attenuations relative to distilled water according to the equation:

$$HU = \frac{\mu_X - \mu_{water}}{\mu_{water} - \mu_{air}} \times 1000$$

where μ_X, μ_{water}, and μ_{air} are the linear attenuation coefficients of that point in the tissue, water, and air, respectively. Essentially, this system normalizes the radiodensity of all tissues relative to water.

A tissue's Hounds Unit (HU) value may serve as a representation of its relative water content, with larger absolute value HU's (because it can be negative as well) containing less water. Thus, one could determine (with some noise) a function of HU that goes in the domain from −1000 (air, minimal radioattenuation) to +1000 (an equivalent difference of higher radioattenuation), where the curve estimates the water content. The data in Table I supports this concept.

TABLE I

Substance	HU	Conductivity, S/m (from literature)
Air	−1000	0
Fat	−120	0.025
Water	0	—
Muscle	+40	0.5
Bone	>+400	.0025

These are general evaluations of conductivity. It does not matter what the conductivity of distilled water is, but it would likely be taken to be that of physiological saline for conductivity estimation (1.2 S/m). From qualitatively assessing the data in Table I, it can be seen that the closer a tissue's HU is to 0, the higher its conductivity. This is also reflected because it is known that muscle has a higher water content than fat, which is closer to the HU of 0 and a higher conductivity, while bone having the least water content of all, is the least conductive.

Although not a comprehensive table, the trends are clearly evident that one may be able to fit an interpolation function between HU and conductivity. With further exploration, it may be seen that this may be a result of higher volumetric water concentrations having higher conductivity. The idea that higher percentage of water causes a tissue to have a radiodensity more similar to that of water is an assumption, but when taking it into account, the relationship between conductivity and %-water may also be used to estimate the tissue's electrical properties, as described in Duck, 1990 (FIG. 8).

Evaluate any Physical Placement Constraints.

Potential physical placement constraints, such as vital structures (nerves, brain, blood vessels, etc.), access orientation preferences (from head, from rear, supine, prone patient positioning, etc.), and/or physical barriers (bones, sensitive structures, etc.) can be identified. The potential constraints can then be used to guide/constrain what angles are possible for the electrodes and if the electrodes should be placed to avoid certain areas more than others.

FIG. 9 shows a graphic 3D reconstruction of the target tumor in relation to surrounding structures within the body, which is useful for developing treatment constraints. The physical location of the tumor relative to the rest of the body (shown in FIG. 9 by arrows pointing out vasculature and nerves, for example) can be demonstrated using the previ-

ously prepared 3D geometric representation of the tumor. This information may be used to constrain or direct where the electrodes should be placed and give priority to regions that should be spared relative to regions that would not cause as significant of problems.

Placement of Electrodes.

Any number of electrodes could be placed into or around the targeted region. Their number, location, orientation, and size could all be adjusted independently.

FIG. 10 is a graphic 3D representation of the imported tumor geometry with electrodes placed. Here, the geometric representation of the targeted region is depicted in red, while representations of electrodes are shown at two locations in blue. The number, orientation, and location of these electrodes is capable of being manipulated to satisfy the desired treatment objectives.

Simulation of the Electric Field Distribution.

Simulation of the electric field distribution (e.g., numerically solved electric field distributions) are capable of being correlated with experimental data to superimpose predicted volumes of affected regions (treated, untreated, thermal damage).

For example, FIG. 11 shows the electrodes depicted in FIG. 10 in an energized state. For the electrode on the left, a section on the end has been set to a voltage while a section on the rest has been set to ground with a section of insulation between, creating a voltage gradient that surrounds the single needle. For the pair of electrodes on the right, the entire length of one electrode has been set to a voltage while the other electrode has been set to ground, creating a voltage gradient between them.

The color maps are representative electric field isocontour regions that may be used in determining predicted treatment regions, reversible regions, or safety margins based on electric field thresholds. For example, if the protocol anticipates an IRE electric field threshold of 500 V/cm, then the entire volume of the tissue exposed to this electric field or higher (depicted in green) would be the predicted treatment region. In addition, if it were desired to ensure sparing of a sensitive structure such as a nerve, and an exact resolution of the above-predicted 500 V/cm IRE electric threshold was insufficient to guarantee sparing, a different electric field may be used to predict a safety margin which would be used to ensure that this threshold is not crossed by the sensitive structure (such as 250 V/cm depicted in red).

Another factor to consider in any analysis for determining proper placement of the electrodes and/or the charge needed for a particular application is the expected behavior of the electric field relative to the electrodes. As shown in FIGS. 11B-D, the electric field distribution is typically at a maximum at the cross-sectional region midway between the lengths of the electrodes and tapers off toward the ends of the electrodes.

More particularly, the image shown in FIG. 11B shows the electric field distribution between 35000 and 150000 V/m looking at both electrodes simultaneously in the xz-plane. The grey rectangles are the electrodes, running along the z-axis, and separated by 1.5 cm (center-to-center) along the x-axis. Here, one can see that the electric field is greatest at z=0, and decreases as one moves towards the tips of the electrodes. The 2-dimensional cross-sectional estimates are calibrated to represent the electric field distribution at z=0, and do not take into account the losses that occur over the length of the electrode.

FIGS. 11C and D in comparison show x-y cross-sectional plane view of the electric field distribution at z=0 and the x-y cross-sectional plane view electric field distribution at z=1 cm

(the tips of the electrodes), respectively. By comparing these two distributions, it can be seen that the electric field distribution decreases as distance from the center of the electrode lengths increases. To accurately predict the treatment regions in three dimensions, these differences should be taken into account for the overall 3D nature of treatments. The methods, systems, and devices according to the invention include consideration of this factor.

Evaluate Success of Outcome.

Determine whether the setup used appropriately meets its treatment demands of affecting the desired regions while preventing unacceptable effects on untargeted and sensitive regions. This could be assessed qualitatively or quantitatively with a fitness function.

Optimization.

The evaluation of physical constraints, placement of electrodes, simulation of the electric field distribution, and evaluation of outcome success can be repeated until a suitable solution is developed. This optimization stage can be performed manually (interactively) by a practitioner or automatically. The Optimization Quality Function of Formula I discussed in more detail below could also be used for manual optimization.

In this embodiment, the optimization phase of the system was performed qualitatively and was iterated with the previous four steps until settling on the electrode array shown in FIGS. **12**A and B. In this embodiment, the resultant representative geometry of compiled ellipsoids (shown in pink) illustrates the satisfactory electroporation protocol developed in order to attain the desired treatment objectives. In FIG. **12**A, it can be seen that a highly complex array of electrodes (blue) was selected, where some electrodes are inserted and exposed an amount (such as 1 or 2 cm), to treat an amount of depth with pulsing, before withdrawing them some and repeating the pulsing. This was done to ensure complete treatment along the depth of the treatment. The blue cylinders depict discrete electrode placements for pulsing, and the ones stacked on top of each other represent this aspect.

Further, as shown in FIG. **12**B, a top view of the graphic representation of the treatment area of FIG. **12**A is provided, in which the electrode insertion paths can be seen. Since the electrodes were all running perpendicular, spacing dimensions have been outlined to aid the placement of the electrodes for the practitioner. The pulses would be administered between each electrode and the electrodes in closest proximity to it. Electric pulse parameters are adjusted between each electrode firing pair based on separation distance and the desired treatment region (based on targeted volume and avoidance of sensitive tissues). The dimensions in red are also used as guidelines for the placement of the outer electrodes relative to the margins of the tumor to prevent excessive treatment of peripheral (untargeted) regions.

Implementation.

Once a desired solution has been developed, the generator system for applying the designated pulsing protocol can be set up for implementation of the desired protocol. More particularly, the practitioner could then place the electrodes according to the prescribed protocol and let the generator apply the pulses.

Also during implementation, the systems, methods, and or devices according to the invention can be operably configured to monitor certain variables. One such variable can include monitoring the temperature of the electrodes and/or surrounding tissue in real time during treatment to ensure limited to no thermal damage to the tissue being treated. If monitored in real time, adjustments could then be made, if necessary, to avoid damage.

One, multiple, or all phases of system embodiments according to the invention can be performed manually or be performed (in whole or in any number of parts) by an automated system capable of performing the phases for the practitioner. Many of these steps can be performed without user input, and could be blocked off into distinct automated processes (with/without coupling to human-performed processes) or could be linked together through a comprehensive system. All of this is able to be done for an initial treatment, or redone for any retreatments that may be necessary, with or without new images (depending on case circumstances).

Example II

Comprehensive Package System: Treatment Planning Software

Due to the great complexity and time required to develop customized treatment protocols for each patient, it is desirable to automate one or more steps, or the entirety, of the treatment planning process. Since Cassini Oval and other analytical solutions are limited by their ability to incorporate many of the complexities commonly found in treatment situations (such as heterogeneities, complex geometries, different electrode dimensions and orientations, etc.), and because the trend seems to be to move treatment planning towards a simpler solution for practitioners so less time is wasted in trying all the different available options—a robust automatic treatment planning system that incorporates numerous variables and runs a self-optimization algorithm to automatically determine the optimal treatment parameters needed to be used to treat a particular patient is highly desired.

Systems according to embodiments of the invention are flexible in that such systems can be operably configured to solve many scenarios numerically and to select the best electrode geometry and pulse parameters for a given situation. Alternatively or additionally, solutions may be obtained analytically, with tables, etc.

Embodiments of the systems according to the invention can be operably configured to be run on an independent system well in advance of treatment administration to allow sufficient computation time, review, and possible re-working of the protocol prior to treatment. The appropriate protocol could then be uploaded directly to the pulse generator.

Model Creation.

Preferred embodiments of systems according to the invention include a model creation stage for establishing an initial model of the target area.

Geometry:

Treatment geometries (information, such as tumor dimensions, electrodes, and peripheral tissue dimensions, for example) may be input manually, by analyzing medical images that were taken and any reconstructions, from computer analyses of medical images/tomography, or other (2D and 3D) mapping techniques.

Properties: Conductivity values for the model subdomains may be obtained by measuring them on the subject directly (placing electrodes within tissue then applying a voltage and measuring the current to get Z/σ), by taking typical values found in the literature for the tissue types, or by noninvasive a measuring techniques such as functional Magnetic Resonance Imaging (fMRI), Electrical Impedance Tomography, etc; and combining these with the relevant equations (for E-field distributions, it is the ratio between tissues/regions that alters the field, absolute values will only be important when considering thermal effects). Medical images that already obtain the conductivity values (fMRI) or coupled to

conductivity values (analyzing and mapping a medical image for the different tissues and coupling the regions to a conductivity value determined as described above) may then be used as the geometries for a numerical/analytical model as the various subdomains, to establish the initial model.

Electrodes.

Once the model geometry has been developed, a single or any set of electrode options (type, number, dimensions, etc.) may be selected to be used or allowed to be selected by the program.

Running the Program.

After setting up the geometry and electrode options to consider, the practitioner would essentially select a "GO" button to let the program run through the many variations to use and solve each using FEM or advanced analytical methods. The program would solve each scenario for various effects (no effect, reversible electroporation, irreversible electroporation, or thermal) and distributions within the model. Thermal considerations will greatly increase the computational cost of the model, but may be desired to determine thermal damage and scarring, especially in very sensitive structures.

Exemplary Optimization Quality Function.

The systems of embodiments of the invention can employ a variety of algorithms (iterative, genetic, etc.) in order to optimize the treatment parameters for the best possible result for a particular patient scenario. Such systems can also be operably configured to employ a function for evaluating the quality of each solution, where desired results, D, (IRE and/or REB throughout the targeted regions) are added; and the undesired results, U, (thermal damage, IRE beyond targeted region, etc.) are subtracted, with each aspect having its own unique scaling (since IRE to entire targeted region is far more important that avoiding IRE to healthy tissues). One such function can include:

$$\Psi(ET,EP,\Phi,\ldots)=A\cdot[IRE]_D+B\cdot[REB]_D-C\cdot[Therm]_D-E\cdot[IRE]_U-F\cdot[REB]_U-G\cdot[Therm]_U \qquad \text{Formula I}$$

wherein D=Desired/Targeted Volume (done as a percentage);

U=Undesired/Peripheral Volume (done as an absolute value);

A, B, C, E, F, G=Scaling factors, with likely situations including: 1) A & B>>C, E, F, and G (treatment success most important); 2) G>>C (thermal to healthy worse than to targeted; 3) B & F may be neglected in purely IRE treatments; and 4) F can typically be assumed to be =0 since no negative effects to the tissue would be associated with this parameter, since it would either have no effect (without chemicals), or will not have an effect on healthy cells (with selective chemicals); but may matter in situations involving nonselective chemicals;

ET=Electrode Type and geometry (single/dual, diameter, length);

EP=Electrode Positioning (location and orientation in 3D space);

ϕ=Applied voltage;

ψ=Quality, the value of the protocol on the entire domain of the targeted and surrounding volumes.

Additional Details on ψ(ET, EP, ϕ, . . .):

This is the value function of a given treatment protocol for the modeled domain previously mentioned as a function of electrode type and geometry, electrode positioning, applied voltage, and any other factors. More specifically: 1) ET (style, number, dimensions), with style referring to the style of the pulse, such as single, multi-unipolar, hybrid, proprietary, etc., with number referring to the number of probes used, and

dimensions referring to the geometry and dimensions of all exposed and insulated regions in all three directions for each electrode used.

EP refers to the position of each or all electrodes in relation to a reference point arbitrarily chosen within the (x, y, z) domain of the model (location and orientation). In one example, the center of the tumor could be selected as the reference point and arbitrarily set to (0, 0, 0). The reference point may also be selected ahead of time or afterwards by the practitioner that will be easy for the practitioner to physically use at the time of treatment administration, such as some anatomical landmark that can be used as a reference for where the electrodes are and the electrode orientation. It is also possible to match the coordinate system from the medical images.

The ψ function may be solved for altered ET and EP, and the ϕ may then be scaled accordingly for the geometry (since it the model geometry and properties that will affect the shape of the distribution, the absolute value of it may be scaled to the applied voltage after this shape is found for each ET and EP). This would dramatically reduce the number of iterations and thus the computational cost.

In embodiments, the system can be operably configured to iteratively adjust ET, EP, etc. and obtain the resulting ψ, storing the top ones (or all those meeting some type of baseline threshold criterion). The resulting stored solutions would then be saved for presentation to the practitioner for conducting a review and visually assessing the value of each solution for selecting the protocol that best meets the demands of the therapy (could range on their arbitrary criterion such as the best quality, most simple to administer and apply the EP in the treatment, most robust, etc.)

The electrical parameters used (number of pulses, repetition rate, shape, pulse length, etc.) can be set as standardized parameters for typical treatments, and optionally these parameters can be flexible in case certain scenarios require different values—such as abdomino-thoracic procedures requiring repetition rate to be synchronized with the patient's heart rate to reduce the risk of pulse-induced arrhythmias. If known or found experimentally, standard electrical parameters can be used to determine the best combination of treatment parameters to use and have been applied to various tissues/tumors to determine the electric field threshold of each for this set of parameters, thus allowing treatment outcome to be reviewed and not just electric field distributions. Table II provides a list of exemplary electric parameters that can be manipulated within the IRE treatments discussed herein.

TABLE II

Parameters	
Pulse length:	ns-ms range
Number of pulses:	1-50,000 pulses
Electric Field Distribution:	1-5,000 V/cm
Frequency of Pulse Application:	0.001-1000 Hz
Frequency of pulse signal:	0-100 MHz
Pulse shape:	square, triangular, trapezoidal, exponential decay, sawtooth, sinusoidal, alternating polarity
Pulse type:	Positive, negative, neutral electrode charge pulses (changing polarity within pulse) Multiple sets of pulse parameters for a single treatment (changing any of the above parameters within the same treatment to specialize outcome)

19

TABLE II-continued

Parameters	
Electrode type:	Parallel plate:
	0.1 mm-70 cm diameter
	(and larger for applications relating to
	e.g., whole organ decellularization)
	Needle electrode(s):
	0.001 mm-1 cm diameter
	Single probe with embedded disk
	electrodes: 0.001 mm-1 cm diameter
	Spherical electrodes:
	0.0001 mm-1 cm diameter
	Needle diameter: 0.001 mm-1 cm
	Electrode length (needle): 0.1 mm to 30 cm
	Electrode separation: 0.1 mm to 5 cm, or
	even 5 cm to 20 cm, or 20 cm to 100 cm,
	and larger (for reversible electroporation,
	gene delivery, or positive electrode with
	ground patch on patient's exterior, e.g.)

Additional considerations, such as multiple pulse protocols that create dynamic tissue properties as a function of electric field, and temperature changes, may need to be investigated or added. Such dynamic properties are demonstrated in FIGS. **13-19**.

FIGS. **13**A-B demonstrate a situation in which there would be little to no change in the physical properties of the tissue as a result of electroporation. More specifically, as shown in FIG. **13**A, an electric field distribution [V/cm] generated by an applied voltage difference of 3000V over the upper two electrodes is shown. FIG. **13**B provides a conductivity map [S/m] displaying a homogeneous distribution that only changes by 0.1% for visualization purposes when irreversible electroporation is accomplished. The white outline represents the region of tissue that is exposed to an electric field magnitude that is sufficient for generating irreversible electroporation.

FIGS. **14**A-B demonstrate an electric field distribution and conductivity map for a treatment region for a given situation in which more than two electrode pairs are energized. In FIG. **14**A, an electric field distribution [V/cm] generated by an applied voltage difference of 3000V over the right two electrodes is shown. FIG. **14**B shows a conductivity map [S/m] displaying a homogeneous distribution that only changes by 0.1% for visualization purposes when irreversible electroporation is accomplished in this set up. In FIG. **14**B, a cumulative visualization of the treatment region is shown.

FIGS. **15**A-B demonstrate a change in the shape and size of the treatment region due to electropermeabilization. More particularly, in FIG. **15**A, an electric field distribution [V/cm] generated by an applied voltage difference of 3000V over the upper two electrodes is shown. FIG. **15**B provides a conductivity map [S/m] displaying a heterogeneous distribution that changes from 0.67 S/m to 0.241 due to electropermeabilization as a result of electroporation. Of particular note in this example, the shape and size of the treatment region is consequently adjusted as a result of this change. In FIG. **15**B the shape and size of the planned treatment region is different than in the above examples (FIGS. **13**B and **14**B) in which the conductivity was assumed to remain constant throughout the delivery of the pulses.

FIG. **16**A provides an electric field distribution [V/cm] generated by an applied voltage difference of 3000V over the right two electrodes, while FIG. **16**B shows a conductivity map [S/m] displaying a heterogeneous distribution that changes from 0.67 S/m to 0.241 S/m due to electropermeabilization. Of particular interest, the first set of pulses using the top two electrodes increased the conductivity of the tissue which in turn modified the electric field distribution (i.e., treatment region) for the second application of pulses (right two electrodes) adjacent to the permeabilized region.

20

The following examples are different than the previously described examples in which the treatment region depended on electropermeabilization, and multiple electrode combinations. In this case, a 2-D model of an irreversible electroporation protocol is shown in which the electric parameters of the protocol included 90 pulses, at 2000V, delivered at a frequency of 1.5 Hz, using 100 µs pulses. The 2D model generates much higher temperatures and thus changes relative to the complete 3D model since the heat has a larger volume in which to diffuse. Nevertheless, this case is reported for illustration purposes and to show that in fact these dynamic effects can be incorporated into treatment planning models. Changes only due to temperature are incorporated in this example to emphasize the importance of accounting for these effects in the models.

To illustrate the thermal effect of electroporation on tissues contacting the electrodes, FIGS. **17-19** are provided. FIG. **17**A provides an electric conductivity [S/m] map at t=0 s in which the irreversible electroporation area is 2.02 cm^2. FIG. **17**B shows a thermal damage assessment by the potential increase in temperature due to the electric pulses which occurs when greater than 0.53.

FIG. **18**A provides an electric conductivity [S/m] map at t=30 s in which the irreversible electroporation region is 2.43 cm^2. FIG. **18**B shows some thermal damage visualized at the electrode-tissue interface 0.11 cm^2.

FIG. **19**A provides an electric conductivity [S/m] map at t=60 s in which the irreversible electroporation area is 2.63 cm^2. FIG. **19**B shows significant thermal damage at the electrode-tissue interface due to thermal effects 0.43 cm^2.

Therapy Application.

Once the practitioner has selected a desired solution from the options on the treatment planning software, the electrical protocol (pulse characteristics, number, sequence, etc.) could be saved and then uploaded to the pulse generator system. At this point, the practitioner would have to do no more than place the electrodes in the predetermined positions and hit "START", at which point the instrument carries out the prescribed pulsing conditions.

Example III

Exemplary Methods for IRE Treatment Planning

Open source image analysis software (OsiriX, Geneva, Switzerland) was used to isolate the brain tumor geometry from the normal brain tissue. The tumor was traced in each of the two-dimensional (2-D) diagnostic T1 post-contrast MRI scans as shown in FIGS. **20**A-B. Attempts were made to exclude regions of peritumoral edema from the tumor volume by composite modeling of the tumor geometry using all available MRI sequences (T1 pre- and post-contrast, T2, and FLAIR) and image planes.

As provided in FIGS. **21**A-H, a three-dimensional (3-D) solid representation of the tumor volume was generated using previously reported reconstruction procedures. The tumor geometry was then imported into a numerical modeling software (Comsol Multiphysics, v.3.5a, Stockholm, Sweden) in order to simulate the physical effects of the electric pulses in the tumor and surrounding healthy brain tissue. The electric field distribution was determined in which the tissue conductivity incorporates the dynamic changes that occur during electroporation. In this model, a 50% increase in conductivity was assumed when the tissue was exposed to an electric field magnitude greater than 500 V/cm, which has been shown as an IRE threshold for brain tissue using specific experimental conditions. Currently, the threshold for brain tumor tissue is unknown so the same magnitude as normal tissue was used for treatment planning purposes.

21   22

Based on the tumor dimensions and numerical simulations, the voltage configurations that would mainly affect tumor tissue were determined and are provided in Table III as well as are displayed in FIGS. 21A-H.

form treatment zone. More specifically, in IRE treatments there is an energized and grounded electrode as the pulses are delivered. In embodiments, charge build-up on the surface of the electrodes can be minimized by alternating the polarity

TABLE III

VOLTAGE (V)	ELECTRODE GAP (CM)	ELECTRODE EXPOSURE (CM)	VOLT-TO-DIST RATIO (V/CM)	PULSE DURATION	NUMBER OF PULSES	FREQUENCY
500	0.5	0.5	1000	50 µs	2 × 20	ECG synchronized
625	0.5	0.5	1250	50 µs	4 × 20	ECG synchronized

IRE Therapy.

Total intravenous general anesthesia was induced and maintained with propofol and fentanyl constant rate infusions. A routine left rostrotentorial approach to the canine skull was performed and a limited left parietal craniectomy defect was created. The craniectomy size was limited to the minimum area necessary to accommodate placement of the IRE electrode configurations required to treat the tumor, as determined from pre-operative treatment plans. Following regional durectomy, multiple biopsies of the mass lesion were obtained, which were consistent with a high-grade (WHO Grade III) mixed glioma.

After administration of appropriate neuromuscular blockade and based on the treatment planning, focal ablative IRE lesions were created in the tumor using the NanoKnife® (AngioDynamics, Queensbury, N.Y. USA), and blunt tip electrodes. The NanoKnife® an electric pulse generator in which the desired IRE pulse parameters (voltage, pulse duration, number of pulses, and pulse frequency) are entered. The NanoKnife® is also designed to monitor the resulting current from the treatment and to automatically suspend the delivery of the pulses if a current threshold is exceeded.

The electrodes were inserted into the tumor tissue in preparation for pulse delivery. The blunt tip electrodes were connected by way of a 6-foot insulated wire (cable) to the generator. After foot pedal activation, the pulses were conducted from the generator to the exposed electrodes.

The two sets of pulse strengths were delivered in perpendicular directions to ensure uniform coverage of the tumor and were synchronized with the electrocardiogram (ECG) signal to prevent ventricular fibrillation or cardiac arrhythmias (Ivy Cardiac Trigger Monitor 3000, Branford, Conn., USA). The sets of pulses were delivered with alternating polarity between the sets to reduce charge build-up on the surface of the electrodes. In addition, shorter pulse durations than those used in previous IRE studies were used in order to reduce the charge delivered to the tissue and decrease resistive heating during the procedure. Previous calculations and experimental data from previous intracranial IRE experiments ensured that no thermal damage would be generated in normal brain. The temperature measured near the electrodes showed a maximum 0.5° C. increase after four sets of twenty 50-µs pulses when using similar parameters to the ones in Table I. In addition, the charge delivered during the procedure was typical or lower than that used in humans during electroconvulsive therapy, a treatment for depression that also uses electric pulses.

Example IV

Treatment Systems, Methods, and Devices Using Bipolar Electric Pulses

It has been found that alternating polarity of adjacent electrodes minimizes charge build up and provides a more uni-

between sets of pulses. It is believed that there are still electrode surface effects that can be associated with negative outcomes.

Further, the use of bipolar pulses (net charge of zero) as seen in FIG. 22 is a way to further minimize the charge delivered to the tissue. FIG. 22 is a graph showing a Bipolar IRE pulse (100 µs duration) with alternating polarity in the middle of the pulse in order to minimize charge delivered to the tissue. In this manner, negative effects can be prevented, reduced, or avoided as part of IRE treatment in the brain, including deleterious electrochemical effects and/or excessive charge delivered to the tissue as in electroconvulsive therapy.

In one experiment, a superficial focal ablative IRE lesion was created in the cranial aspect of the temporal lobe (ectosylvian gyrus) using the NanoKnifeB (AngioDynamics, Queensbury, N.Y.) generator, blunt tip bipolar electrode (AngioDynamics, No. 204002XX) by delivering 9 sets of ten 50 µs pulses (voltage-to-distance ratio 2000 V/cm) with alternating polarity between the sets to prevent charge build-up on the stainless steel electrode surfaces. These parameters were determined from ex-vivo experiments on canine brain and ensured that the charge delivered during the procedure was lower than the charge delivered to the human brain during electroconvulsive therapy (an FDA approved treatment for major depression).

Other undesirable consequences of various electroporation protocols have also been experienced. More specifically, with the application of electric potentials, electrical forces may drive ions towards one electrode or the other. This may also lead to undesirable behavior such as electrolysis, separating water into its hydrogen and oxygen components, and leading to the formation of bubbles at the electrode-tissue interface. These effects are further exacerbated for multiple pulse applications. Such effects may cause interference with treatment by skewing electric field distributions and altering treatment outcomes in a relatively unpredictable manner. By altering the polarity between the electrodes for each pulse, these effects can be significantly reduced, enhancing treatment predictability, and thus, outcome. This alternating polarity may be a change in potential direction for each pulse, or occur within each pulse itself (switch each electrode's polarity for every pulse or go immediately from positive to negative potential within the pulse at each electrode).

FIG. 23A is a schematic diagram of a representative circuit model for switching polarity between pulses and multipolar pulses. As shown in FIG. 23A, a basic circuit according to embodiments of the invention may contain a) a generator supply circuit containing a voltage source and capacitor bank to accumulate sufficient charge for pulse delivery; b) a simultaneous switching mechanism; c) electrodes for pulse deliv-

ery (here, 2 electrodes are shown); and d) a parallel capacitor-resistor equivalent to represent the behavior of biological tissues. FIG. 23B shows an exemplary bipolar pulse that can be created using the circuit of FIG. 23A.

The circuit can be operably configured to function in the following representative manner. At Time **0**, the switches are in position **0**. The voltage source would be used to charge an array of capacitors to the desired electric potential for a given pulse. At Time t_1, the switches move to position **1**. This causes rapid initiation of capacitor discharge, generating a high-slope ΔV between the electrodes placed in the tissue (the first half of a square wave). This gives electrode **1** a "negative" voltage and electrode **2** a "positive" voltage (based on their relative electric potentials). The capacitor(s) continue delivering the electric charge over time, causing a logarithmic decay of the electric potential to which the tissue is exposed. At Time t_2, the switches move to position **2**. This changes which electrode is connected to which end of the circuit, rapidly reversing the polarity of the electric potential, making electrode **1** "positive" and electrode **2** "negative." The peak of this reversal is the same as the remaining charge on the capacitors after the decay between t_1 and t_2. The remaining charge on the capacitors continues to decay. At Time t_3, the switches return to position **0**. This disconnects the circuits, creating a rapid drop in the electric potential between the electrodes, returning ΔV to zero. Alternatively, at Time t_3, the switch could return to position **1**, then alternate between positions **1** and **2** for a desired period of time to deliver several bipolar pulses in rapid succession. Such switching circuitry would enable delivery of a bipolar pulse train comprising individual pulses having a duration ranging from 10 ms to 1 ns, much faster than any human could achieve.

It should be mentioned that the electric potential difference is arbitrary, and the polarity of any of the pulses in the above-mentioned example are for demonstration only, and are not the sole method of obtaining multipolar pulses. Alternative approaches are possible and this basic circuitry representation may be adapted to generate any series of complex pulses by changing the pattern of switch behavior.

For instance, unipolar pulses may have their polarity reversed every pulse or after any number of pulses by moving the switches from position **0** to **1** for pulse delivery, then back to **0** (first pulse); then from position **0** to **2** for delivery, then back to **0** (second pulse of opposite polarity). As shown in FIGS. **24**A-D, a unipolar pulse of any polarity can be reversed after one or more pulses up to any number of desired pulses for a particular application. For example, a time delay between the unipolar pulse and the reversed polarity unipolar pulse can be any desired duration as well, including from 5 times the pulse length (FIG. **24**A), to 3 times the pulse length (FIG. **24**B), to 1 time the pulse length (FIG. **24**C), to no delay (or effectively no delay) at the time of switching (FIG. **24**D).

As shown in FIGS. **24**E-G, the pattern of alternating between pulse polarities can be repeated any number of times to accomplish a desired result. For example, the bipolar pulse of FIG. **24**D is shown repeated at timing intervals of 3 times the pulse length (FIG. **24**E), to 2 times the pulse length (FIG. **24**F), to 1 time the pulse length (FIG. **24**G). The delay between bipolar pulses can also be zero (or effectively zero) and/or the bipolar pulses can be repeated any number of time to establish a particular desired pulsing protocol or pattern.

The pulses could also be made multipolar by switching from position **0** to **1** (first polarity), then to position **2** (reversed polarity), then back to position **1** (returning to initial polarity), and so on, all within the same pulse.

Even further, the bipolar pulses can be configured in a manner to deliver a charge to the tissue where the net effect of

the pulse is something other than zero. For example, the magnitude of the positive portion of the pulse can be different than the magnitude of the negative portion of the pulse. More specifically, the pulse can be 90% positive and 10% negative or 90% negative and 10% positive. Indeed, any ratio of positive:negative charge can be used, including from 0:100 (mono-polar and positive) to 100:0 (mono-polar and negative). Specifically, 50:50 (net charge of zero) is preferred, but 90:10, 80:20, 75:25, 60:40 and the reverse can be used depending on the desired effect.

Additionally, the time between any switch could be used to alter the length of any pulse or change the pulse repetition rate. And, if varying combinations of different capacitor banks were used in the system, then depending on which ones were connected, it would be possible to change the applied voltage to the electrodes between pulses or within a pulse (of any polarity).

The shape and type of pulse can also be varied for particular applications. In various embodiments, the individual electric pulses can be unipolar while in other embodiments, the individual electric pulses can be bipolar. In certain preferred embodiments, a train of unipolar pulses is delivered in one direction, followed by a subsequent pulse train of opposite polarity. Depending on the outcome desired, the waveforms of the electric pulses are triangular, square, sinusoidal, exponential, or trapezoidal. Other geometric shapes are contemplated as well. In some embodiments, an electrode is connected to a system for employing electrical impedance tomography (EIT), computed tomography (CT), Magnetic Resonance Imaging (MRI), or ultrasound to image the tissue prior to treatment by applying small alternating currents that themselves do not damage the tissue.

A large variety of other parameters can influence the efficiency of membrane poration, such as the shape of the electrical pulses, polarity, size of target cells, and thermal conditions during and after the pulses.

Another method for avoiding excessive charge build up in tissues being treated by electroporation is to deliver counteracting pulses simultaneously from one or more pulse generator. In embodiments, the pulses delivered by the generators can overlap in time for some portion of the pulse and be offset from one another.

FIG. **25**A illustrates the concept of overlapping the equal but opposite charges delivered from separate pulse generators. In particular, a first pulse generator administers a first positive pulse for a desired amount of time. Here, the pulse has a duration in the 10 ns to 10 ms range. At some time after the first pulse is generated, a second pulse from a second pulse generator is administered. In this example, the second pulse is of the same magnitude as the first pulse yet opposite in polarity. By overlapping the pulses, or simultaneously applying the pulses, the net effect during the overlap is that the tissue does not experience a charge. In effect the overlap of the pulses creates a delay and the charge delivered to the tissue is only the portion of each pulse that is outside of the overlap, i.e., the offset.

FIG. **25**B illustrates one example of administering opposing polarity pulses from two pulse generators simultaneously, but offset and with no overlap. As shown, a first positive electrical pulse is initiated by a first pulse generator. At a desired time following administration of the first pulse, a second pulse equal in magnitude to the first pulse but opposite in charge is initiated using a second pulse generator. It is noted that in this figure that although a summation of the two individual signals offset by a delay (pulse duration) is shown, one of skill in the art could easily incorporate additional signals in order to manipulate additional pulse parameters. Further, and

as with all embodiments described in this specification, the positive and negative applied voltages do not have to be of equal magnitude.

In one such embodiment, electrical pulses are delivered in a series of two pulses of alternating polarity (from millisecond to nanosecond range). Use of alternating polarities reduces or eliminates charge buildup on the electrode(s). For example, two NanoKnife™ (AngioDynamics, Queensbury, N.Y.) devices can be linked to the same electrode array, and programmed to deliver synched or slightly offset pulses to the electrodes. The first pulse can generate a 2500 V/cm electric field of 500 ns duration. This pulse is followed immediately (yet slightly offset) by the onset of a second pulse, which generates a −2500 V/cm electric field for 500 ns. The net effect of the pulses in the tissue is a net charge of zero and an additional benefit is avoiding the need for complex circuitry as the need for abrupt switching of the polarity is obviated.

Also during implementation of a desired treatment protocol, the systems, methods, and or devices according to the invention can be operably configured to monitor certain variables, such as temperature of the electrodes and/or surrounding tissue. If monitored during the procedure and in real time, adjustments to the protocol, including adjustments to the type, length, number, and duration of the pulses, could then be made, if necessary, to avoid damage of the tissue being treated.

It is important to note that bipolar pulses are only effective for electroporation if each pulse within the train is long enough in duration to charge the plasma membrane to a permeabilizing level. If this is not the case, the pulses offset each other from fully charging the plasma, and supra-poration effects dominate when the pulse amplitude is increased. Additionally, a delay can be included between pulses within the train, or the total number of pulses within the train can be controlled, to limit the Joule heating in the tissue while still delivering a lethal dose of energy. Embodiments of the invention are equally applicable to any electroporation-based therapy (EBT), including therapies employing reversible electroporation, such as gene delivery therapy and electro-chemotherapy, to name a few. One of skill in the art is equipped with the skills to modify the protocols described herein to apply to certain uses.

The repetition rate of pulse trains can also be controlled to minimize interference with, and allow treatment of vital organs that respond to electrical signals, such as the heart. The concept of alternating polarity of pulses can be extended to the use of multiple electrodes. For example, a combination of three electrodes can be used to deliver three sequential sets of alternating polarity pulses to a target tissue. More specifically, Electrode A can be used to deliver a 500 ns pulse at 1000 V at a starting time (T=0) and a 500 ns pulse at −1000 V at T=1 μs. Electrode B can be used to deliver a 500 ns pulse at 1000 V at T=500 ns, and a 500 ns pulse at −1000 V at T=1.5 μs. Electrode C can be used to deliver a 500 ns pulse at 1000 V at T=1 μs, and a −1000V pulse at T=2.0 μs. Of course, this concept can be applied using any numbers of electrodes and pulse times to achieve highly directed cell killing.

Example V

Monitoring Temperature During Electroporation Procedures

One of the main advantages of N-TIRE over other focal ablation techniques is that the pulses do not generate thermal damage due to resistive heating, thus major blood vessels, extracellular matrix and other tissue structures are spared. See B. Al-Sakere, F. Andre, C. Bernat, E. Connault, P. Opolon, R. V. Davalos, B. Rubinsky, and L. M. Mir, "Tumor ablation with irreversible electroporation," *PLoS ONE*, vol. 2, p. e1135, 2007; and J. F. Edd, L. Horowitz, R. V. Davalos, L. M. Mir, and B. Rubinsky, "In vivo results of a new focal tissue ablation technique: irreversible electroporation," *IEEE Trans Biomed Eng*, vol. 53, pp. 1409-15, July 2006, both of which are incorporated by reference herein in their entireties. The inventors have found that with real time temperature data measured at the electrode-tissue interface, the non-thermal aspect of the technique can be confirmed. One such way to measure temperature in-vivo during the pulse delivery is to use fiber optic probes.

In an experiment performed by the inventors, temperatures were measured in the brain during an N-TIRE procedure using the Luxtron® m3300 Biomedical Lab Kit Fluoroptic® Thermometer (LumaSense™ Technologies, Santa Clara, Calif. USA). STB medical fiber optic probes (LumaSense™ Technologies, Santa Clara, Calif. USA) were placed at the electrode-tissue interface and 7.5 mm along the insulation. FIG. 26A is a photograph showing the N-TIRE electrodes with attached fiber optic probes, which were used in this intracranial treatment of white matter to measure temperature during pulse delivery.

After insertion of the electrodes, four sets of twenty 50 μs pulses were delivered with a voltage-to-distance ratio of 1000 V/cm between the electrodes. The electrode exposure and separation distance were each 5 mm. The polarity of the electrodes was alternated between the sets to minimize charge build-up on the electrode surface. These parameters were determined from previous in-vivo N-TIRE procedures which showed sufficient ablation of tissue. The NanoKnife® was synchronized with the dog's heart rate in order to prevent any ventricular defibrillation or arrhythmias.

For treatment planning purposes, in order to model accurate N-TIRE treatment, it is beneficial to incorporate changes in conductivity due to permeabilization of the tissue (as described in detail in the treatment planning section of this specification), as well as incorporate information relating to temperature changes. See P. A. Garcia, J. H. Rossmeisl, R. E. Neal, II, T. L. Ellis, J. Olson, N. Henao-Guerrero, J. Robertson, and R. V. Davalos, "Intrracranial Non-Thermal Irreversible Electroporation: In vivo analysis," *Journal of Membrane Biology*, p. (in press), 2010, which is incorporated by reference herein in its entirety. Conductivity changes due to thermal effects could have important implications with a number of different treatment parameters, including electrode geometry and pulse parameters (i.e., duration, number, amplitude, and repetition rate, etc.).

FIG. 26B is a graph showing temperature [° C.] distribution during an N-TIRE treatment in the white matter of a canine subject. More particularly, what is shown is the temperature distribution measured by the probe located at the electrode-tissue interface and 7.5 mm above the insulation. It is important to note that the starting temperature was approximately 33° C. due to the anesthesia effects and this is neuro-protective during brain procedures in general and that the total pulse delivery took around 300 seconds. For the probe at the interface, four sets of mild increase in temperatures are seen. The probe in the insulation also shows some very mild increase in temperature that is probably due to heat conduction from the treatment region.

The changes in the temperature resulting from N-TIRE are less than 0.5° C. and they are not sufficient to generate thermal damage. This confirms that any cell death achieved by the procedure was a direct result of N-TIRE since at the electrode-tissue interface the highest thermal effects are expected

to be achieved. It is also apparent from this data that it can be assumed in numerical modeling that electrical conductivity changes due to electroporation only and not temperature.

The present invention has been described with reference to particular embodiments having various features. It will be apparent to those skilled in the art that various modifications and variations can be made in the practice of the present invention without departing from the scope or spirit of the invention. One skilled in the art will recognize that these features may be used singularly or in any combination based on the requirements and specifications of a given application or design. Other embodiments of the invention will be apparent to those skilled in the art from consideration of the specification and practice of the invention. It is intended that the specification and examples be considered as exemplary in nature and that variations that do not depart from the essence of the invention are intended to be within the scope of the invention.

The invention claimed is:

1. A treatment planning system for determining a patient-specific electroporation-based treatment protocol comprising:

a processing module operably configured for performing the following stages:

receiving and processing information from medical images of a target structure and preparing a 3-D reconstruction model of the target structure;

performing a numerical model analysis using as inputs in the analysis the 3-D reconstruction and electrical conductivity; and

constructing one or more protocols each providing a treatment region with parameters for electroporating the target structure; and

a processor for executing the stages of the processing module.

2. The treatment planning system of claim 1, wherein the processing module is capable of performing the stages in real time.

3. The treatment planning system of claim 2, wherein the processing module further comprises functionality for monitoring electrode or tissue temperature in real time and for considering electrode or tissue temperature in the analysis.

4. The treatment planning system of claim 1, wherein the information from medical images is extracted from an array of images obtained from one or more imaging modalities chosen from radiographs, tomography, nuclear scintigraphy, CT, MRI, fMRI, PET, or US.

5. The treatment planning system of claim 1, wherein the numerical model analysis comprises finite element modeling (FEM).

6. The treatment planning system of claim 5, wherein the target structure is a targeted region or mass; or is a targeted region or mass with neighboring regions; or is a 3D map of voxels to be treated as independent elements in the finite modeling software.

7. The treatment planning system of claim 1, wherein the 3D reconstruction is a surface or a solid volume.

8. The treatment planning system of claim 1, wherein the numerical model analysis involves accounting for physical constraints, tissue heterogeneities, dynamic effects of electropermeabilization, dynamic thermal effects, and multiple-treatment effects.

9. The treatment planning system of claim 1, further comprising a self-optimization algorithm for constructing the protocols.

10. The treatment planning system of claim 9, wherein the self-optimization algorithm is capable of repeatedly evaluat-

ing one or more of physical constraints, placement of electrodes, electric field distribution simulations, and outcome success of the protocols, and evaluation of outcome success until one or more effective protocol is constructed.

11. The treatment planning system of claim 1, wherein the treatment region and parameters for electroporating are determined automatically, interactively, or automatically and interactively with or without user input.

12. The treatment planning system of claim 1, capable of constructing protocols for an initial patient treatment or retreatment with or without additional medical images.

13. The treatment planning system of claim 1, further adapted for instructing an electrical waveform generator to perform the protocol.

14. The treatment planning system of claim 13, further comprising an electrical waveform generator in operable communication with the processing module and capable of receiving and executing the treatment protocol.

15. The treatment planning system of claim 14, wherein the generator is operably configured for delivering a bipolar pulse train.

16. The treatment planning system of claim 13, wherein instructing comprises specifying a number of bipolar pulses to be delivered, a length of pulse duration at any pole, and a length of any delay between pulses.

17. The treatment planning system of claim 1, wherein the electrical conductivity is provided as a conductivity map.

18. A treatment planning method comprising:

receiving and processing information from medical images of a target structure and preparing a 3-D reconstruction model of the target structure;

performing a numerical model analysis using as inputs in the analysis the 3-D reconstruction and electrical conductivity;

and constructing an electroporation protocol based on results of the analyzing;

wherein the receiving, processing, analyzing, and constructing is performed in real time.

19. The treatment planning system of claim 18, wherein the electrical conductivity is provided as a conductivity map.

20. The method of claim 18, wherein the information from medical images is extracted from images obtained from one or more imaging modalities chosen from radiographs, tomography, nuclear scintigraphy, CT, MRI, fMRI, PET, or US.

21. The method of claim 18, wherein the numerical model analysis comprises finite element modeling (FEM).

22. The method of claim 21, wherein the target structure is a targeted region or mass; or is a targeted region or mass with neighboring regions; or is a 3D map of voxels to be treated as independent elements in the finite modeling software.

23. The method of claim 18, wherein the 3D reconstruction is a surface or a solid volume.

24. The method of claim 18, wherein the numerical model analysis involves accounting for physical constraints, tissue heterogeneities, dynamic effects of electropermeabilization, dynamic thermal effects, or multiple-treatment effects.

25. The method of claim 18, wherein the electroporation protocol is determined automatically, interactively, or automatically and interactively with or without user input.

26. The method of claim 18, capable of constructing protocols for an initial patient treatment or retreatment with or without additional medical images.

27. The method of claim 18, further comprising instructing an electrical waveform generator to perform the electroporation protocol.

28. The method of claim **27**, wherein the instructing comprises specifying a number of bipolar pulses to be delivered, a length of pulse duration at any pole, and a length of any delay between pulses.

29. The method of claim **27**, wherein the instructing comprises instructions for delivering a bipolar pulse train.

30. The method of claim **18**, further comprising monitoring electrode or tissue temperature in real time and considering electrode or tissue temperature in the analyzing.

* * * * *